GLUCOCORTICOID INDUCED OSTEOPOROSIS AND

MECHANISMS OF INTERVENTION

Amy Yoshiko Sato

Submitted to the faculty of the University Graduate School

in partial fulfillment of the requirements

for the degree

Doctor of Philosophy

in the Department of Anatomy and Cell Biology,

Indiana University

March 2017

Accepted by the Graduate Faculty, Indiana University, in partial

fulfillment of the requirements for the degree of Doctor of Philosophy.

_____

Teresita Bellido, Ph.D., Chair

_____

Lilian I. Plotkin, Ph.D.

Doctoral Committee

_____

Fredrick M. Pavalko, Ph.D.

_____

Alexander G. Robling, Ph.D.

January 13, 2017

© 2017

Amy Yoshiko Sato

Dedication

To my mother and father, for always believing I could achieve anything and everything.

Truly, the inspiration I draw from you is never-ending.

To Dr. Bellido, for countless moments of guidance and encouragement,

and when needed chocolate.

To my committee, department and clinical advisors, for their sharing

their expertise and providing insightful questions.

I would also like to thank the Department of Anatomy and Cell Biology, the IBMG

program, and Indiana University School of Medicine for providing this opportunity and

creating the perfect learning environment.

Amy Yoshiko Sato

GLUCOCORTICOID INDUCED OSTEOPOROSIS AND

MECHANISMS OF INTERVENTION

Glucocorticoid excess is a leading cause of osteoporosis. The loss of bone mass and strength corresponds to the increase in fractures exhibited after three months of glucocorticoid therapy. Glucocorticoids induce the bone cellular responses of deceased bone formation, increased osteoblast/osteocyte apoptosis, and transient increased bone resorption, which result in rapid bone loss and degradation of bone microarchitecture.

The current standard of care for osteoporosis is bisphosphonate treatment; however, these agents further suppress bone formation and increase osteonecrosis and low energy atypical fracture risks. Thus, there is an unmet need for interventions that protect from glucocorticoid therapy. The purpose of these studies was to investigate novel mechanisms that potentially interfere with glucocorticoid-induced bone loss. We chose to explore pathways that regulate endoplasmic reticulum stress, the canonical Wnt pathway, and Pyk2 activity. Pharmacologic reduction of endoplasmic reticulum stress through salubrinal administration protected against glucocorticoid-induced bone loss by preservation of bone formation and osteoblast/osteocyte viability. In contrast, inhibition of Wnt antagonist Sost/sclerostin and inhibition of Pyk2 signaling did not prevent glucocorticoid-induced reductions in bone formation; however, both Sost/sclerostin and Pyk2 deficiency protected against bone loss through inhibition of increases in resorption. Overall, these studies demonstrate the significant contributions of reductions in bone formation, increased osteoblast/osteocyte apoptosis, and elevations in resorption to the rapid 6-12% bone loss exhibited during the first year of glucocorticoid therapy.

However, glucocorticoid excess also induces skeletal muscle weakness, which is not reversed by bisphosphonate treatment or the interventions reported here of

salubrinal, Sost/sclerostin inhibition, or Pyk2 deficiency. Further, the novel finding of increased E3 ubiquitin ligase atrophy signaling induce by glucocorticoids in both bone and muscle, by tissue-specific upstream mechanisms, provides opportunities for therapeutic combination strategies. Thus, future studies are warranted to investigate the role of E3 ubiquitin ligase signaling in the deleterious glucocorticoid effects of bone and muscle.

Teresita Bellido, Ph.D., Chair

Table of Contents

Chapter 1

Introduction

Glucocorticoid-induced osteoporosis

Excess of glucocorticoids (GC), either due to an endogenous elevation or due to administration as immunosuppressants, is one of the leading causes of increased bone fragility and osteoporosis worldwide (1;2). Glucocorticoids are secreted by the adrenal glands under the regulation of the hypothalamus-pituitary-adrenal (HPA) axis in response to biological stress and regulate numerous physiological processes such as carbohydrate and amino acid metabolism, maintenance of blood pressure, and modulation of stress and inflammatory responses (3-5). Glucocorticoid-induced osteoporosis was first described by Dr. Cushing as patients with endogenous elevation of GC, either due to Cushing's disease or syndrome, exhibited an increased tendency for bone fractures (6). Aging also leads to endogenous elevation of GC action with progressive increases in adrenal production of the hormone and increases in the 11β-hydroxysteroid-dehydrogenase 1 (11β-HSD1) activity that favors conversion of inactive cortisone to active cortisol (7). The level of 11β-HSD1 activity is also highly predictive for the degree of bone formation suppression induced by GC, with higher 11β-HSD1 activity levels correlating to further reductions in circulating markers of bone formation (8). Administration of GC as immunosuppressant therapy is commonly prescribed for a wide range of conditions including rheumatoid arthritis, asthma, inflammatory bowel disease, lung diseases, chronic liver disease, skin diseases, multiple myeloma, and organ transplantation, resulting in long-term GC therapy with the consequent bone loss and fragility for many of these conditions (9;10).

Excess of GC, from either endogenous or exogenous sources, leads to adverse effects in the musculoskeletal system as well as several other tissues and organs involving ocular, cardiovascular, nervous, and metabolic-related systems (5;10-14). For

instance, rapid increases in vertebral, hip, and nonvertebral (forearm) fracture risks have been reported as early as 3 months after initiation of systemic GC therapy with daily doses as low as 2.5 mg prednisolone (15). Glucocorticoid therapy induces loss of cortical and cancellous bone, reductions in bone strength, and atraumatic fractures for an estimated 30-50% of long-term therapy patients with the consequent morbidity and mortality (2;9;16-19). The GC deterioration of bone microarchitecture, through trabecular and cortical bone thinning, further contributes to the increased bone fragility, by precariously altering the threshold for fractures (20;21). Unfortunately, bone mineral density (BMD) assessments underestimate fracture risks of GC therapy patients as impaired bone microarchitecture cannot be detected by standard dual energy X-ray absorptiometry (DXA) measurements (20;22;23). In addition, GC induce muscle weakness, reduce body balance, and increase the prevalence of falls which when combined with lower bone mass greatly elevate the risk and occurrence of bone fractures (10;15;22).

Biphasic nature of GC-induced bone loss

GC induce osteoporosis by increasing bone resorption, decreasing bone formation, and increasing apoptosis of osteocytes and osteoblasts, resulting in bone fragility with elevated fracture risk, as indicated by human and animal models of GC excess (2;9;17-19;24-28). The initial phase of GC-induced bone disease involves a rapid, early bone loss with reports ranging from 6-12% losses during the first year of GC therapy (29). The rapid bone loss is attributed to increased resorption due to both a prolongation of preexisting osteoclast lifespan and increased osteoclastogenesis (24;30;31). Bone formation is also reduced in the initial phase (32) as GC downregulate the expression of OCN (33;34) and Col1A1 (35;36) resulting in decreased matrix mineral production. Prevalence of apoptotic osteoblasts and osteocytes is also elevated with GC administration, exhibited as early as 10 days after treatment *in vivo* (32). Overall, these

bone cellular responses to GC administration result in rapid bone loss with significant reductions in lumbar spine BMD occurring as early as 3 to 5 months with mean doses of 7.5 mg/day prednisolone, with greater than 15 mg/day prednisolone doses considered typically as high doses (22;37;38).

The initial phase of high bone resorption is followed by a low bone remodeling phase associated with reductions in both osteoclasts and osteoblasts numbers leading to chronic bone loss. The suppression of bone formation and increased osteoblast/osteocyte apoptosis continues throughout the chronic phase and the loss of these RANKL supporting cells has been attributed as the cause of reductions in resorption activity (9). The continuation of reduced bone formation corresponds with strong correlations between cumulative GC doses and reductions with BMD of the spine, hip, distal radius, and mid-radius as each consecutive year of GC therapy contributes to further bone loss (22).

Current therapeutic anti-catabolic options

While several therapeutic options inhibit the resorption-driven bone loss by GC administration, these therapeutic options have undesirable side effects attributed to the severe reductions in bone turnover, without addressing bone formation reductions or muscle weakness pathology associated with glucocorticoid-induced osteoporosis (GIO).

Currently, bisphosphonates are the standard of care for GIO and are widely-used anti-resorption agents for GIO internationally (2;10). Patients under immunosuppressant therapy and co-treated with the bisphosphonate alendronate exhibited higher BMD of the total body, lumbar spine, femoral-neck, and trochanter when compared to GC-treated controls (14). Similar BMD conserving results have also been reported with administration of zoledronic acid or risedronate bisphosphonates in immunosuppressant therapy patients (39). However, while BMD is protected from resorption driven GC-induced bone loss with bisphosphonates, the use of these agents significantly

suppresses bone turnover resulting in even further reductions of bone formation compared with GC treatment alone (14;32;40;41). Prolonged use of bisphosphonates is also associated with decreased bone tissue toughness, which increases the risk for low-energy atypical fractures as the bone's capacity to absorb energy before failure is diminished (42-44). Treatment with anti-RANKL antibodies in patients receiving GC induces even more pronounced reductions in bone formation, with roughly -30% lower circulating levels of N-terminal type I procollagen propeptide (P1NP) and OCN, when compared to treatment with bisphosphonates (45). The long-term prevention of resorption activity, whether due to bisphosphonate or anti-RANKL antibody administration, results in a loss of normal bone turnover which promotes microdamage and advanced glycation endproducts (AGEs) accumulation and increases risks for osteonecrosis of the jaw (42;43;46;47). Overall, these anti-catabolic agents preserve pre-existing bone to maintain BMD and lower fracture risk, but also further suppress the formation of new bone, which is not ideal for the GC chronic phase of bone loss or the long-term treatment nature of GC therapy.

Current therapeutic anabolic agent

Currently, teriparatide, recombinant human parathyroid hormone (1-34), is the only FDA approved anabolic therapy. In contrast to anti-catabolic agents, that reduce bone formation to lower levels than GC treatment alone, teriparatide stimulates bone formation to increase BMD and lower fracture risks (40;48). The anabolic stimulation by teriparatide leads to the addition of new bone resulting in higher gains in BMD at critical bone sites of the lumbar spine (38;40;48), total hip (40;48), and femoral neck (48) than alendronate administration in GIO patients. The incidence of vertebral fractures is also significantly lower with teriparatide than alendronate therapy (40;48). Further, whereas circulating bone formation markers P1NP and bone alkaline phosphatase (ALP) as well as remodeling marker OCN are elevated with teriparatide, bisphosphonate

administration further reduced the levels of these circulating markers when compared to baseline GIO levels (40;48). However, currently there is a lack of long-term anabolic interventions as teriparatide therapy is only approved for 24 months in patients (49).

Thus, understanding the mechanisms of GC action on the musculoskeletal system and identification the development of long-term therapeutic agents that prevent the detrimental side effects of anabolic bone suppression are imperative. The purpose of these studies was to investigate potential therapeutic targets for GC-induced skeletal effects within pathways regulating endoplasmic reticulum stress, canonical Wnt signaling, and Pyk2-induced apoptosis signaling. Future studies will investigate the role of E3 ubiquitin ligase signaling in the deleterious GC skeletal effects of bone and skeletal muscle.

Chapter 2

Prevention of glucocorticoid induced-apoptosis of osteoblasts and osteocytes

by protecting against endoplasmic reticulum (ER) stress *in vitro* and *in vivo*

in female mice

Introduction

Excess of glucocorticoids (GC), either endogenous as in aging or due to glucocorticoid administration as immunosuppressants, leads to loss of bone (2). Chronic GC therapy is prescribed for a multitude of medical conditions including autoimmune diseases such as rheumatoid arthritis, organ transplants, asthma, as a component of cancer chemotherapies, and a variety of inflammatory afflictions (9;50). Patients with chronic GC exposure exhibit a consistent reduced bone formation rate and histomorphometric features of increased bone resorption (2;27;51). Studies with experimental animals in which GC action is blocked in osteoclasts or in osteoblasts/osteocytes support the notion that GC-induced bone loss occurs in two phases: an early bone loss caused by osteoclast-driven bone resorption, followed by a steady decline in both bone formation and bone resorption (26;30;52). Between 30 to 50% of patients experience at least one bone fracture, with the consequent morbidity and mortality. Approximately 25% of patients also develop osteonecrosis due to accumulation of apoptotic osteocytes, which increases the risk of femoral head collapse (25). Thus, understanding the mechanisms of GC action on bone cells and designing therapeutic strategies that prevent the deleterious effects of these drugs are imperative.

Increased apoptosis of osteoblasts and osteocytes is one of the mechanisms that underlie the reduced bone formation and bone fragility that characterize GC-induced osteoporosis (2). Apoptosis by GC is due to direct hormonal effects on osteoblasts and osteocytes (28;53;54) and is abolished by overexpressing in these cells the enzyme that inactivates GC, 11beta-hydroxysteroid dehydrogenase type 2 (26). The pro-apoptotic effects of GC are mediated through the classical GC receptor and are triggered by rapid activation of the kinases Pyk2 and JNK (54). GC-induced JNK phosphorylation lies downstream of increased reactive oxygen species (ROS) generation and subsequent activation of pro-apoptotic signaling in osteoblasts (55). Phosphorylation of eukaryotic

translation initiation factor 2α (eIF2α) by double-stranded RNA-activated protein kinase-like ER kinase (PERK) protects cells from oxidative stress and apoptosis under ER stress conditions (56). Phosphorylated eIF2α slows global rate of protein translation to provide time for the ER to recover from the excessive protein load, allowing the cell to escape from apoptosis (56;57). Earlier findings showed that selective inhibition of eIF2α phosphatases with salubrinal or guanabenz protects from apoptosis induced by ER stress (58;59). Salubrinal increases the levels of phosphorylated eIF2α and protects PC12 pheochromocytoma cells from apoptosis induced by the ER stressor tunicamycin, in a dose dependent manner at concentrations varying from 1-100 μM (58). Further, guanabenz, another eIF2α phosphatase inhibitor, antagonizes the effect of tunicamycin on several cell types at concentrations up to 50 μM (59). We hypothesized that the pro-apoptotic effect of GC on osteoblasts and osteocytes is at least in part due to induction of ER stress, and we investigated here whether the compounds salubrinal and guanabenz that inhibit eIF2α dephosphorylation will promote osteoblastic cell viability and oppose the deleterious effects of GC *in vitro* and *in vivo*.

Materials and Methods

Cell lines. Primary osteoblastic cells were isolated from the neonatal calvarial bones of C57BL/6 mice, as previously published (60). Murine primary osteoblastic cells, bone marrow-derived OB-6 osteoblastic cells, and MLO-Y4 osteocytic cells were cultured as previously described (61;62).

Quantification of cell detachment, apoptosis, and cell viability. Cell and nuclear morphology was quantified in MLO-Y4 osteocytic cells stably transfected with green fluorescent protein targeted to the nucleus (nGFP), as published (54). Briefly, cell detachment was assessed by quantifying the number of cytoplasmic processes per cell. Cells were then categorized into one of two groups: having 3 or less processes or having more than 3 processes; and data is reported as percentage of cells with 3 or less processes. Apoptosis was evaluated by quantifying the percentage of cells with chromatin condensation and nuclear fragmentation in the same cultures. Data is reported as percentage of apoptotic cells.

Cells were treated with the anti-oxidant agents N-acetyl cysteine (NAC, 10 mM), ebselen (20 µM), or catalase (1250 U/ml), the eIF2α phosphatase inhibitors salubrinal (1-100 µM) and guanabenz (10 µM) (58;59), the bisphosphonate alendronate (0.1 µM), or corresponding vehicle (named control in the figures), for 1 hour. Subsequently, cells were exposed to the pro-apoptotic agents dexamethasone (1 µM), etoposide (50 µM), brefeldin A (2.7 µM), or tunicamycin (2.7 µM) or corresponding vehicle (named control in the figures), for the indicated times. Cell viability was assessed by trypan blue uptake as previously published (54;60). Cells that excluded the dye were considered alive, and stained cells were considered dead. Data is reported as the percentage of dead cells.

Mineralization assay. Primary osteoblasts or OB-6 cells were plated at a density of 5000 cells/cm^2 in growth medium consisting of MEM Alpha medium supplemented with 10% fetal bovine serum and 1% penicillin/streptomycin. Once cultures reached

confluence, medium was replaced by osteogenic medium containing 50 ug/ml ascorbic acid and 10 mM β-glycerophosphate together with 1 μM dexamethasone or its corresponding vehicle (ethanol), and 10 μM salubrinal or guanabenz or the corresponding vehicle (DMSO). Medium was replaced every 2-3 days. Mineralization was visualized using von Kossa phosphate staining (63), Alizarin Red S (Sigma-Aldrich) staining (64), or OsteoImage Mineralization Assay Kit (Lonza). Mineralization was quantified using a microplate reader for Alizarin Red S staining (405 nm absorbance) and Lonza staining (492/520 nm) excitation/emission fluorescence).

In vivo study. C57BL/6 female mice (n=7-11 per group) were purchased from Harlan (Indianapolis, IN). After a 2 week acclimation period, four-month-old mice were implanted with 60 day slow-release pellets delivering placebo, 1.4 mg/kg/day (GC1) prednisolone, or 2.1 mg/kg/day (GC2) prednisolone (Innovative Research of America, Sarasota, FL) while under isoflurane anesthesia. For this, a small area between the shoulder blades was shaved and cleaned with 70% EtOH prior to incision. Daily subcutaneous injections of salubrinal (1 mg/kg/day, Tocris Bioscience, USA) or equal volume of vehicle (propylene glycol, Sigma Aldrich, named control) began 3 days prior to pellet implantation and continued until experiment termination. An additional group of GC2 implanted mice (n=10) received 5.25 mg/kg/week alendronate subcutaneous injections starting 3 days before pellet implantation. Mice were sacrificed 28 days after pellet implantation. Institutional Animal Care and Use Committee at Indiana University School of Medicine approved all animal procedures.

Bone mineral density (BMD) measurements. BMD was determined in live mice by dual-energy x-ray absorptiometry (DXA) scanning using a PIXImus II densitometer (G.E. Medical Systems, Lunar Division, Madison, WI) (65). Experimental group assignment was randomized by basal spine BMD determined by DXA scanning

10

performed 5 days prior to pellet implantation. DXA scanning was also performed 28 days after pellet implantation.

Bone histomorphometry and apoptosis. Distal femora were fixed in 10% neutral buffered formalin. After 48 hours in fixative, samples were transferred to 70% ethanol, and then embedded undecalcified in methyl methacrylate as previously described (28). Dynamic histomorphometry measurements were performed in 7-µm unstained bone sections under epifluorescence microscopy. For this purpose, 0.6% calcein and 1.0% alizarin red solutions were intraperitoneally injected 8 and 3 days prior to sacrifice. Histomorphometric analysis was performed with a computer and digitizer tablet (OsteoMetrics, Decatur, GA) interfaced to an Olympus BX51 fluorescence microscope (Olympus America Inc., Melville, NY) with a drawing tube attachment (66). Apoptotic cells were detected by transferase-mediated biotin-dUTP nick end-labeling (TUNEL) reaction in undecalcified longitudinal sections of the distal femur, as previously described (28). Analysis was performed in cancellous and cortical bone, starting 200 µm below the growth plate and ending at the mid-diaphysis.

Statistical analysis. Data is expressed as means ± standard deviation (SD). Sample differences were assessed using SigmaPlot 12.0 (Systat Software Inc., San Jose, CA), following the appropriate method for each measurement, as indicated in the figure legends. Means were considered significantly different at $p < 0.05$.

Results

Glucocorticoids induce apoptosis of osteocytic and osteoblastic cells by gernerating ROS. The synthetic glucocorticoid dexamethasone induced retraction of osteocytic MLO-Y4 cytoplasmic processes, an early sign of cell detachment that triggers apoptosis (anoikis) (54), as revealed by a reduction in the percentage of cells exhibiting 3 or more cytoplasmic projections (**Figure 2-1A**). Dexamethasone also induced apoptosis of MLO-Y4 osteocytic cells, as quantified by evaluating chromatin condensation and nuclear fragmentation (**Figure 2-1B** and **C**). Further, dexamethasone increased the percentage of MLO-Y4 and OB-6 osteoblastic cells exhibiting trypan blue uptake (**Figure 2-1D**), another sign of apoptotic cell death induced by GC previously shown to be blocked by inhibiting caspase 3 activity (28;54;60). Pre-treatment with the anti-oxidants NAC, ebselen, or catalase prevented GC-induced apoptosis of either cell type, although for OB-6 cells the inhibitory effect of catalase was incomplete.

Inhibition of eIF2α dephosphorylation with salubrinal and guanabenz prevents apoptosis induced by glucocorticoids, etoposide, and ER stressors in osteoblastic cells. Because ROS induce ER stress, we next investigated whether reduction of ER stress by inhibiting eIF2α dephosphorylation with salubrinal was able to prevent apoptosis induced by dexamethasone or etoposide, another pro-apoptotic stimulus that induces apoptosis by inhibiting topoisomerase II and DNA repair. Dexamethasone or etoposide consistently increased MLO-Y4 and OB-6 cell death (**Figure 2-2**). Salubrinal did not significantly affect cell viability, except for the increasing trypan blue uptake of MLO-Y4 cells at 100 μM for 6 hours (**Figure 2-2A**). The mechanism behind the decreased viability induced by high concentrations of salubrinal is not known. However, it might be related to a transient increase in the expression of pro-apoptotic protein CHOP as found by Zhang et al. in MC3T3 osteoblastic cells (67). Further, 1-100 μM salubrinal prevented cell death induced by dexamethasone in both MLO-Y4 and OB-6 cells (**Figure 2-2A** and **B**).

Salubrinal also inhibited the effects of etoposide, but with less efficiency. The 10 µM salubrinal concentration was used for subsequent experiments as it consistently prevented dexamethasone-induced apoptosis in MLO-Y4 and OB-6 cells at both 6 and 24 hour time points. Salubrinal and guanabenz, another inhibitor of eIF2α dephosphorylation, also inhibited apoptosis of OB-6 osteoblastic cells and primary osteoblasts induced by the inducers of ER stress brefeldin A, and inhibitor of the ER/Golgi apparatus vesicle transport, and tunicamycin, a protein glycosylation inhibitor (58) (**Figures 2-3A-C**). In contrast, alendronate, an agent previously shown to effectively inhibit apoptosis of osteocytic MLO-Y4 cells, osteoblastic OB-6 cells, and primary calvaria derived osteoblasts induced by dexamethasone or etoposide (28;65;68), was unable to prevent the increase in OB-6 cell death induced by the ER stress inducers (**Figure 2-3B**).

Salubrinal and guanabenz ameliorate the inhibitory effects of glucocorticoids on matrix mineralization. We next investigated whether inhibitors of the ER stress alter the effects of GC on matrix mineralization. GC decreased mineral deposition in OB-6 osteoblastic cells cultured under osteogenic conditions, as shown by staining with von Kossa (that detects phosphate) or Alizarin Red S (that detects calcium) (**Figures 2-4A** and **B**), or in primary osteoblasts measured by hydroxyapatite accumulation (**Figure 2-4C**). Treatment with salubrinal or guanabenz increased mineralization of OB-6 cells (**Figures 2-5A** and **B**). Further, either compound partially prevented the decreased mineralization induced by GC in OB-6 or primary osteoblasts (**Figure 2-5**). Thus, salubrinal increased mineral content in cells treated with GC compared to GC alone after 7 and 10 days of culture (**Figure 2-5A**). However, salubrinal treatment could not block GC reductions in mineralization after 14 days of GC exposure, but guanabenz remained effective throughout the two week GC treatment period (**Figures 2-5A-C**).

Salubrinal protects against osteoblast and osteocyte apoptosis in vivo and partially prevents the bone loss induced by glucocorticoids. We next investigated whether inhibition of eIF2α dephosphorylation promoted bone cell viability also *in vivo*. Guanabenz appeared to be more potent in opposing the *in vitro* effects of GC compared to salubrinal. However, guanabenz is also an α2 adrenergic receptor agonist used in the treatment of hypertension (69). To avoid potential skeletal effects of activating these receptors, we decided to use salubrinal for the *in vivo* study. C57BL/6 female mice implanted with pellets containing two different doses of the GC prednisolone (GC1 = 1.4 or 2.1 mg/kg/day) received daily injections of salubrinal (1 mg/kg/day). Mice treated with prednisolone exhibited increased apoptosis of osteoblasts in cancellous bone and of osteocytes in both cancellous and cortical bone (**Figure 2-6**). Salubrinal completely blocked GC1-induced apoptosis of both osteoblasts and osteocytes, whereas it only partially prevented the increase in GC2-induced apoptosis of osteoblasts and did not inhibit GC2-induced osteocyte apoptosis. On the other hand and consistent with previous findings (65), alendronate effectively prevented GC2-induced apoptosis of both osteoblasts and osteocytes in cancellous bone, although it did not inhibit GC2-induced cortical osteocyte apoptosis. Administration of prednisolone induced a significant decrease in BMD in total body, spine, and femur, at both doses compared to placebo (**Figure 2-6B**). Mice implanted with placebo pellets and treated with salubrinal lost significantly less spinal BMD compared to those treated with vehicle. Similarly, mice implanted with GC1 pellets and injected with salubrinal lost significantly less bone compared to mice implanted with GC1 pellets and injected with vehicle. On the other hand, salubrinal did not prevent the loss of bone induced by GC2. In contrast, inhibition of resorption with alendronate not only prevented GC2-induced bone loss, as previously shown (65), but also increased BMD over placebo treated mice. Moreover, GC1 and GC2 reduced bone formation rate (BFR) in cancellous bone by a combination of

14

reduction in MS/BS and in MAR (**Figure 2-6C**). Salubrinal reversed the decreased BFR induced by GC1 but not GC2. Alendronate reduced further GC2-mediated inhibition of BFR by decreasing both MS/BS and MAR.

Discussion

Apoptosis of osteoblasts and osteocytes contributes to the reduced bone formation and increased bone fragility in glucocorticoid-induced osteoporosis (25;26;52). Therefore, understanding the mechanisms by which GC induce apoptosis of osteoblastic cells is critical for the development of intervention therapies. Earlier studies demonstrated that apoptosis of osteocytes and osteoblasts is caused by loss of attachment to the extracellular matrix mediated by inside-out signaling down-stream of Pyk2/JNK kinases (54) and that GC increase ROS production in bone *in vivo* and in osteoblastic cells *in vitro* (55). We investigated in this study the effect on GC action of salubrinal and guanabenz, eIF2α dephosphorylation inhibitors that block ROS-induced ER stress (58;59). These compounds prevented the pro-apoptotic effect of GC on osteoblasts and osteocytes *in vitro* and the decrease in mineral deposition induced by GC in osteoblastic cell cultures. Further, salubrinal prevented apoptosis of osteoblasts and osteocytes induced by GC *in vivo* and the concomitant decrease in bone mass and bone formation.

Consistent with the current study demonstrating inhibition of apoptosis of osteoblasts and osteocytes and improved mineralization by decreasing ER stress, recent evidence demonstrates increased apoptosis of osteoblastic cells and changes in osteoblast differentiation associated with elevated ER stress *in vitro* with thapsigargin or tunicamycin (70;71). Remarkably, increased ER stress appears to have a time-dependent biphasic effect inducing rapid increase in osteoblast markers Runx2 and osterix, followed by a reduction in the expression of these transcription factors as well as osteocalcin (70). Further, ER stress-mediated apoptosis of osteoblasts and impaired osteoblast differentiation was also demonstrated in a model of osteogenesis imperfecta (72) and in mice lacking the ER-localization protein Arl6ip5 in osteoblasts (73). Consistent with the pro-apoptotic and inhibitory effect of ER stress on osteoblast

16

differentiation, in the current manuscript we show that opposing ER stress by inhibiting eIF2α dephosphorylation prevents osteoblast and osteocyte apoptosis and the decrease in osteoblast function induced by GC *in vitro* and *in vivo*. Our findings agree with previous evidence showing that salubrinal increases the number of alkaline phosphatase positive colonies in bone marrow cell cultures (74) and osteocalcin expression in MC3T3-E1 cells (75).

In contrast to the protective effect of salubrinal against the action of low GC dose (GC1), salubrinal was unable to protect the skeleton from the high GC dose (GC2). Similarly, whereas salubrinal or guanabenz effectively prevented the inhibition of mineralization induced by short-term treatment of cultured osteoblasts with GC, only guanabenz was able to reverse the effects of prolonged treatment with GC. The mechanism of the different outcome of guanabenz compared to salubrinal is not known. It remains unclear also the reason for the incomplete inhibition of cortical osteocyte apoptosis by alendronate in this experiment, since in earlier studies alendronate completely prevented apoptosis of osteoblastic cells in both cancellous and cortical bone (65). A potential explanation is that in the previous study alendronate was administered daily instead of in a weekly 7-day cumulative dose. Nevertheless, these findings suggest that the potency of the pro-apoptotic signals delivered by GC, either due to high dose or prolonged exposure, determines the ability of the protective compound to induced survival and that once a pro-apoptotic threshold is reached, salubrinal is not able to reverse it.

Consistent with the *in vitro* and *in vivo* data showing that inhibition of eIF2α dephosphorylation preserves osteoblast viability, treatment with salubrinal reversed the inhibition in BFR induced by low dose of GC mainly by reversing the decrease in MS/BS. These findings together with the demonstration that salubrinal prevents the reduction in mineralization induced by GC *in vitro* strongly suggest that the preservation of bone

mineral density by salubrinal is due to its protective effects on osteoblasts. In contrast, alendronate further reduced BFR in GC treated animals, as expected due to its potent inhibitory effects on osteoclasts and resorption. Salubrinal, like alendronate, has been also shown to inhibit osteoclastogenesis (75) and to protect from ovariectomy-induced bone loss (76). However, in the setting of GC excess, the main mechanism of salubrinal action appears to be related to osteoblasts. Thus, the bone sparing actions of salubrinal and bisphosphonates on GC excess are mediated by distinct cellular mechanisms. Whereas alendronate inhibits osteoclast activity and reduces bone turnover, salubrinal preserves the viability and the bone forming function of osteoblasts.

Protein misfolding is a common feature of several human diseases including neurodegenerative conditions such as Alzheimer's and Parkinson's diseases, as well as type 2 diabetes (77). Lack of functional PERK, the sensor of the unfolded protein response and a major eIF2α kinase, causes the Wolcott-Rallison syndrome (WRS) in humans, which characterized by early onset diabetes and aberrant skeletal development (78). PERK deletion in the mouse prevents the unfolded protein response induced by ER stressors and inhibits phosphorylation of eIF2α (79). Homozygous PERK null mice are born normal but loose β cells rapidly and develop early diabetes (80). As with WRS patients, PERK knockout mice develop skeletal dysplasia and defective bone mineralization (81). Osteoblast and osteocyte number, mineral apposition rate MAR, and markers of osteoblasts and osteocytes are decreased in PERK null mice. Osteoblast survival appears not to be affected *in vitro,* albeit *in vivo* studies were not shown. Together with the current study in which increased osteoblast and osteocyte apoptosis, decreased bone formation, and decreased bone mass induced by glucocorticoids are partially prevented by salubrinal, these findings suggest that inhibition of eIF2α dephosphorylation is a potential novel target for the treatment of glucocorticoid-induced

18

osteoporosis and other conditions with deficient osteoblast differentiation and bone mineralization.
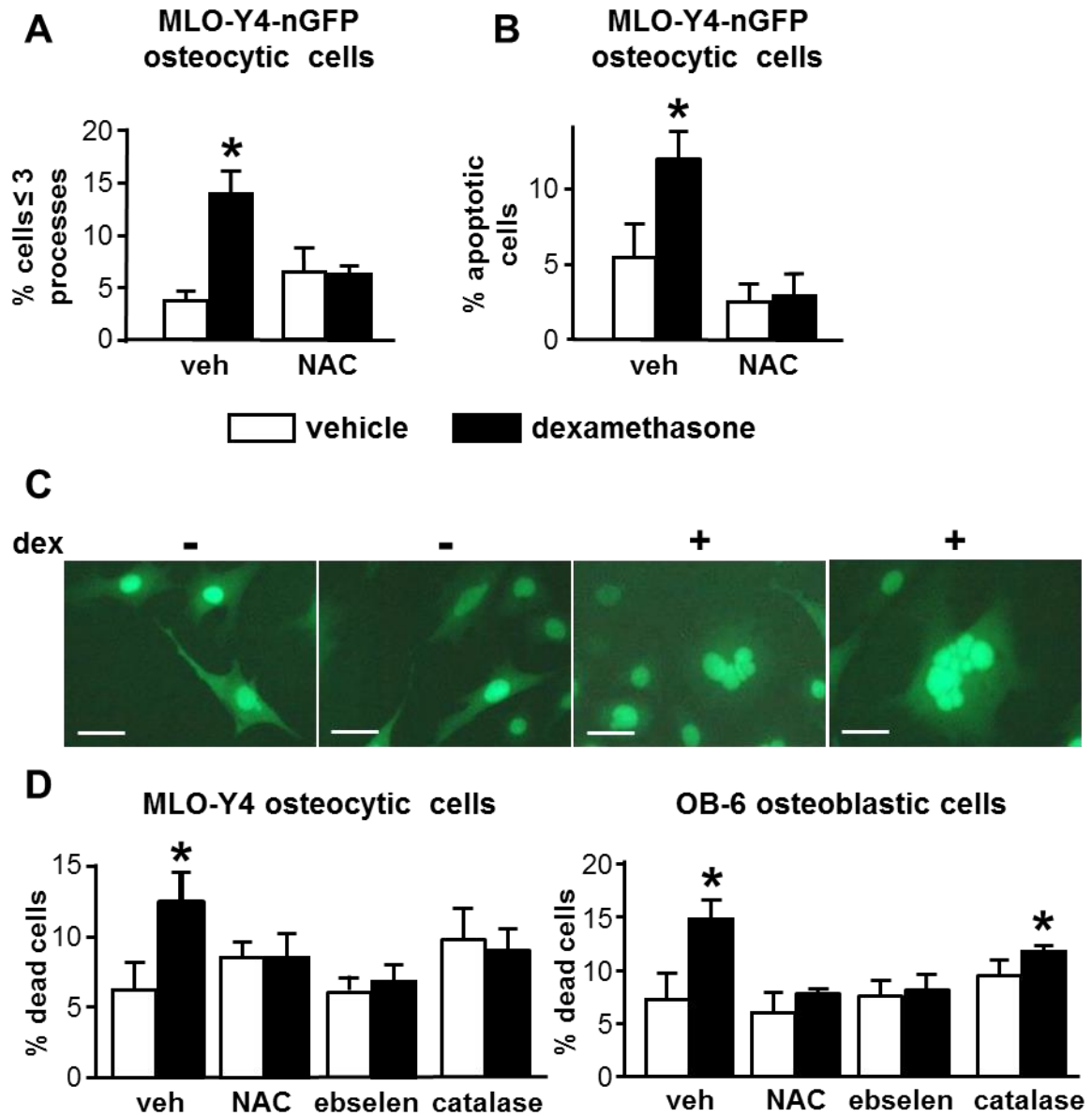
Acknowledgments

Figure 2-1. Glucocorticoid-induced apoptosis of osteocytic and osteoblastic cells is prevented by inhibiting ROS generation. (A-D) Cells were exposed to vehicle (ethanol) or dexamethasone for 6 hours. **(A)** Quantification of cytoplasmic retraction in stably transfected nGFP MLO-Y4 cells treated with or without NAC for 1 hour prior to addition of dexamethasone. **(B)** Apoptosis quantification of nGFP-transfected MLO-Y4 cells. **(C)** Representative images of nGFP-expressing MLO-Y4 osteocytic cells treated with vehicle or dexamethasone showing changes in cell morphology, chromatin

condensation, and nuclear fragmentation. Lines correspond to 200 µm. **(D)** Quantification of cell death in MLO-Y4 osteocytic or OB-6 osteoblastic cells with or without pretreatment of the indicated anti-oxidant agent, assessed by trypan blue uptake. Bars represent the means ± SD of N=3 independent wells/treatment. *p<0.05 vs. the corresponding vehicle-treated cells, by one-way ANOVA.

A

MLO-Y4 osteocytic cells

6h

24h

vehicle salubrinal

B
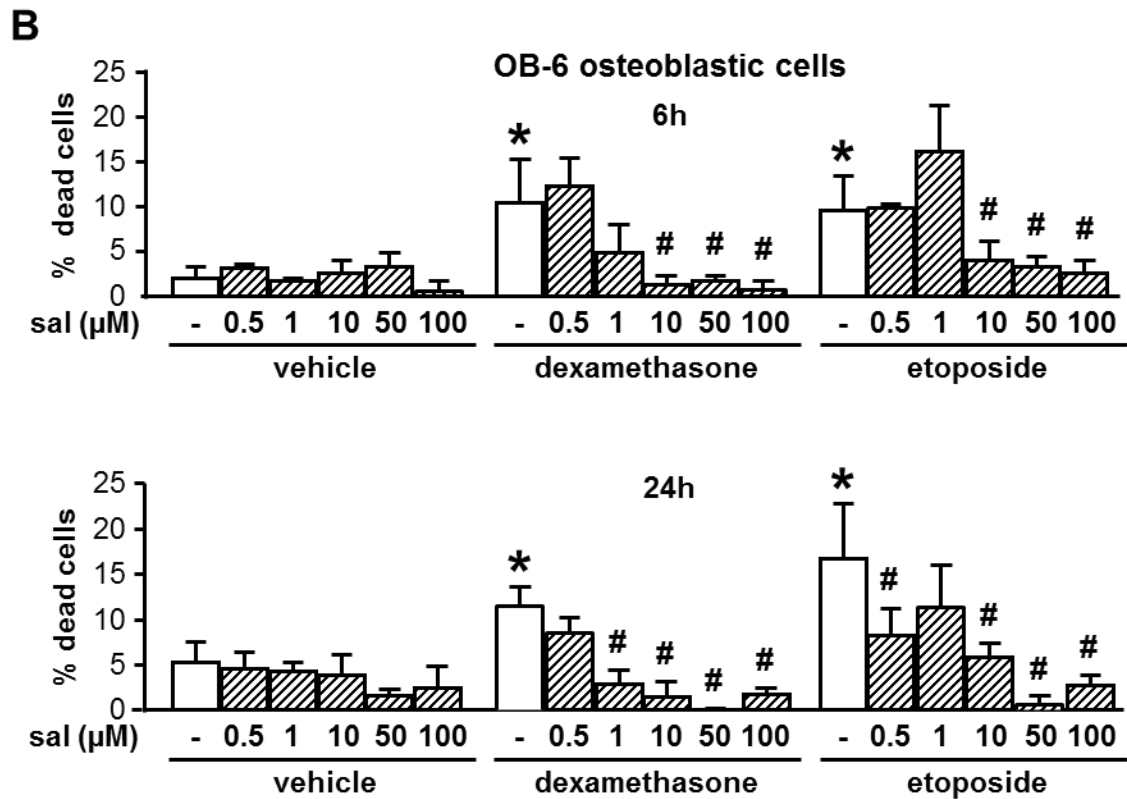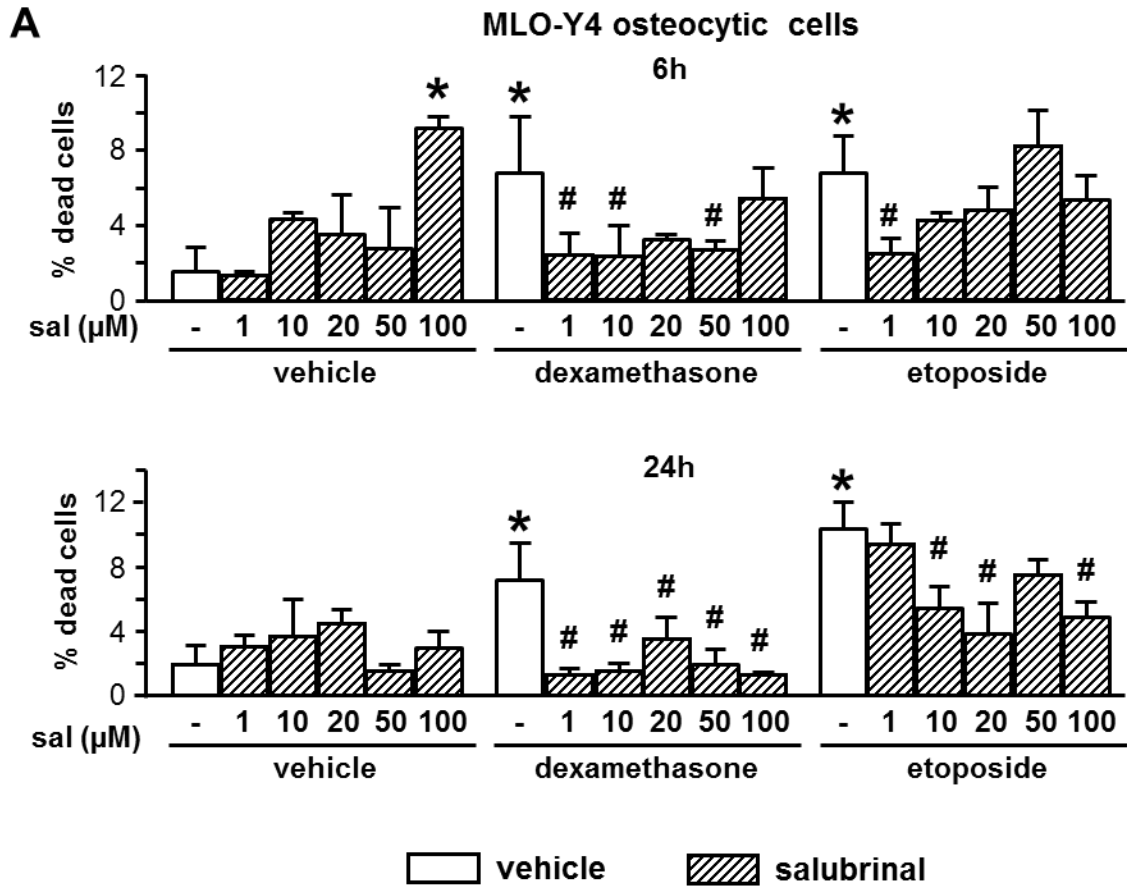
OB-6 osteoblastic cells

6h

24h

23

Figure 2-2. Protection against ER stress with salubrinal prevents dexamethasone and etoposide induced apoptosis of osteocytic MLO-Y4 and osteoblastic OB-6 cells. Cell death quantification in MLO-Y4 osteocytic **(A)** or OB-6 osteoblastic **(B)** cells treated with or without salubrinal prior to addition of vehicle, dexamethasone, or etoposide, assessed by trypan blue uptake. Bars represent the means ± SD of N=3 samples per treatment. *$p < 0.05$ vs. cells treated with vehicle without salubrinal and #$p < 0.05$ vs. corresponding apoptotic agent without salubrinal for each time point, by one-way ANOVA.
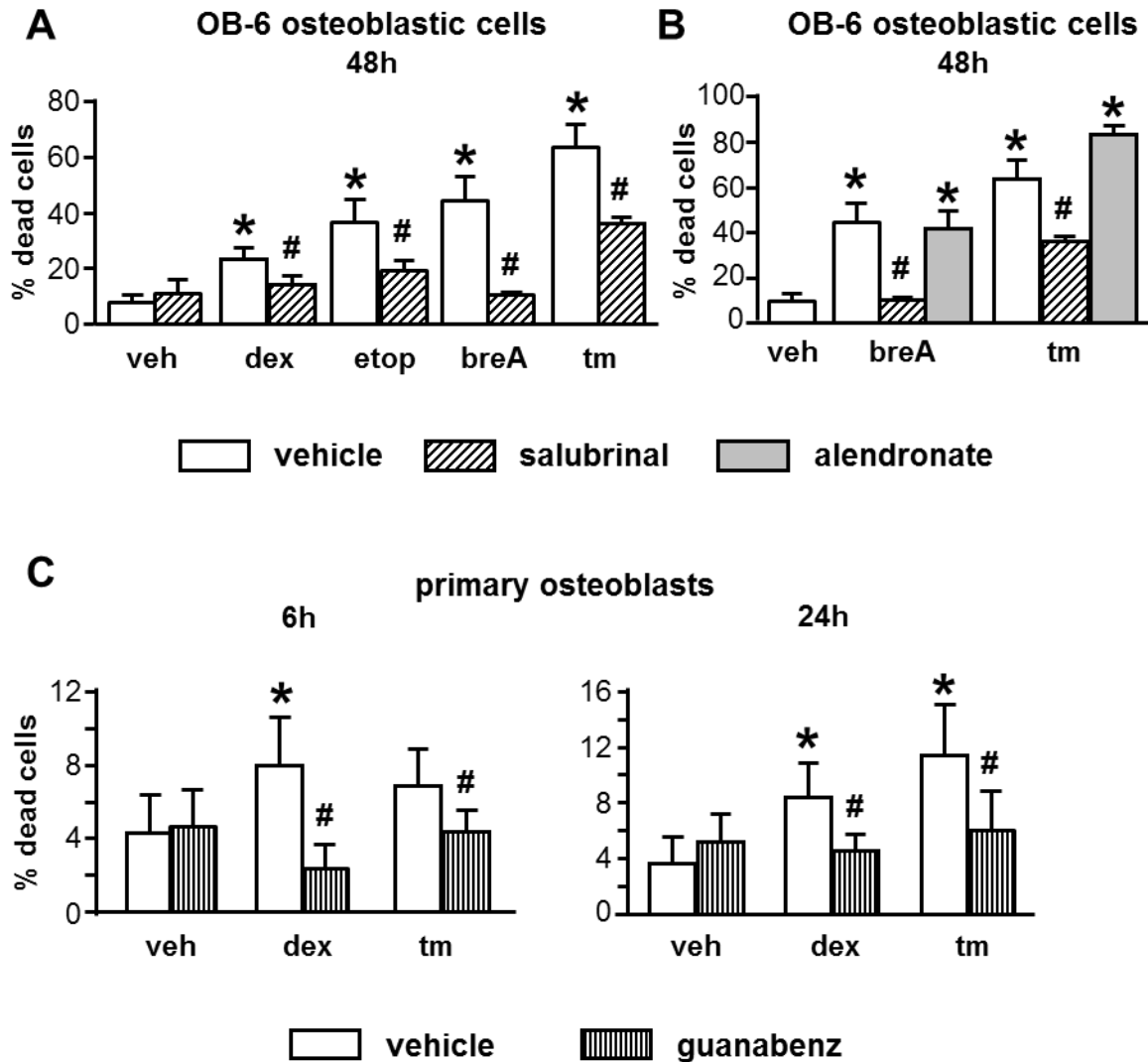
Figure 2-3. Salubrinal or guanabenz protects from apoptosis induced by dexamethasone, etoposide, and ER stressors in osteoblastic cells. Cell death quantification in OB-6 osteoblastic **(A** and **B)** or primary osteoblastic **(C)** cells treated with or without anti-apoptotic agents salubrinal, alendronate, or guanabenz prior to addition of dexamethasone (dex), etoposide (etop), brefeldin A (breA), tunicamycin (tm), or vehicle (veh). Bars represent the means ± SD of N=3 samples per group. *p<0.05 vs. veh-treated cells and #p<0.05 vs. corresponding apoptotic agent without designated eIF2α phosphatase inhibitor for each time point, by Student's *t*-test in **(A)** and **(C)** and by one-way ANOVA in **(B)**.
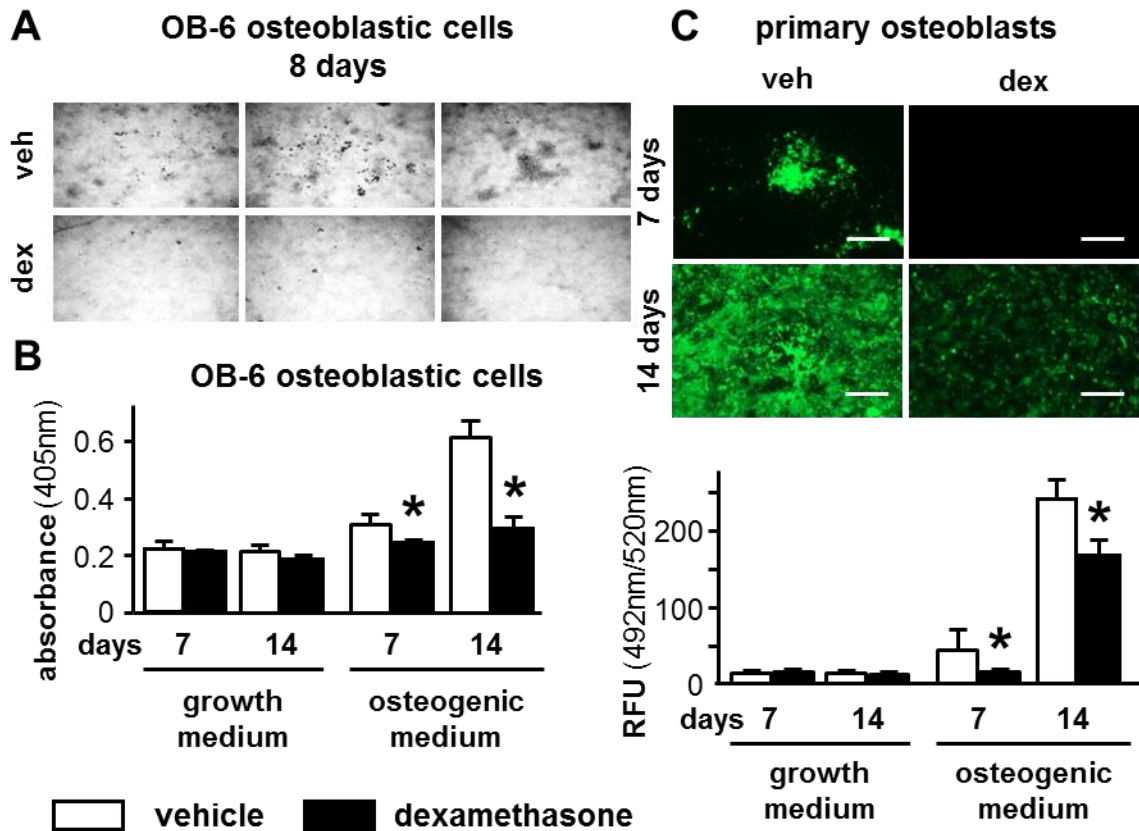
Figure 2-4. Glucocorticoid decreases matrix mineralization in cultures of osteoblastic cells and primary osteoblasts. (A and **B)** OB-6 osteoblastic cells cultured with or without dexamethasone (dex) and the degree of mineralization was assessed by von Kossa staining for 8 days **(A)** and by Alizarin Red S staining for 1 or 2 weeks **(B)**. **(C)** Calvaria-derived osteoblastic cells were cultured with or without osteogenic medium for 1 or 2 weeks together with vehicle (veh) or dexamethasone (dex) and mineralization was assessed using the OsteoImage Mineralization Assay Kit. Lines correspond to 200 μm. Bars represent the means ± SD of N=3 for **(A)** and **(B)**, N=6 for **(C)** samples per group. *p<0.05 vs. veh-treated cells in corresponding medium condition for each time point, by two-way ANOVA.

A OB-6 osteoblastic cells
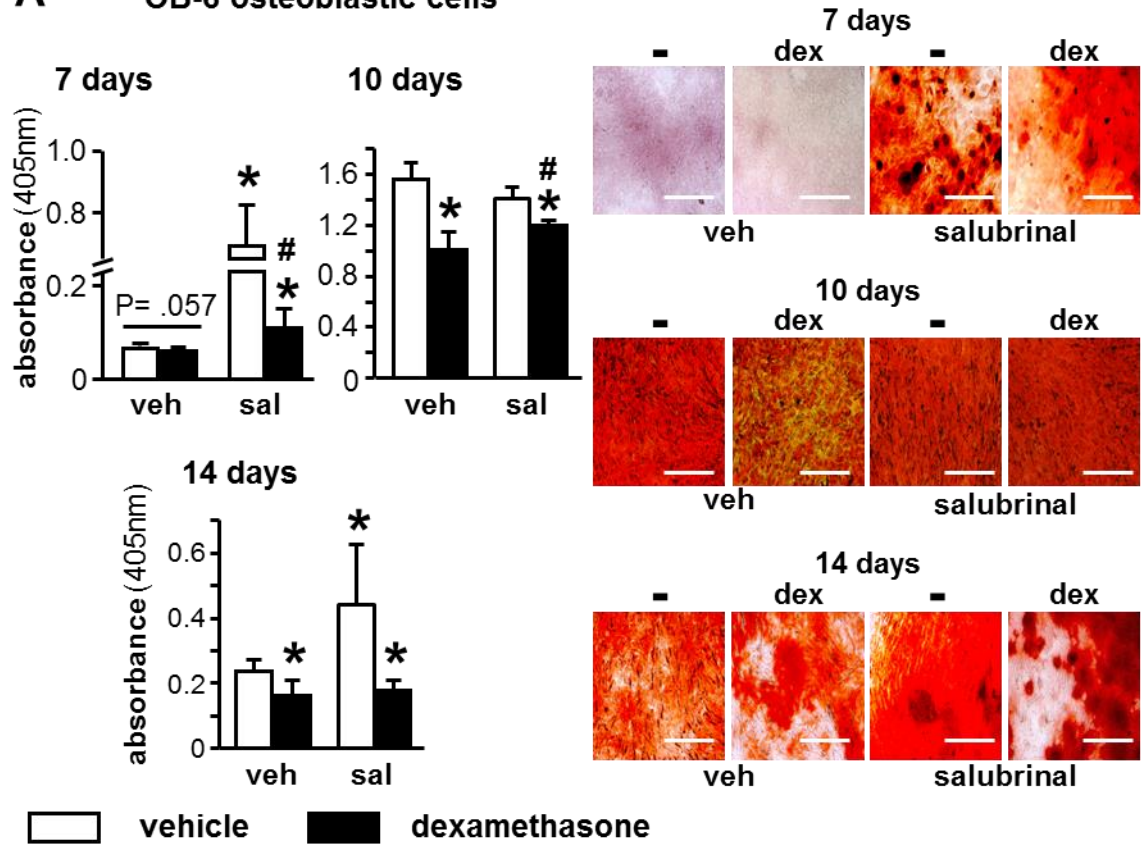
B OB-6 osteoblastic cells
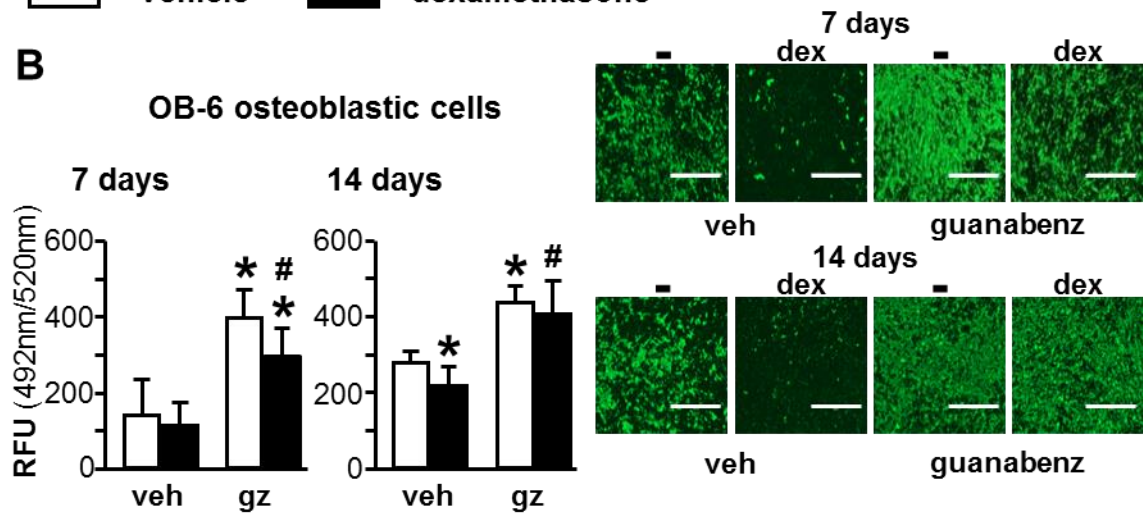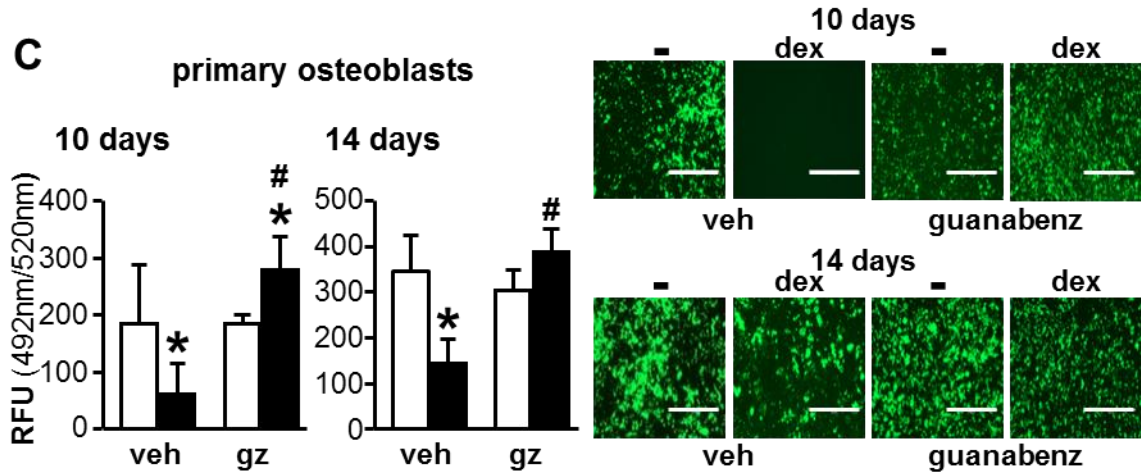
Figure 2-5. Salubrinal and guanabenz ameliorate the inhibitory effects of GC on matrix mineralization. (A) Mineralization was determined in vehicle (veh) or dexamethasone (dex) treated differentiated OB-6 cells without (control) or with salubrinal (sal) pre-treatment for 7, 10, and 14, days by Alizarin Red S staining. **(B)** and **(C)** quantification of mineralization in OB-6 **(B)** and calvaria-derived **(C)** osteoblastic cells treated with vehicle or dexamethasone with or without guanabenz (gz) for the indicated incubation periods. Hydroxyapatite accumulation was measured by OsteoImage Mineralization Assay Kit. Lines correspond to 400 µm. Bars represent the means ± SD of N=3 for **(A)** and N=12 for **(B-C)**. *p<0.05 vs. veh-treated control cells and #p<0.05 vs. dex-treated control cells, by one-way ANOVA.

A apoptosis

vehicle salubrinal alendronate

cancellous osteoblasts   cancellous osteocytes   cortical osteocytes

B BMD

total   spine   femur

C bone formation

MS/BS   MAR   BFR/BS

vehicle   salubrinal

placebo   GC1   placebo   GC1
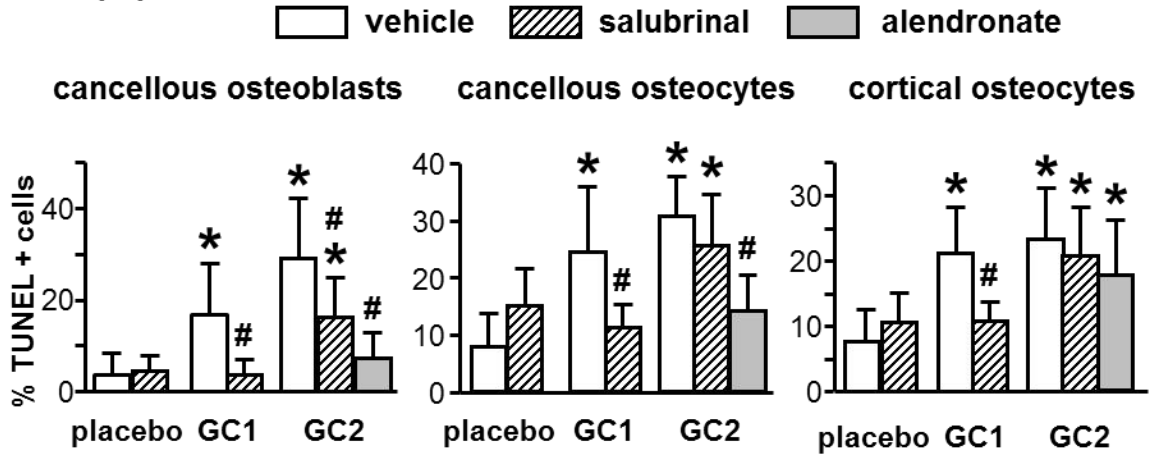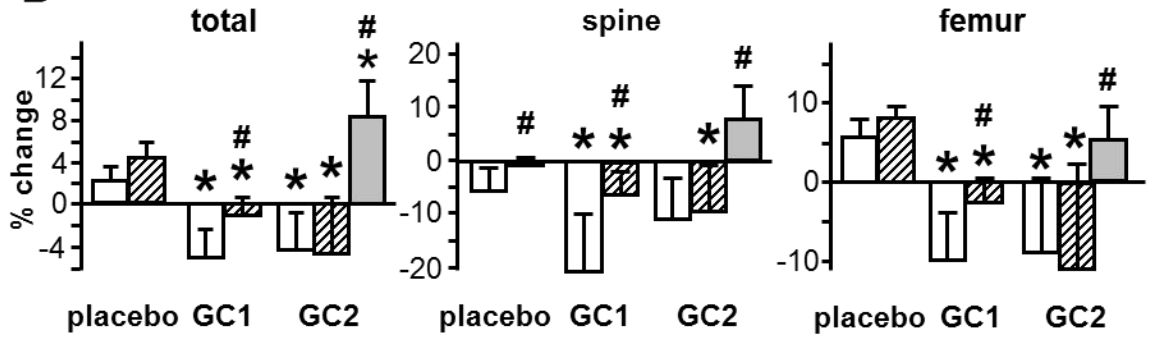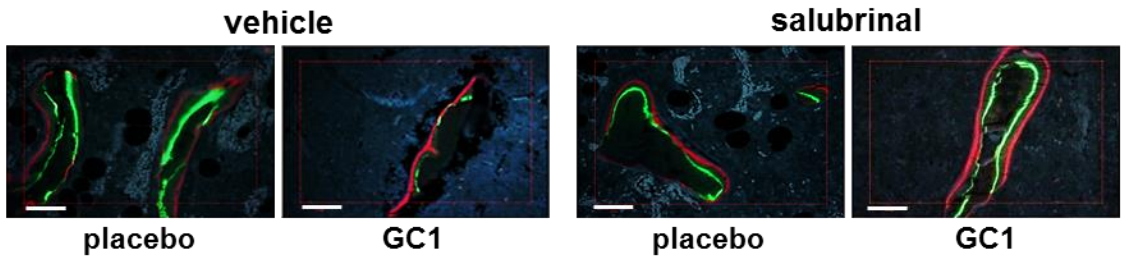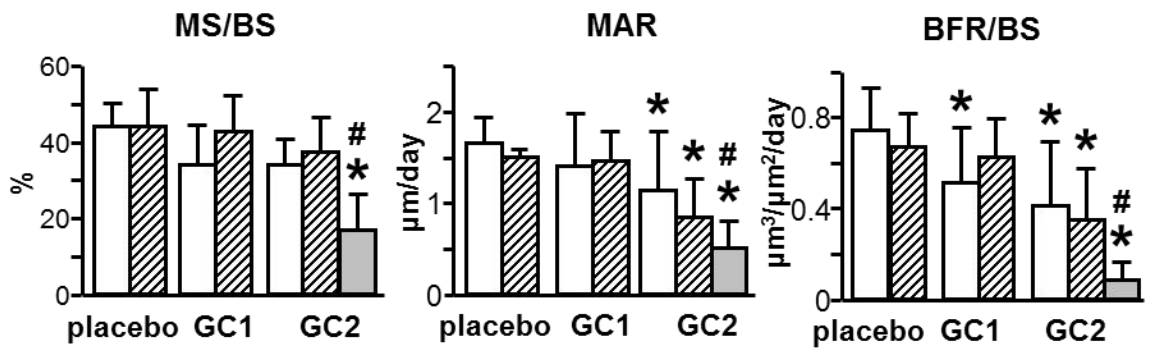
Figure 2-6. **Salubrinal protects against glucocorticoid-induced apoptosis and consequent bone loss *in vivo.* (A)** TUNEL and **(C)** dynamic histomorphometric data was obtained from longitudinal distal femur sections. Representative images of fluorochrome labeled bones are shown. Bars correspond to 50 µm. **(B)** BMD percent changes for placebo, 1.4 mg/kg/day prednisolone (GC1), or 2.1 mg/kg/day prednisolone (GC2) pellet implanted mice with or without salubrinal intervention were determined by DXA analysis. Bars represent the means ± SD of N=7-10 for **(A)** and **(C)** and N=6-10 for **(B)**. Statistical analysis for placebo, GC1, and GC2 treated mice treated with vehicle (control) or salubrinal was performed by two-way ANOVA. *$p < 0.05$ vs. placebo mice injected with vehicle (control) or salubrinal. #$p < 0.05$ vs. corresponding GC treated mice injected with vehicle (control). The effect of alendronate on GC2 treated mice was analyzed by comparing placebo, GC2, and GC2 plus alendronate by one-way ANOVA. *$p < 0.05$ vs. placebo mice injected with vehicle (control) and #$p < 0.05$ vs. GC2 treated mice injected with vehicle (control).

Chapter 3

Protection from glucocorticoid-induced osteoporosis by anti-catabolic signaling

in the absence of Sost/sclerostin

Introduction

Excess of glucocorticoids, either endogenously or iatrogenically-induced, leads to loss of bone and is one of the leading causes of increased bone fragility worldwide (82). Glucocorticoids, produced and released by the adrenal glands in response to biological stress, regulate numerous physiological processes in a wide range of tissues (3;4). Exaggerated production of glucocorticoids is found in patients with pituitary tumors producing adrenocorticotrophin hormone (ACTH) (Cushing's disease), or exhibiting Cushing's syndrome due to ectopic ACTH production or autonomous adrenal production of cortisol. Further, glucocorticoid action progressively increases with age due to elevated hormonal adrenal secretion as well as conversion of inactive to active metabolites catalyzed by 11β-hydroxysteroid-dehydrogenase 1 in target tissues. In addition, glucocorticoids are extensively used for the treatment of immune and inflammatory conditions including rheumatoid arthritis, for the management of organ transplantation, and as components of chemotherapy regimens for hematological cancers including multiple myeloma. Both endogenous and pharmacologic increase in glucocorticoid levels are associated with severe adverse side effects manifested in several tissues and organs, in particular the skeleton (10-14). Prolonged treatment with glucocorticoids leads to a dramatic loss of bone mineral and strength in cortical and cancellous bone, and increases atraumatic fractures in approximately 30-50% of patients (2;9;16-19). Excess glucocorticoids also causes muscle weakness with the consequent loss of body balance and increased falls, which in turn contribute to elevate the risk of bone fractures (10). It is estimated that 4.4 million individuals in United States and United Kingdom are chronically treated with oral glucocorticoids (10;83) and the use of these agents extends worldwide.

Human and animal studies demonstrate that the mechanism of glucocorticoid-induced osteoporosis involves increased bone resorption, decreased bone formation,

and increased apoptosis of osteocytes and osteoblasts, which together contribute to bone weakness and elevated fracture risk (2;9;17-19;24-28). There is a rapid, early bone loss ascribed to both prolongation of life span of preexisting osteoclast and increased generation of new osteoclasts (24;30;31). This initial phase is followed by a less pronounced chronic bone loss associated with reduction of osteoblasts and osteoclasts and low bone remodeling, due to reduced synthetic activity of osteoblasts through downregulation of critical genes, including osteocalcin (OCN), increased osteoblast apoptosis, and reduced generation of osteoclasts resulting from the loss of supporting cells (2;9;82).

The Wnt/β-catenin pathway has a critical role in the control of bone acquisition and maintenance. Wnt/β-catenin signaling is activated by ligands of the Wnt family that bind to frizzled receptors and co-receptors, and also by downregulation of antagonists, including Dkk1 and Sost/sclerostin (84). Human mutations responsible for high bone mass conditions, including gain-of-function of the LRP5 Wnt co-receptor (OMIM603506.0013), loss of expression of the Sost/sclerostin inhibitor in Van Buchem disease (OMIM239100) and sclerosteosis type 1 (OMIM269500), and loss-of-function of the sclerostin chaperone LRP4 in sclerosteosis type 2 (OMIM614305), demonstrate that activation of the Wnt/β-catenin pathway is linked to increased bone formation and bone gain (85-87). In addition, genetic manipulation of β-catenin, the mediator of the canonical Wnt pathway, affects bone resorption due to regulation of the expression of osteoprotegerin (OPG), the decoy receptor for RANKL, receptor activator of nuclear factor kappa B ligand, demonstrating that this pathway is also linked to resorption (88;89). Therefore, the Wnt/β-catenin signaling cascade can regulate bone mass by both bone anabolic and anti-catabolic mechanisms. Further, activation of Wnt/β-catenin signaling promotes osteoblast and osteocyte survival (90). Based on these pieces of evidence, we investigated whether activation of Wnt/β-catenin signaling in female mice

lacking Sost/sclerostin opposes glucocorticoid-induced loss of bone mineral and strength, and examined the cellular and molecular mechanisms involved.

Materials and Methods

Mice and tissue procurement. Four-month-old female Sost^{-/-} mice of C57BL/6 background generated by Li et al. 2008 (91) or wild type (WT) littermate controls, 10 mice per group, were implanted with 90 day slow-release pellets delivering placebo, 1.4 mg/kg/day (GC1), or 2.1 mg/kg/day (GC2) prednisolone (Innovative Research of America) while under anesthesia. Previous studies showed that these doses reproduce in the mouse the hallmarks of glucocorticoid-induced osteoporosis and are equivalent to medium and high therapeutic glucocorticoid doses in humans (41;52). Moreover, the C57BL/6 mouse is a reliable and reproducible model for glucocorticoid-induced skeletal deterioration, as demonstrated by consistent decreases in BMD, reduction in bone formation, and increased osteoblast/osteocyte apoptosis (26;41). Mice were injected 10 and 3 days prior to sacrifice with 0.6% calcein and 1.0% alizarin red solutions, respectively. Twenty-eight days after pellet implantation mice were sacrificed. Bones and muscles were dissected. Bones were processed as indicated below. Wet weight of indicated muscles from both hind limbs was taken and averaged for each mouse. Analysis was performed in a blinded fashion.

BMD measurement and micro-CT analysis. BMD of the total body excluding the head and the tail, the lumbar spine (L1-L6), and the femur, and lean body mass were measured by dual energy X-ray absorptiometry (DXA) scanning by using a PIXImus II densitometer (G.E. Medical System, Lunar Division). Body weight and DXA measurements were performed 2-4 days before (initial) and 28 days (final) after pellet implantation (65;92). Mice were randomized to the experimental groups based on spine BMD. Percent changes in body weight, lean body mass, and BMD were calculated with the following formula: [(final–initial)/initial] multiplied by 100.

For micro-CT analysis, L6 vertebrae were cleaned of soft tissue, fixed in 10% buffered formalin, and stored in 70% ethanol until scanned at 6-µm resolution (Skyscan

1172, SkyScan). Measurements were done 60 µm away from the growth plates as previously described (93;94).

Serum biochemistry. Blood was collected 2 and 4 weeks after pellet implantation from the facial vein of 3-hour fasted mice. N-terminal propeptide of type I procollagen (P1NP), C-terminal telopeptides of type I collagen (CTX), and tartrate-resistant acid phosphatase form 5b (TRAP 5b) were measured using enzyme-linked immunosorbent assays (Immunodiagnostic Systems Inc.) (32;92). Alkaline phosphatase was measured on a Randox Daytona analyzer (Randox Laboratories Limited).

Quantitative PCR (qPCR). Total RNA extraction and qPCR were performed as previously reported (95). Briefly, total RNA was extracted from lumbar vertebrae L5, femur, *ex vivo* cultured bones, using TRIzol (Invitrogen). cDNA was synthesized by using high capacity cDNA reverse transcriptase kit (Applied Biosystems). Gene expression was analyzed using primer probe sets from Applied Biosystems or from Roche Applied Science. Relative mRNA expression levels were normalized to the housekeeping gene ribosomal protein S2 (Rplp2) by using the ΔCt method (94;95). Data are expressed as fold change, where the ratio between the gene of interest and the housekeeping gene for WT mice receiving placebo was considered as 1.

Bone histomorphometry and apoptosis analysis. L1-3 vertebrae were fixed in 10% neutral buffered formalin and embedded undecalcified in methyl methacrylate as previously described (28). Dynamic histomorphometry measurements were performed in 7-µm unstained bone sections under epifluorescence microscopy. Histomorphometric analysis was performed using OsteoMeasure high resolution digital video system (OsteoMetrics) interfaced to an Olympus BX51 fluorescence microscope (Olympus America Inc.) (66). Osteoclasts were quantified on lumbar vertebra L2 thin sections stained for tartrate-resistant acid phosphatase (TRAP) and counterstained with Toluidine Blue as previously published (32;92). An osteoclast was defined as a TRAP positive cell

attached to the bone surface with more than 1 nucleus. Apoptosis of osteoblasts and osteocytes was detected by the transferase-mediated biotin-dUTP nick end-labeling (TUNEL) reaction (Fisher) in undecalcified vertebral bone sections counterstained with 2% methyl green, mounted on silane-coated glass slides (Scientific Device Lab, Inc.), as previously described (28). The prevalence of apoptotic osteoblasts and osteocytes was calculated by enumerating the total number and TUNEL positive cells exhibiting condense chromatin, nuclear fragmentation or cell shrinkage.

Immunohistochemistry. The expression of sclerostin was visualized in paraffin-embedded femora from 5 month-old WT and Sost$^{-/-}$ mice 28 days after pellet implantation, as previously described (93;96). Sclerostin was visualized in deparaffinized sections of decalcified femora, treated with 3% H_2O_2 to inhibit endogenous peroxidase activity, blocked with serum, and then incubated with goat polyclonal anti-mouse sclerostin antibody (1:100; Abcam, catalog Ab63097) (92). Sections were then incubated with anti-goat biotinylated secondary antibody followed by avidin conjugated peroxidase (Vectastain Elite ABC Kit; Vectora Laboratories, catalog PK-6105). Color was developed with a diaminobenzidine substrate chromogen system (Dako Corp.). Cells expressing the protein of interest are stained in brown, whereas negative cells are green-blue.

Mechanical testing. Mechanical properties of L6 vertebrae were determined by axial compression after removal of vertebral processes and the cranial and caudal endplates. Vertebral bodies were loaded at a rate of 0.5 mm/min until failure (100P225 Modular Test Machine) as previously described (97;98). Structural properties were obtained from the load/displacement curves and material-level properties were calculated using published equations to normalize to vertebral height, cross-sectional area, and bone volume (46).

Ex vivo cultures. Femoral and tibial long bones were harvested from WT and Sost$^{-/-}$ mice, and then maintained in α-MEM containing 10% FBS and 1% penicillin/streptomycin for 24 hours. Bones were treated with 1 µM dexamethasone or vehicle (ethanol) with or without an anti-sclerostin antibody (99) (10µg/mL; Acris Antibodies, catalog AP13235PU-N) or vehicle (PBS) for 6 hours. mRNA was isolated and gene expression was measured by qPCR, as indicated above.

Mineralization assay. Primary osteoblastic cells were isolated from the neonatal calvarial bones of C57BL/6 mice, Sost$^{-/-}$, or WT littermate control mice, and plated at 5000 cells/cm^2 density in MEM Alpha medium with 10% fetal bovine serum and 1% penicillin/streptomycin as previously described (41;60). Osteogenic medium was used after cultures reached confluence consisting of 50µg/ml ascorbic acid and 10mM β-glycerophosphate and treated with 1µM dexamethasone or the corresponding vehicle (ethanol). Medium was replaced every 2-3 days, and mineralization was visualized using the OsteoImage Mineralization Assay Kit (Lonza), and then quantified by microplate reader for 492/520 nm excitation/emission fluorescence.

Statistical analysis. Data are expressed as means ± standard deviations (SD). Sample differences were evaluated using SigmaPlot 12.0 (Systat Software Inc.). Data of the *in vivo* experiments were analyzed by two-way ANOVA using genotype and treatment as independent variables. When ANOVA detected a significant interaction between the variables or a significant main effect of genotype, a post-hoc test was used to determine the significance of the effect of the treatment within each genotype. The only exception was the analysis of the mechanical testing data in which one-way ANOVA for each genotype using treatment as independent variable was used, because the marked differences between WT and Sost$^{-/-}$ mice in these parameters precluded the detection of the effect of glucocorticoids when two-way ANOVA was used. All Pairwise Multiple Comparison Procedures within one- or two-Way ANOVA tests using the Tukey

method were utilized to detect genotype and/or treatment differences. Results of the ANOVA and post-hoc test are presented in the Supplementary Information online at jbmr2869-sup-0001-SuppData-S1.docx. Data of the *in vitro* experiments were analyzed by two-tailed Student's *t*-test. Data of the *ex vivo* experiments, in which bones from each leg of the same mouse were treated with vehicle or dexamethasone, were analyzed by paired *t*-test. Means were considered significantly different at $p < 0.05$.

   Study approval. All animal procedures were approved by the Institutional Animal Care and Use Committee of Indiana University School of Medicine, and animal care was carried out in accordance with institutional guidelines.

Results

Sost^{-/-} mice are protected from bone loss and decreased bone strength induced by glucocorticoids, but not from the loss of muscle mass. Mice lacking the osteocyte-derived antagonist of Wnt/β-catenin signaling Sost/sclerostin (Sost^{-/-} mice) displayed high bone mass and strength compared to wild type (WT) littermate controls (**Figure 3-1**), consistent with earlier reports (91). Glucocorticoid administration at two different doses of prednisolone (GC1=1.4 or GC2=2.1 mg/kg/day) significantly decreased total and spinal BMD (**Figure 3-1A**), cancellous bone trabecular thickness (Tb.Th.), cortical bone area (BA/TA) in lumbar vertebra of WT mice (**Figure 3-1B** and **C**), although no changes in cancellous BV/TV were detected. The high GC does also decreased cortical thickness (Ct.Th.). The decreased thickness of cortical bone was driven by thinning of the dorsal surface. Glucocorticoid excess also reduced the mechanical properties of WT bones, at both the structural level (ultimate force and energy to ultimate load) and at the material level (toughness), although modulus and ultimate stress were not altered (**Figure 3-1D**). In contrast, Sost^{-/-} mice were protected from glucocorticoid-induced decrease in bone mass, changes in bone architecture in cancellous and cortical sites, as well as the reduction in bone strength (**Figure 3-1**). Ultimate stress is an estimate of the strength of the material – calculated as ultimate force normalized by the amount of bone. Therefore, the lack of changes in ultimate stress by glucocorticoids in either genotype indicates that the decrease in ultimate force is driven by structural changes as opposed to changes in tissue properties (such as mineralization or collagen alterations).

The protection from loss of tissue mass by Sost/sclerostin deficiency was specific to bone, since Sost^{-/-} mice exhibited glucocorticoid-induced sarcopenia similar to WT mice (**Figure 3-2**). Thus, both WT and Sost^{-/-} mice treated with prednisolone displayed decreased lean body mass, an index of skeletal muscle mass, with a loss of 6-9% in lean body mass over the 4 week-treatment (**Figure 3-2A**). In addition, the weight of the

fast twitch type II dominated muscles from glucocorticoid-treated mice of both genotypes was equally decreased about 22-23% and 13-15% for gastrocnemius and tibialis anterior, respectively (**Figure 3-2B**). On the other hand, glucocorticoids did not decrease in either genotype the weight of the slow twitch type I dominated soleus muscle, a muscle type shown to be less sensitive to the action of the hormones (100). These changes in bone and muscle mass induced by glucocorticoids occurred in the absence of alterations in total mouse body weight (**Figure 3-2C**).

Sost/sclerostin deficiency does not prevent glucocorticoid-induced decrease in bone formation, increase in osteoblast/osteocyte apoptosis, or reduced mineral deposition. Consistent with the recognized bone anabolism induced by Wnt/β-catenin activation, Sost$^{-/-}$ mice exhibited increased bone formation indexes at the tissue level (mineralizing surface, MS/BS; mineral apposition rate, MAR; and bone formation rate, BFR/BS) and in the circulation (procollagen type 1 N terminal propeptide, P1NP; and alkaline phosphatase, ALP); as well as increased mRNA expression in bone of the osteoblast marker osteocalcin, OCN (**Figure 3-3A-D**).

In spite of the elevated bone formation exhibited by the Sost deficient mice under basal conditions, glucocorticoids decreased MAR and BFR/BS to a similar extent compared to placebo in WT and Sost$^{-/-}$ mice (**Figure 3-3A**). Specifically, BFR/BS was reduced by about 30-40% in both WT and Sost$^{-/-}$ mice. Further, circulating P1NP and ALP were decreased by glucocorticoids in both genotypes at 2 weeks (**Figure 3-3B** and **C**). In addition, glucocorticoids reduced P1NP in the Sost$^{-/-}$ mice. In addition, glucocorticoids markedly decreased OCN expression in bones from both WT and Sost$^{-/-}$ mice (**Figure 3-3D**). Further, both WT and Sost$^{-/-}$ mice receiving prednisolone exhibited high prevalence of osteoblast and osteocyte apoptosis in cancellous and cortical bone (**Figure 3-3E**), consistent with the relationship between decreased bone formation and promotion of osteoblast (and osteocyte) apoptosis by glucocorticoids (26;28;52).

41

Moreover, addition of the glucocorticoid dexamethasone to cultured primary calvarial osteoblasts decreased mineral deposition in cells isolated from WT or Sost$^{-/-}$ mice (**Figure 3-3F**).

Sost/sclerostin deficiency prevents glucocorticoid-induced increase in bone resorption. Sost$^{-/-}$ mice exhibited overall unremarkable changes in osteoclasts and resorption compared to WT mice under basal conditions (**Figure 3-4**). Compared to WT mice, Sost deficient mice showed no differences in osteoclast surface (Oc.S/BS), blood bone resorption marker C-terminal telopeptide fragments of type I collagen (CTX) at 4 weeks or osteoclast marker tartrate-resistant acid phosphatase 5b (TRAP5b) at 2 and 4 weeks; and only a minor decrease in osteoclast number (N.Oc/BS) at 4 weeks and a transient increase in CTX at 2 weeks. Further, glucocorticoids increased osteoclast number (N.Oc/BS) and surface (Oc.S/BS) and raised CTX and TRAP5b circulating levels in WT mice. In contrast, glucocorticoids failed to do so at any dose or time point in Sost$^{-/-}$ mice.

Glucocorticoids differentially alter the anti-catabolic versus anabolic/survival molecular signature of the Wnt/β-catenin pathway in a Sost/sclerostin-dependent manner. Treatment with glucocorticoids increased Sost mRNA and the prevalence of sclerostin positive osteocytes in WT mice; and, as expected, Sost or sclerostin expression was not detectable in bones from Sost$^{-/-}$ mice (**Figure 3-5A** and **B**). Consistent with the recognized antagonistic function of Sost/sclerostin on Wnt/β-catenin activation, glucocorticoids decreased the expression of several target genes of the pathway, including OPG, Cx43, BMP4, cyclin D1, Axin2, and Smad6 in WT mice (**Figure 3-5C**). However, glucocorticoids only decreased the expression of a set of these genes in Sost$^{-/-}$ mice, suggesting that sustained activation of Wnt/β-catenin signaling due to Sost/sclerostin deficiency only partially opposes glucocorticoid effects on gene expression. Overall, similar patterns of expression were found in bones from the

appendicular (femur) and axial (lumbar vertebra) skeleton. Specifically, glucocorticoids decreased the expression of cyclin D1, Smad6, and Axin2 in both WT and Sost^{-/-} mice. In contrast, they decrease the expression of OPG, Cx43, and BMP4 only in WT mice. Increased cyclin D1 is associated with bone anabolism and anti-apoptosis (94;101-103); and increased OPG is responsible for inhibition of osteoclast formation and resorption (88;89;104). Thus, whereas glucocorticoids oppose all Wnt/β-catenin signaling in the presence of Sost/sclerostin, the hormones only oppose signaling associated with bone formation/survival in the absence of Sost/sclerostin.

Genetic or pharmacologic activation of Wnt/β-catenin signaling blocks downregulation of OPG expression induced by glucocorticoids. The lack of downregulation of OPG in Sost^{-/-} mice (**Figure 3-5C**) resulted in lower RANKL/OPG ratio in prednisolone-treated Sost^{-/-} mice compared to WT mice (**Figure 3-6A**). The differential regulation of OPG in WT and Sost^{-/-} mice was due to direct action of glucocorticoids on osteocytes as evidenced in *ex vivo* cultures of bones enriched in osteocytes. Genetic deletion of Sost or pharmacologic inhibition of sclerostin with the neutralizing antibody in *ex vivo* bone organ cultures mimicked the *in vivo* regulation of OPG in Sost^{-/-} mice. Thus, glucocorticoids increased Sost and decreased OPG expression, resulting in increased RANKL/OPG ratio in cultured bones from WT mice (**Figure 3-6B** and **C**). In contrast, bones from Sost^{-/-} mice were protected from glucocorticoid-induced decrease in OPG and increase in RANKL/OPG ratio (**Figure 3-6B**). Similarly, glucocorticoids failed to decrease OPG and increase the RANKL/OPG ratio in WT bones in which sclerostin function was blocked with an anti-sclerostin antibody (Scl-Ab), even when Sost mRNA expression was still increased by glucocorticoids (**Figure 3-6C**). RANKL expression was not consistently regulated by glucocorticoids either *in vivo* or *ex vivo* (**Figure 3-6**), demonstrating that OPG expression is responsible for the differential regulation of the RANKL/OPG ratio observed in the presence or absence of Sost/sclerostin deficiency.

Discussion

Glucocorticoid-induced osteoporosis is a leading cause of bone fragility worldwide and better therapies are critically needed. This study provides insights into novel mechanisms of glucocorticoid action and the cellular and molecular basis by which activation of Wnt/β-catenin signaling interferes with the detrimental effect of glucocorticoid excess in bone, but not in muscle, using *in vivo*, *ex vivo*, and *in vitro* approaches.

We report that glucocorticoids hinder the expression of target genes of the Wnt/β-catenin pathway, regardless of whether they are associated with bone anabolism (i.e. bone gain) or anti-catabolism (i.e. inhibition of bone loss). Glucocorticoids exert this action, in part, by increasing the expression of Sost/sclerostin, the osteocyte-derived Wnt/β-catenin antagonist and potent inhibitor of bone formation. Future investigations are warranted to determine whether this phenomenon is due to direct regulation of transcription of the Sost gene or whether is exerted through indirect mechanisms. Nevertheless, Sost/sclerostin deficiency protected against the loss of bone mass, deterioration of microarchitecture, and reduction of extrinsic/structural and intrinsic/material mechanical properties induced by glucocorticoids. Remarkably, however, the bone protective effect of Sost/sclerostin deficiency against glucocorticoids was not due to an opposing action to increase bone formation and maintain anabolic signaling. Instead, it was due to preservation of the Wnt/β-catenin anti-catabolic cellular and molecular signature (**Figure 3-7**). These results indicate that a pathway predominantly anabolic for bone is switched to anti-catabolic in the frame of glucocorticoid excess. Our findings suggest that therapeutic interventions activating Wnt/β-catenin signaling could effectively halt the high bone resorption responsible for the profound and rapid bone loss induced by glucocorticoids, which in humans can reach up to 12% during the first year of treatment (2).

Consistent with our current findings in skeletally mature Sost/sclerostin deficient mice, previous studies showed that pharmacologic inhibition of sclerostin with a neutralizing antibody opposed the lack of bone gain and the loss of strength induced by glucocorticoids in growing mice (105;106). Although it was proposed that these effects were due to preservation of osteoblast activity (106), mice treated with glucocorticoids and the anti-sclerostin antibody in these earlier studies exhibited lower circulating TRAP 5b (105) or CTX-1 (106), but still markedly reduced bone formation markers osteocalcin and P1NP (105), compared to the corresponding mice treated with glucocorticoids alone. Likewise, our *in vivo* studies show that sustained activation of the Wnt/β-catenin signaling in Sost deficient mice abolishes the increase in resorption induced by glucocorticoids but not the decreased bone formation. Moreover, our *ex vivo* results demonstrate that glucocorticoids are unable to decrease OPG and increase the RANKL/OPG ratio in bones from Sost$^{-/-}$ mice or in WT bones treated with an anti-sclerostin antibody. Taking together, these findings demonstrate that Sost/sclerostin deficiency, either genetic or pharmacologically achieved with the neutralizing anti-sclerostin antibody, maintains bone mass and strength in conditions of glucocorticoid excess by inhibiting bone resorption, through sustained anti-catabolic signaling driven by OPG.

In our mouse model of glucocorticoid-induced osteoporosis, the bone loss in this early phase is accompanied by both decreased bone formation and increased bone resorption, with the latter being the only one opposed by Sost/sclerostin deficiency. In view of the striking reduction in bone formation that remains in both genotypes, we speculate that during the second phase of glucocorticoid-induced osteoporosis that occurs with prolonged treatment and that is driven by reduced bone formation, bone loss could occur even in the Sost KO mice. Future investigations are warranted to address this issue.

Although bone mass, shape, and microarchitecture are the major recognized contributors to bone strength, accumulating evidence supports also an important role of osteocyte viability (26;32;107). Our findings demonstrate that Sost KO mice treated with glucocorticoids maintain structural and material mechanical properties despite of increased osteocyte apoptosis, highlighting the relative contribution of these factors. Evidently, the high bone mass and strong architecture exhibited by the Sost KO mice compensate for the bone weakening effects of increased osteocyte apoptosis under glucocorticoid excess.

A clinical case reported that glucocorticoids stop the exaggerated bone gain and reduced the high circulating P1NP in a patient with Van Buchem disease, a condition that results from lack of sclerostin expression and in which continuous bone anabolism causes life-threatening increased intracranial pressure (108). Prior to glucocorticoid intervention, the patient exhibited annual BMD gains of 4 to 9% in the lumbar spine and of 4 to 24% in the hip. Treatment with prednisone blunted the anabolic effect of Sost deficiency as evidenced by no gain in BMD after two years (-0.7% in lumbar spine and 0.4% in the hip). Our report showing that bone formation and Wnt/β-catenin anabolic signaling is still decreased in Sost/sclerostin deficient mice treated with glucocorticoids provides a mechanistic explanation for these clinical findings. Taken together with the current study, these pieces of evidence demonstrate that glucocorticoids oppose the effects of Sost/sclerostin deficiency on bone formation in both humans and mice.

Inhibition of resorption with bisphosphonates is the current standard of care for glucocorticoid-induced osteoporosis (2;10). These drugs protect from the loss of bone mass induced by glucocorticoids in animal models and patients. However, bone formation is decreased even further by bisphosphonates compared to glucocorticoids alone (14;32;40;41). Treatment with anti-RANKL antibodies induces even more pronounced reductions in bone formation compared to treatment with bisphosphonates

in patients receiving glucocorticoids (45). Profound reduction in bone turnover is not desirable since it leads to accumulation of microdamage and advanced glycation endproducts (AGEs), and the potential for developing osteonecrosis of the jaw with long-term treatments (42;43;46;47). Severe suppression of turnover by bisphosphonates can also lead to reduced toughness (42-44), the energy that bone tissue absorbs before failure, which in turn could be the cause of increased risk for low-energy atypical fractures (109;110). In contrast to purely antiresorptive agents, Sost deficiency confers high bone formation *per se*; thus, Sost deficient mice treated with glucocorticoids exhibit bone formation levels comparable to WT mice treated with placebo. Even when the reduction in P1NP induced by glucocorticoids in Sost KO mice is more severe than in WT mice, the reduced P1NP is similar to that of placebo-treated WT mice (Figure 3B). Similarly, the reduced bone formation exhibited by Sost KO mice treated with glucocorticoids is equivalent to bone formation in placebo-treated WT mice (Figure 3A). These findings suggest that Sost/sclerostin deficiency maintains tissue-level toughness by preserving modest amounts of bone formation while preventing glucocorticoid-induced increases in resorption. This mechanical finding points to a potential benefit compared to the current therapeutic approach to treat glucocorticoid-induced bone fragility.

Another unwanted consequence of excess glucocorticoids, either endogenous or iatrogenic, is muscle weakness; which reduces body balance and, when combined with lower bone mass, increases the risk of bone fractures. Due to their intimate association as a mechanical unit, changes in bone might impact skeletal muscle and vice versa. Our mouse model of glucocorticoid elevation faithfully reproduces the bone and skeletal muscle atrophy exhibited by humans. However, the bone preservation resulting from Sost/sclerostin deficiency in our studies did not protect from muscle atrophy; and conversely, the marked loss of muscle mass experienced by the Sost deficient mice did

not translate into apparent detrimental effects on bone volume or mechanical properties. These findings demonstrate that Sost/sclerostin deficiency protects exclusively bone, but not muscle, from the action of glucocorticoids, and show a lack of crosstalk between these two tissues in the frame of glucocorticoid-induced musculoskeletal atrophy. Future studies are warranted to investigate whether muscle-derived factors contribute to the low bone formation and high prevalence of osteoblast and osteocyte apoptosis still exhibited by Sost/sclerostin deficient mice treated with glucocorticoids. Nevertheless, more recent findings of ours showed that glucocorticoids induce bone and muscle atrophy by distinct mechanisms upstream of the atrophy-related E3 ligases atrogin1 and MuRF1 (111). Taken together with the current study, these findings support the contention that combination of bone- and muscle-specific therapeutic interventions might be required to interfere with the damaging actions of glucocorticoids in the musculoskeletal system.

We demonstrate that glucocorticoids differentially regulate anabolic/survival versus anti-catabolic Wnt/β-catenin signaling depending on the expression of Sost/sclerostin. Thus, whereas cyclin D1 is downregulated and bone formation is inhibited regardless of whether Sost is expressed or not, the decrease in OPG and increase in bone resorption is strictly dependent on Sost expression. The basis for this differential regulation of Wnt/β-catenin target genes by glucocorticoids remains unknown. However, glucocorticoids might regulate some of these genes by interfering with the Wnt/β-catenin pathway itself, whereas they might control other genes either directly by repressing the activity of their promoters or through regulation of alternative pathways including kinase signaling or induction of ROS/endoplasmic reticulum (ER) stress (41;54;55;103;112;113).

In closing, the current report demonstrates that the deleterious effects of glucocorticoids on the skeleton are linked to increased expression of the osteocyte-derived Wnt/β-catenin antagonist Sost/sclerostin and to downregulation of Wnt/β-catenin

target genes; and that Sost/sclerostin deficiency prevents glucocorticoid-induced osteoporosis by anti-catabolic, not anabolic, actions.

Acknowledgments

Figure 3-1. Sost^{-/-} mice are protected from bone loss and decreased bone strength induced by glucocorticoids. (A) Percent change in BMD for WT or Sost$^{-/-}$ mice treated with placebo, 1.4 mg/kg/d prednisolone (GC1), or 2.1 mg/kg/d prednisolone (GC2) for 28 days, measured by DXA. N=7-10. **(B)** Representative reconstructed micro-CT images of L6 vertebral cancellous bone (3D, top row) and cortical bone (2D, lower row). The dorsal surface of cortical bone for which thickness was also quantified is indicated by the gray boxes. **(C)** Bone volume/tissue volume (BV/TV), trabecular thickness (Tb.Th.), separation (Tb.Sp.), and number (Tb.N.), cortical bone area/total area (BA/TA), thickness of cortical bone (total Ct.Th.), and thickness of the dorsal surface of cortical bone (dorsal Ct. Th.) are shown. N=7-10. **(D)** Biomechanical properties were measured in vertebral bone (L6) by axial compression testing; N=6-9. Bars represent means ± SD. *$p<0.05$ vs. corresponding placebo-treated mice and #$p<0.05$ vs. placebo-treated WT mice, by two-way ANOVA; §$p<0.05$ vs. corresponding placebo-treated mice by one-way ANOVA, Tukey post-hoc test.

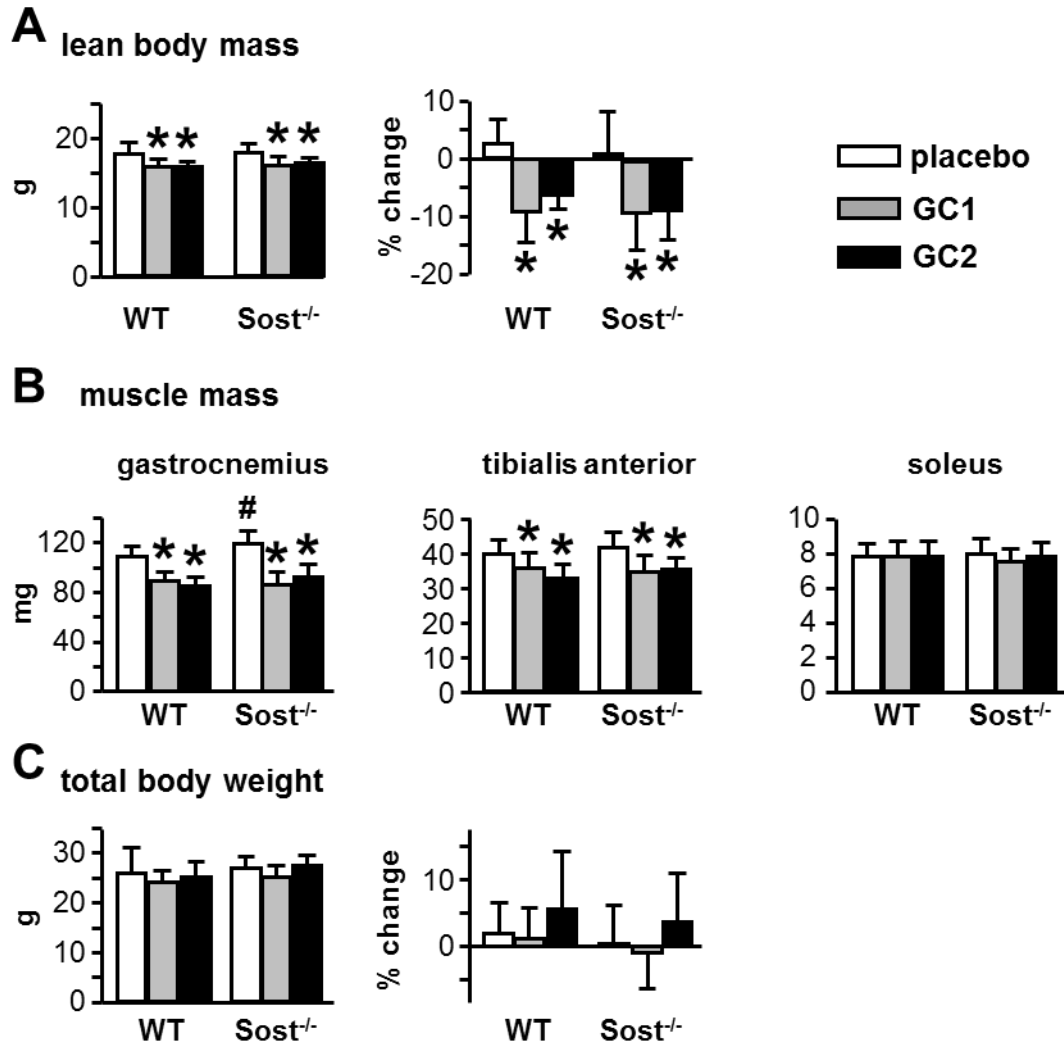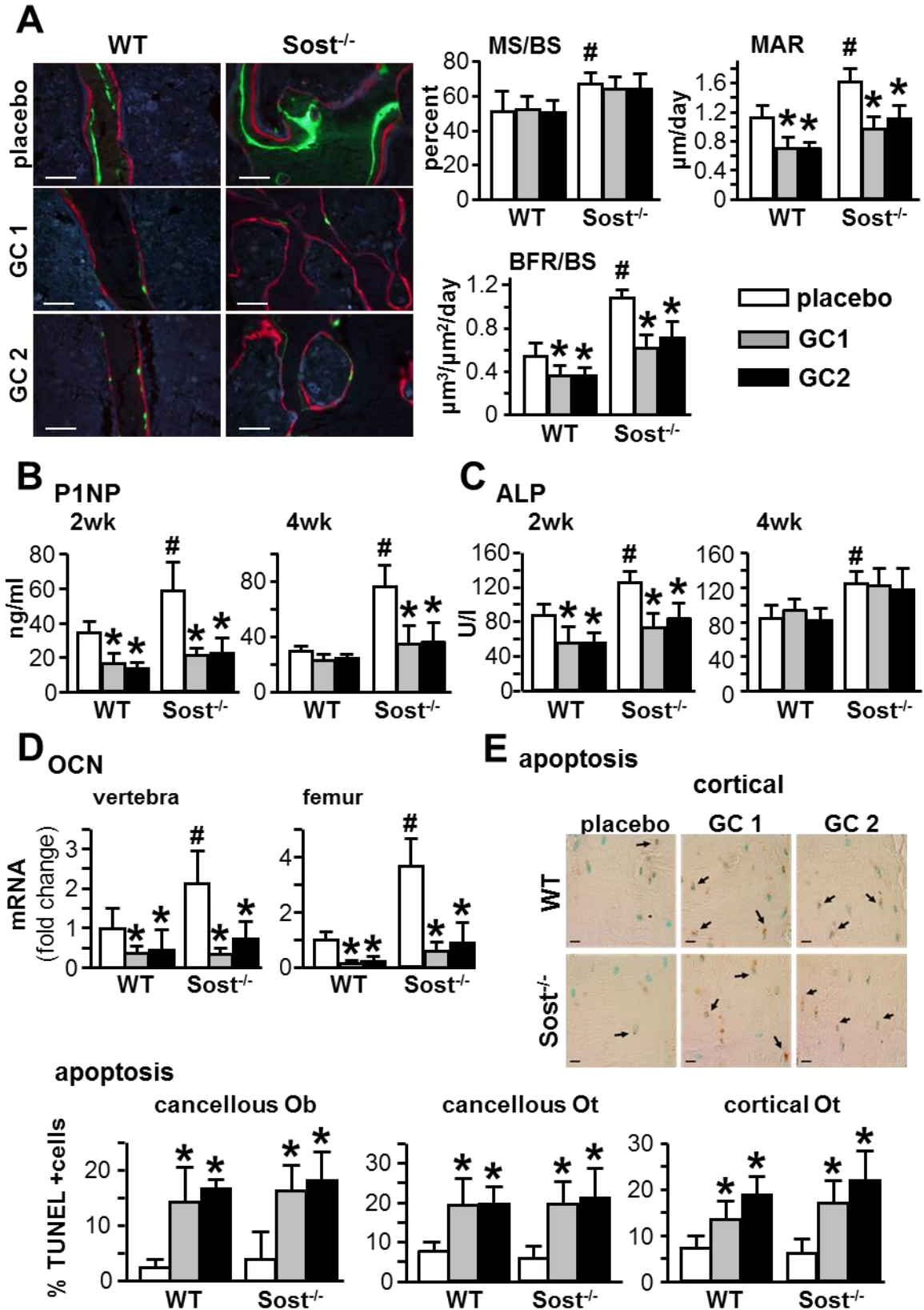**Figure 3-2. Sost/sclerostin deficiency does not prevent glucocorticoid-induced sarcopenia.** Final and percent change in lean body mass **(A)**, the mass of the indicated muscles **(B)**, and final and percent change in total body weight **(C)** are shown; N=8-10. Bars represent means ± SD. *p<0.05 vs. corresponding placebo-treated mice and #p<0.05 vs. placebo-treated WT mice by two-way ANOVA, Tukey post-hoc test.
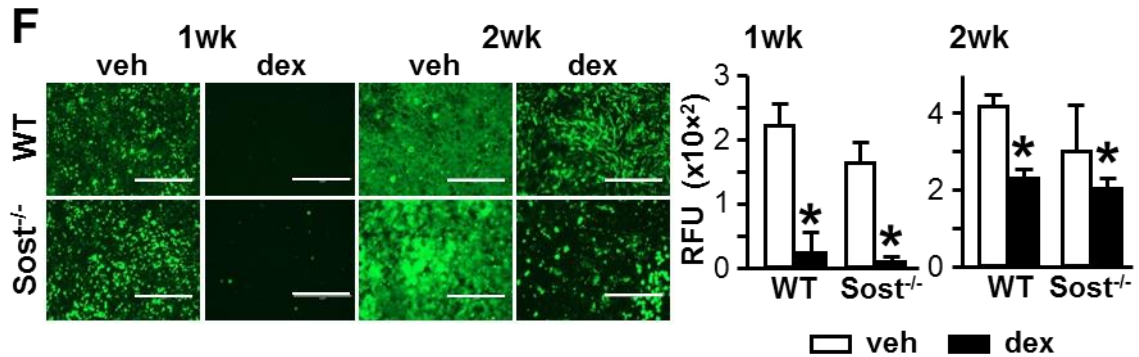
Figure 3-3. Sost/sclerostin deficiency does not prevent glucocorticoid-induced decrease in bone formation or increase in osteoblast/osteocyte apoptosis. (A) Representative images of fluorochrome incorporation and dynamic histomorphometric data measured in longitudinal sections of lumbar vertebra (L1-L3). Mineralizing bone surface per bone surface (MS/BS), mineral apposition rate (MAR), and bone formation rate per bone surface (BFR/BS) are shown. Scale bars: 50 μm, N=8-10. P1NP, N=6-10 **(B)**, and alkaline phosphatase, N=7-10 **(C)** were measured in blood collected 2 or 4 weeks after pellet implantation. **(D)** Osteocalcin (OCN) gene expression was quantified by qPCR in L5 lumbar vertebra and femur. N=7-10 for WT and N=6-8 for Sost^{-/-} mice. mRNA levels were normalized to the housekeeping gene ribosomal protein large P2 (Rplp2). **(E)** Apoptosis of osteoblasts (Ob) and osteocytes (Ot) was quantified in cancellous and cortical bone in longitudinal sections of lumbar vertebrae (L1-L3) stained for TUNEL. N=6. Representative images of cortical bone are shown. Scale bar: 20 μm. **(F)** Quantification of mineralization in cultures of calvaria-derived primary osteoblastic cells from WT or Sost^{-/-} mice treated with vehicle (veh) or dexamethasone (dex) for 1 or 2 weeks stained using the OsteoImage Mineralization Assay Kit (RFU 492nm/520nm excitation/emission fluorescence). Scale bars: 400 μm. N=7-8. Bars represent means ± SD. **(A-E)** *$p<0.05$ vs. corresponding placebo-treated mice and #$p<0.05$ vs. placebo-treated WT mice by two-way ANOVA, Tukey post-hoc test. **(F)** *$p<0.05$ vs. corresponding vehicle-treated primary osteoblasts by Student's *t*-test.
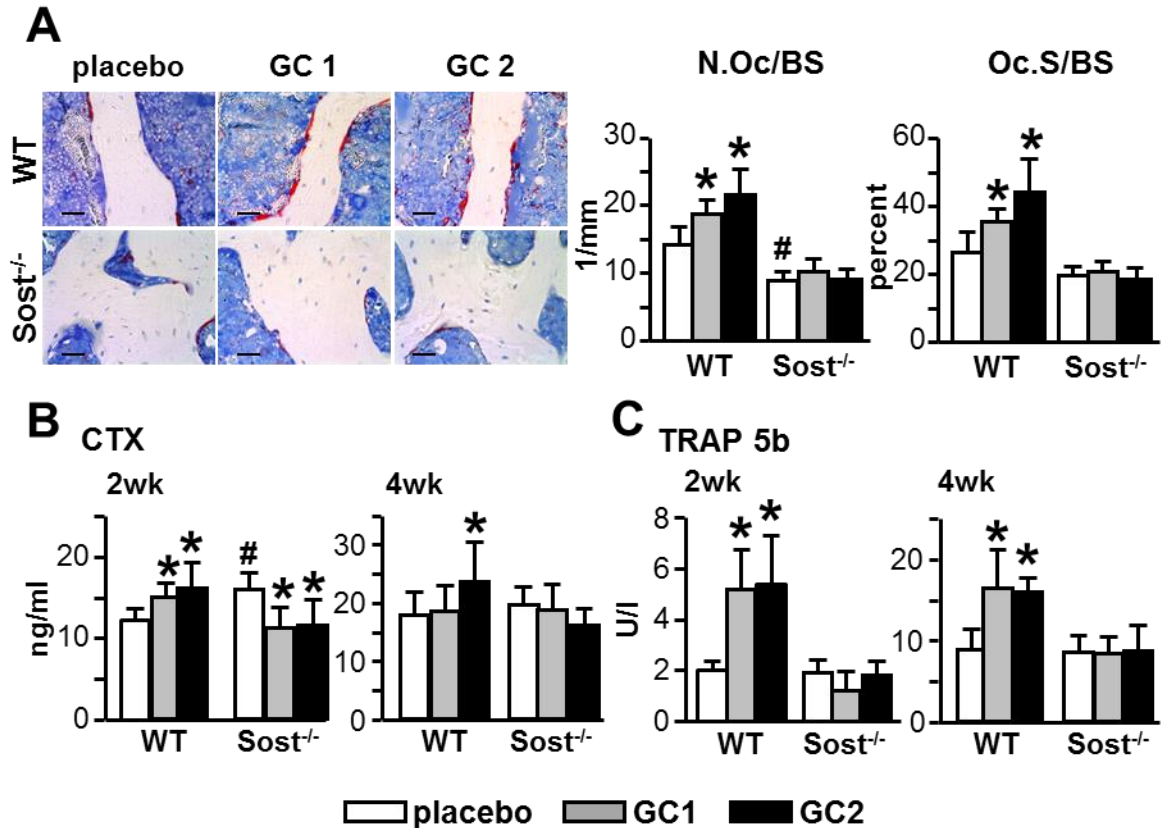
Figure 3-4. Sost^{-/-} mice are protected from the increase in bone resorption induced by glucocorticoid. (A) Representative microscopy images of osteoclasts on cancellous bone surface in lumbar vertebra (L2) stained for TRAPase. Osteoclast number (N.Oc/BS) and surface (Oc.S/BS) normalized to bone surface were measured. Scale bars: 30 µm, N=5. CTX, N=6-11 **(B)** and TRAP 5b, N=6-7 **(C)** were measured in blood collected 2 and 4 weeks after pellet implantation. Bars represent means ± SD. *p<0.05 vs. corresponding placebo-treated mice and #p<0.05 vs. placebo-treated WT mice by two-way ANOVA, Tukey post-hoc test.

A Sost

B % sclerostin positive osteocytes

WT: placebo 42 ± 7 | GC 1 47 ± 5 | GC 2 59 ± 5 §

Sost⁻/⁻: placebo N.D.

C

femur: OPG, Cx43, BMP4

vertebra: OPG, Cx43, BMP4

femur: cyclin D1, axin2, Smad6

vertebra: cyclin D1, axin2, Smad6

placebo | GC1 | GC2
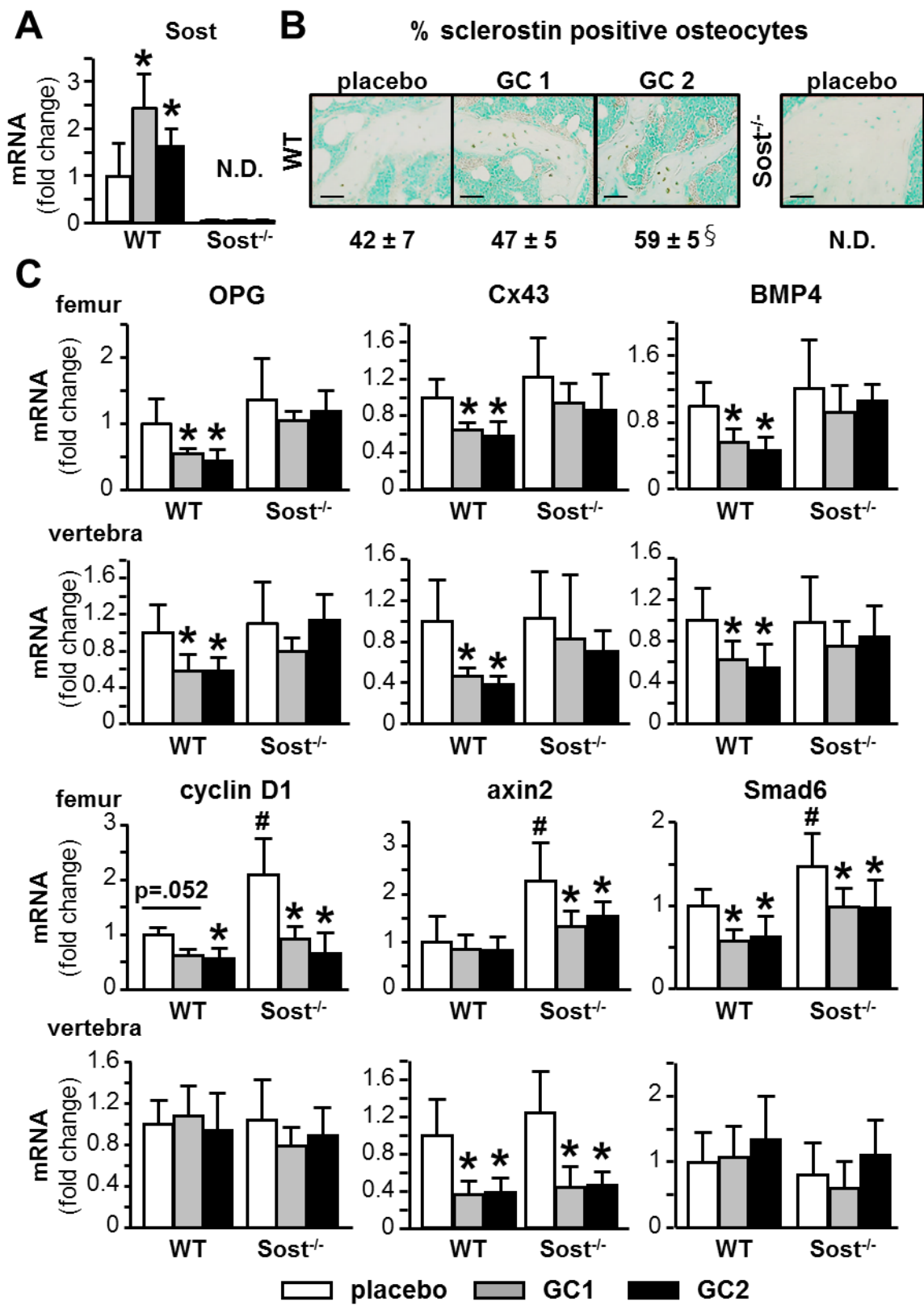
Figure 3-5. Glucocorticoids differentially alter Wnt/β-catenin signaling in a Sost/sclerostin-dependent manner. (A) Sost gene expression was quantified by qPCR in L5 lumbar vertebra. N=7-10 for WT and N=6-8 for Sost$^{-/-}$. **(B)** The percentage of sclerostin positive osteocytes was quantified in longitudinal sections of femoral bone stained with an anti-sclerostin antibody and is shown as percentage ± SD shown, N=3-4. Scale bars: 50 μm. **(C)** Expression of the indicated genes normalized to the housekeeping gene Rplp2 in femur and lumbar vertebra (L5). N= 7-10 for WT and N= 6-8 for Sost$^{-/-}$. Bars represent means ± SD. *p<0.05 vs. corresponding placebo-treated mice and #p<0.05 vs. placebo-treated WT mice by two-way ANOVA and Tukey post-hoc test. §p<0.05 vs. placebo-treated WT mice, by one-way ANOVA and the Tukey post-hoc test.
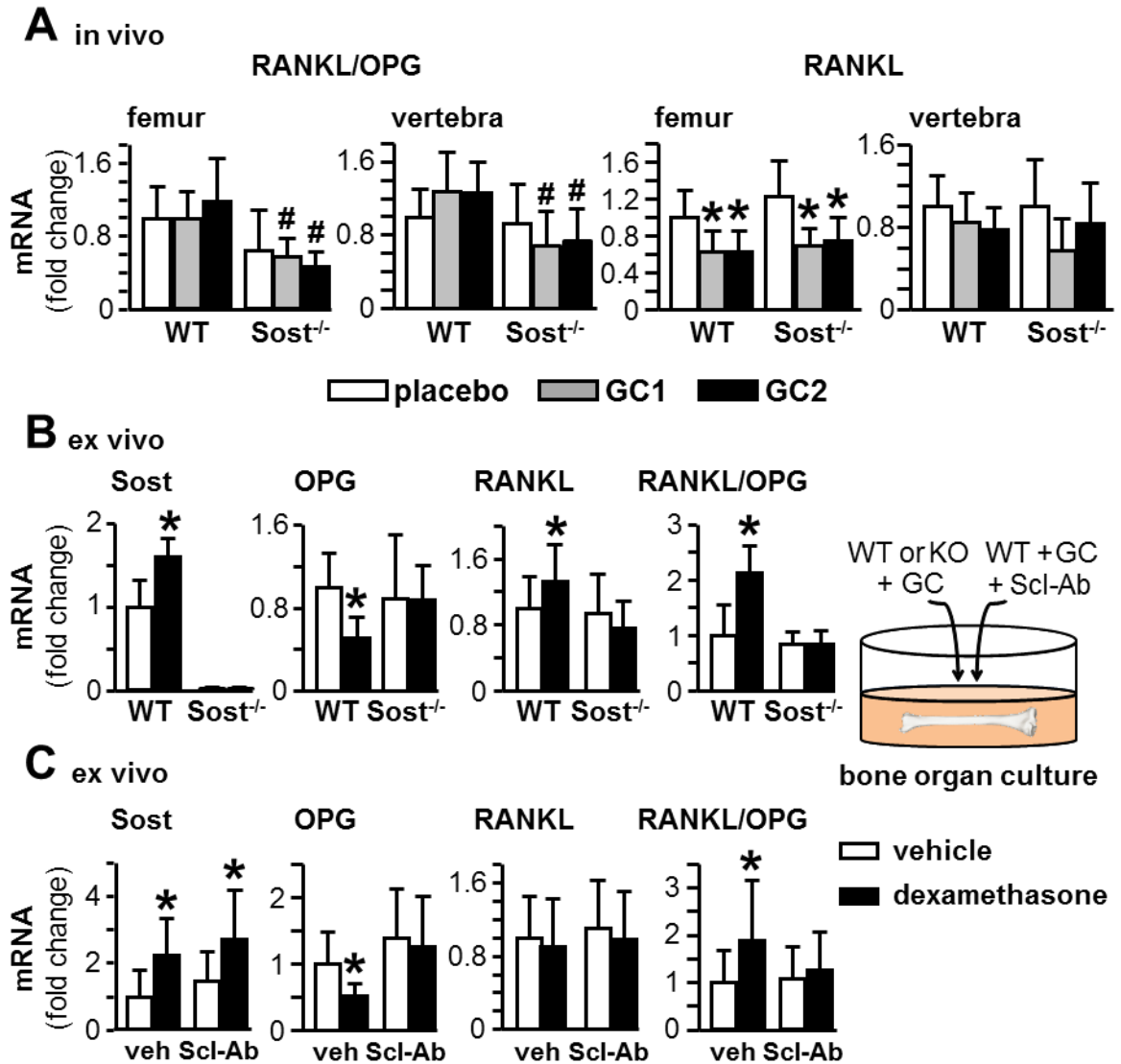
Figure 3-6. Genetic or pharmacologic inhibition of Sost/sclerostin blocks downregulation of OPG expression and the increase in RANKL/OPG ratio induced by glucocorticoid. (A) Expression of the indicated genes normalized to the housekeeping gene Rplp2 in femur and lumbar vertebra (L5). N= 7-10 for WT and N= 6-8 for Sost^{-/-}. *p<0.05 vs. corresponding placebo-treated mice and #p<0.05 vs. WT mice treated with the same glucocorticoid dose by two-way ANOVA, Tukey post-hoc test. **(B and C)** Gene expression in bones from WT or Sost^{-/-} mice, N=6 **(B)** or from WT mice cultured with or without anti-sclerostin antibody (Scl-Ab), N=16 **(C)** were treated *ex vivo*

with vehicle or dexamethasone for 6 hours. *$p < 0.05$ vs. corresponding vehicle-treated bones, by paired t-test.
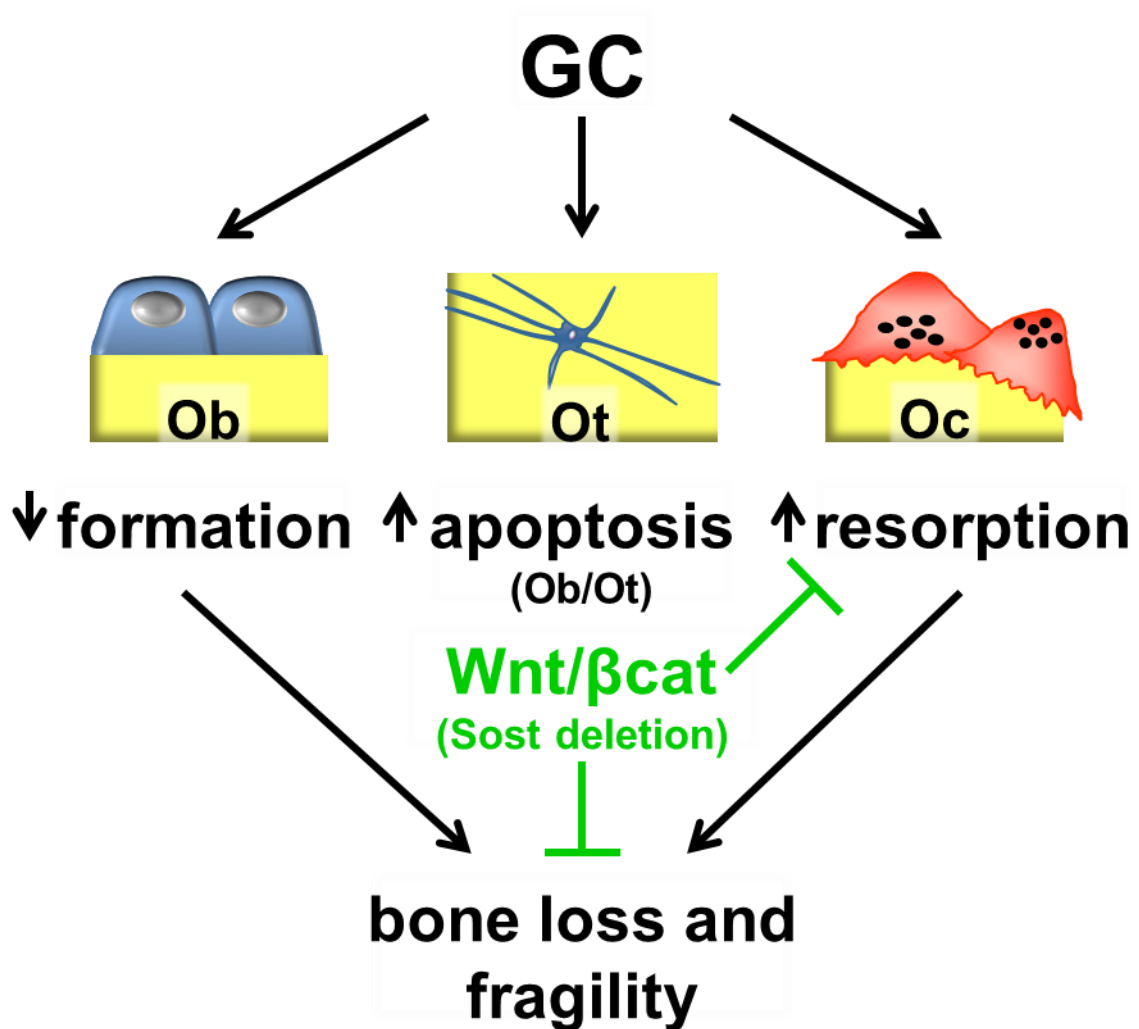
Figure 3-7. Sost/sclerostin deficiency prevents glucocorticoid-induced bone loss. Glucocorticoid-induced osteoporosis is characterized by decreased bone formation, increased apoptosis of osteocytes (Ot) and osteoblasts (Ob), and increased osteoclasts (Oc) and bone resorption, which combined induced bone loss and fragility. Activation of Wnt/β-catenin signaling resulting from Sost/sclerostin deletion protects from glucocorticoid-osteoporosis by inhibiting bone resorption through sustained anti-catabolic signaling driven by osteoprotegerin, OPG.

Chapter 4

Pyk2 deficiency protects from glucocorticoid-induced bone resorption and osteoblast and osteocyte apoptosis, but not from the decrease in bone formation

In this study, we demonstrate that Pyk2 deficiency prevents the bone loss and weakening effects of glucocorticoids *in vivo* due to a lack of GC-induced bone resorption. Pyk2 KO mice were also protected from glucocorticoid-induced apoptosis of osteoblasts and osteocytes; however, the glucocorticoid-induced suppression of bone formation occurred independently of Pyk2 expression and activity. To our knowledge, this is the first report demonstrating that Pyk2 deficiency leads to increased prevalence of osteoclast apoptosis, and inhibition of Pyk2 blocks the anti-apoptotic effects of glucocorticoids on osteoclasts.

Introduction

Glucocorticoid excess is the leading iatrogenic cause of osteoporosis world-wide and the third cause of osteoporosis overall, and novel therapeutic interventions are sorely needed (2). Glucocorticoid administration as immunosuppressant therapy is commonly used for a wide range of conditions, such as rheumatoid arthritis, asthma, inflammatory bowel disease, lung diseases, chronic liver disease, skin diseases, myeloma, and organ transplantation (9;10). However, glucocorticoids have direct, detrimental effects on the skeleton, resulting in bone fractures for an estimated 30-50% of long-term glucocorticoid-treated patients (2;10;22;27;114). Further, the bone loss and microarchitectural thinning of trabecular bone all contribute to the increased bone fragility and fracture risks associated with glucocorticoid administration.

Glucocorticoid-induced bone loss is accompanied by increased prevalence of osteoblast and osteocyte apoptosis, decreased formation, and increased resorption. Glucocorticoids lead to the phosphorylation of proline-rich tyrosine kinase 2 (Pyk2) in MLO-Y4 osteocytic cells, and silencing Pyk2 or expression of a kinase inactive Pyk2 prevents GC-induced apoptosis (54). Thus, the pro-apoptotic glucocorticoid effect on osteocytic cells requires Pyk2 expression and function *in vitro* (54). Another study showed that Pyk2 KO mice, as well as rats treated with a Pyk2 kinase inhibitor, also exhibit increased bone formation (115). Moreover, work from the Baron and Schlessinger groups reported that Pyk2 KO mice exhibit high bone volume and increased osteoclasts, which exhibit disorganized podosomes and impaired attachment to dentin *in vitro* (116). Collectively, this evidence raises the possibility that Pyk2 is involved in the effects of glucocorticoids on bone cells. The purpose of the current study was to investigate whether Pyk2 is required for the bone loss induced by glucocorticoids, and if so by which cellular mechanism, by interfering with resorption, apoptosis, or formation.

Materials and Methods

Mice and tissue procurement. Four-month-old female Pyk2$^{-/-}$ mice of C57BL/6 background generated by Okigaki et al. 2003 (117) or wild type (WT) littermate controls, 10 mice per group, were implanted with 90 day slow-release pellets delivering placebo, 1.4 mg/kg/day (GC1), or 2.1 mg/kg/day (GC2) prednisolone (Innovative Research of America) while under anesthesia. Mice were injected 10 and 3 days prior to sacrifice with 0.6% calcein and 1.0% alizarin red solutions, respectively. Twenty-eight days after pellet implantation mice were sacrificed. Bones were dissected and processed as indicated below. Analysis was performed in a blinded fashion.

BMD measurement and micro-CT analysis. BMD of the total body excluding the head and the tail, the lumbar spine (L1-L6), and the femur, and lean body mass were measured by dual energy X-ray absorptiometry (DXA) scanning by using a PIXImus II densitometer (G.E. Medical System, Lunar Division). DXA measurements were performed 2-4 days before (initial) and 28 days (final) after pellet implantation (65;92). Mice were randomized to the experimental groups based on initial spine BMD. Percent changes in BMD were calculated with the following formula: [(final–initial)/initial] multiplied by 100.

For micro-CT analysis, L6 vertebrae were cleaned of soft tissue, fixed in 10% buffered formalin, and stored in 70% ethanol until scanned at 6-μm resolution (Skyscan 1172, SkyScan). Measurements were done 60 μm away from the growth plates as previously described (93;94).

Mechanical testing. Mechanical properties of L6 vertebrae were determined by axial compression after removal of vertebral processes and the cranial and caudal endplates. Vertebral bodies were loaded at a rate of 0.5 mm/min until failure (100P225 Modular Test Machine) as previously described (97;98). Structural properties were obtained from the load/displacement curves and material-level properties were

calculated using published equations to normalize to vertebral height, cross-sectional area, and bone volume (46).

Serum biochemistry. Blood was collected 2 and 4 weeks after pellet implantation from the facial vein of 3-hour fasted mice. N-terminal propeptide of type I procollagen (P1NP), C-terminal telopeptides of type I collagen (CTX), and tartrate-resistant acid phosphatase form 5b (TRAP 5b) were measured using enzyme-linked immunosorbent assays (Immunodiagnostic Systems Inc.) (32;92). Osteocalcin was measured using the Mouse Osteocalcin KIA Kit (Biomedical Technologies Inc.).

Bone histomorphometry and apoptosis analysis. L1-3 vertebrae were fixed in 10% neutral buffered formalin and embedded undecalcified in methyl methacrylate as previously described (28). Dynamic histomorphometry measurements were performed in 7-μm unstained bone sections under epifluorescence microscopy. Histomorphometric analysis was performed using OsteoMeasure high resolution digital video system (OsteoMetrics) interfaced to an Olympus BX51 fluorescence microscope (Olympus America Inc.) (66). Osteoclasts were quantified on lumbar vertebra L2 thin sections stained for tartrate-resistant acid phosphatase (TRAP) and counterstained with Toluidine Blue as previously published (32;92). An osteoclast was defined as a TRAP positive cell attached to the bone surface with more than 1 nucleus. A marrow osteoclast was defined as TRAP positive cells with 2 or more nuclei separated from the bone surface by at least one cell.

Apoptosis of osteoblasts and osteocytes was detected by the transferase-mediated biotin-dUTP nick end-labeling (TUNEL) reaction (Fisher) in undecalcified vertebral bone sections counterstained with 2% methyl green, mounted on silane-coated glass slides (Scientific Device Lab, Inc.), as previously described (28). Apoptosis of osteoclasts and marrow osteoclasts was detected in double stained TRAPase, to identify osteoclasts, and TUNEL, to identify apoptotic cells, in paraffin-embedded femora from 5-

month-old WT and Pyk2$^{-/-}$ mice 28 days after pellet implantation. The prevalence of apoptotic osteoblasts, osteocytes, osteoclasts, and marrow osteoclasts was calculated by enumerating the total number of TUNEL positive cells exhibiting condense chromatin, nuclear fragmentation, or cell shrinkage.

Mineralization assay. Primary osteoblastic cells were isolated from the neonatal calvarial bones of C57BL/6 mice, Pyk2$^{-/-}$, or WT littermate control mice, and plated at 5000 cells/cm^2 density in MEM Alpha medium with 10% fetal bovine serum and 1% penicillin/streptomycin as previously described (41;60). Osteogenic medium was used after cultures reached confluence consisting of 50 µg/ml ascorbic acid and 10 mM β-glycerophosphate and treated with 1 µM dexamethasone or the corresponding vehicle (ethanol), and Pyk2 inhibitor (PF-431396) or the corresponding vehicle (DMSO). Medium was replaced every 2-3 days, and mineralization was visualized using the OsteoImage Mineralization Assay Kit (Lonza) or Alizarin Red S (Sigma-Aldrich) staining (41). Mineralization was quantified using a microplate reader for Lonza staining (492/520 nm excitation/emission fluorescence) or for Alizarin Red S staining (405 nm absorbance) (41).

Osteoclast apoptosis assay in vitro. Primary bone marrow cells were flushed with sterile PBS from tibiae and femora of C57BL/6 mice or WT and Pyk2$^{-/-}$ mice and cultured in MEM Alpha medium with 10% fetal bovine serum and 1% penicillin/streptomycin for 48 hours, as previously described (24). Nonadherent cells were collected, re-plated at 300,000 cells/cm^2 density, and differentiated with 80 ng/ml recombinant murine soluble RANKL (PeproTech) and 20 ng/ml recombinant murine M-CSF (PeproTech) for 4-6 days. Medium was replaced every 2 days and cells were treated with 10^{-5}M alendronate or corresponding vehicle (PBS) one hour prior to 1 µM dexamethasone or the corresponding vehicle (EtOH) addition. After 24 hours, cells were fixed with 10% buffered formalin, rinsed with dH$_2$O, and stained for TRAPase (Sigma-Aldrich) with

hematoxylin counterstaining. Apoptotic osteoclasts were identified by the presence of morphologic characteristics such as the loss of cell membrane integrity, nuclear condensation, and fragmentation.

Statistical analysis. Data are expressed as means ± standard deviations (SD). Sample differences were evaluated using SigmaPlot 12.0 (Systat Software Inc.). Data of the *in vivo* and *in vitro* experiments were analyzed by two-way ANOVA using genotype and treatment as independent variables. When ANOVA detected a significant interaction between the variables or a significant main effect of genotype, the post-hoc test Tukey was used to determine the significance of the effect of the treatment within each genotype.

Study approval. All animal procedures were approved by the Institutional Animal Care and Use Committee of Indiana University School of Medicine, and animal care was carried out in accordance with institutional guidelines.

Results

Pyk2 deficiency protects from GC-induced bone loss and reductions in bone strength. Mice lacking Pyk2 displayed high bone mass at all sites (**Figure 4-1A**) when compared to wild type (WT) littermate controls. Pyk2$^{-/-}$ mice also exhibited increased cancellous bone (BV/TV), trabecular thickness, trabecular number, and decreased trabecular separation (**Figure 4-1B**). Both doses of prednisolone (GC1=1.4 or GC2=2.1 mg/kg/day) significantly decreased total, spine, and femur BMD in WT mice (**Figure 4-1A**). GC-induced a significant loss of cancellous BV/TV bone at the high dose and the characteristic trabecular thinning at both doses in WT mice (**Figure 4-1B**). In contrast, Pyk2 deficient mice were resistant to these effects, as reductions in BMD, cancellous bone, or trabecular thickness did not occur in GC treated Pyk2$^{-/-}$ mice.

Pyk2$^{-/-}$ vertebral bones also exhibited increased structural mechanical properties of ultimate force, energy to ultimate load, and stiffness (**Figure 4-1C**) when compared to WT vertebral bones. However, no differences in material properties were detected between the two genotypes of placebo treated mice, which indicates that the gains in bone strength of Pyk2$^{-/-}$ mice is due to structural changes and not tissue level alterations (i.e. mineralization or collagen alterations). Both doses of GC reduced the ultimate force, energy to ultimate load, and toughness of vertebral bones from WT mice, with exception for the low GC dose regarding ultimate force. In contrast, bones from Pyk2$^{-/-}$ mice were protected from these GC-induced bone weakening effects.

Pyk2 deficiency protects from osteoblast and osteocyte apoptosis, but not the suppression of bone formation or mineral deposition induced by GC. Consistent with the previously published *in vitro* results showing that GC-induced apoptosis of MLO-Y4 osteocytic cells requires Pyk2 kinase expression and activity (54), GC increased the prevalence of osteoblast and osteocyte apoptosis in cancellous bone and of osteocyte apoptosis in cortical bone in WT mice, but not in Pyk2 KO mice (**Figure 4-2A**). These

findings demonstrate that Pyk2 deficiency protects from osteoblast and osteocyte apoptosis induced by GC also *in vivo*. In contrast, GC reduced serum levels of bone formation marker P1NP and of OCN at both doses in WT as well as in Pyk2 KO mice (**Figure 4-2B**). Further, GC decreased bone formation indexes to the same extent in WT and in Pyk2 KO mice with decreases of MS/BS, MAR, and BFR (**Figure 4-2C**). GC treatment also decreased hydroxyapatite deposition *in vitro* in osteoblast cultures from both WT and Pyk2 KO mice (**Figure 4-2E**). Interestingly, mineral deposition was increased in cultures of Pyk2 KO osteoblasts or WT osteoblasts treated with .02 μM Pyk2 kinase inhibitor (**Figure 4-2E-F**) in the absence of GC, resembling the increased bone formation in the femur reported by Buckbinder et al. 2007 (115). As a dose response toxicity effect was exhibited with 2 μM or higher Pyk2 kinase inhibitor concentrations (**Figure 4-2F**), doses of .02 and .2 μM were selected for following experiments. Similarly to the Pyk2 KO *in vivo* and *in vitro* results, GC also decreased calcium deposition in the absence or presence of the Pyk2 kinase inhibitor PF-431396. Thus, GC-induced suppression of bone formation or mineral deposition does not require Pyk2 expression or activity.

Pyk2 deficiency protects from GC-induced bone resorption. Both doses of GC induced the expected increases in serum CTX, an index of bone resorption, and in TRAP 5b, an index of osteoclast number, of WT mice (**Figure 4-3A-B**). In contrast, GC failed to increase serum CTX in Pyk2 KO mice. TRAP 5b was already elevated in Pyk2 KO mice, and GC did not further increase TRAP 5b circulating levels. Consistently with the mismatch between CTX and TRAP 5b the ratio of CTX/TRAP 5b, an index of the activity of individual osteoclasts, was reduced in Pyk2 KO mice (**Figure 4-3C**). Moreover, GC did not change the CTX/TRAP 5b ratio in WT mice, indicating that the

increase in resorption in WT mice was due to an increase in osteoclast number, and not due to an increase in osteoclast activity.

GC increased osteoclast number in bone of WT as well as of Pyk2 KO mice (**Figure 4-3D**). Remarkably however, GC increased osteoclast surface only in WT mice and not in Pyk2 KO mice. Close examination of the bone sections showed that whereas osteoclasts in WT treated with GC were attached to the bone, osteoclasts in Pyk2 KO mice treated with GC were not completely attached to bone (**Figure 4-3E-F**). This phenomenon explains the mismatch between osteoclast number and surface, and is consistent with the reduced CTX/TRAP 5b found in the circulation of Pyk2 KO mice. Moreover, compared to WT bones, Pyk2 KO bones exhibited more than double number of osteoclasts in the bone marrow (**Figure 4-3D**). Marrow osteoclasts were identified as TRAP positive cells with 2 or more nuclei, separated from the bone surface by at least one cell. Thus, Pyk2 deficiency protects from the increase in osteoclast surface induced by GC.

Pyk2 deficient mice exhibit increased osteoclast apoptosis, which is not altered by GC. We next explored the possibility that the osteoclasts from the Pyk2 KO mice that exhibit impaired attachment to bone were undergoing premature death by apoptosis. Bone sections were double stained with TRAPase to identify osteoclasts and TUNEL to identify apoptotic cells. High magnification images show a living osteoclast in WT bone and an apoptotic, TUNEL positive osteoclasts in Pyk2 KO bone (**Figure 4-4A**). Quantification of TUNEL and TRAPase double stained osteoclasts revealed that Pyk2 KO bones exhibited increased prevalence of apoptotic osteoclasts on bone surfaces as well as osteoclasts in the bone marrow when compared to WT controls. The increase in osteoclast apoptosis induced by Pyk2 deficiency was not altered by GC treatment.

Taken together these findings demonstrate that impaired attachment in osteoclasts lacking Pyk2 leads to apoptosis.

Consistent with previous reports (116), Pyk2 deficient osteoclasts also exhibited abnormal morphology with the absence of organized podosome belt structures and impaired osteoclast spreading (**Figure 4-4B**). Also, osteoclasts derived from Pyk2 KO mice exhibited approximately 95% reduction in the number of TRAP positive cells with 3 or more nuclei when compared to WT derived osteoclasts, which led to the quantification of TRAP positive cells with less than 3 nuclei for Pyk2 deficient osteoclasts.

As previously shown (24), the bisphosphonate alendronate increased apoptosis of mature osteoclasts generated *in vitro* with RANKL and MCSF for 5 days from marrow precursors of WT mice (**Figure 4-4B**). Normal osteoclasts show intact cell membrane, TRAPase staining evenly distributed in the cytoplasm, and round nuclei. Apoptotic osteoclasts exhibited the characteristic features of apoptotic cells, i.e. loss of cell membrane integrity, nuclear condensation and fragmentation, and the TRAPase staining is condensed in darker areas. Consistent with previous published reports (24), addition of dexamethasone partially prevented apoptosis induced by the bisphosphonate alendronate of osteoclasts derived from WT mice. Similar to the Pyk2 KO *in vivo* results, overall osteoclast apoptosis was more prevalent in the absence of Pyk2 *in vitro*, regardless of the number of nuclei. Also, osteoclasts derived from Pyk2 deficient mice did not exhibit the glucocorticoid pro-survival effects against alendronate-induced apoptosis of osteoclasts derived from WT mice. Similarly, osteoclasts treated with the Pyk2 kinase inhibitor (**Figure 4-4C**) derived from C57BL/6 mice were not protected from bisphosphonate-induced apoptosis by GC. Therefore, prevention of osteoclast apoptosis by GC requires Pyk2 kinase activity. Taken together, these pieces of evidence

demonstrate that the inherent osteoclast dysfunction conferred by lack of Pyk2 overrides

GC induced resorption.

Discussion

This study provides insights into novel mechanisms of glucocorticoid action and the cellular basis by which inactivation of Pyk2 signaling interferes with the detrimental skeletal effects of glucocorticoid excess in bone.

The findings reported here demonstrate that Pyk2 is required for glucocorticoid-induced bone loss and bone fragility *in vivo* as glucocorticoid stimulated cellular responses of increased osteoblast/osteocyte apoptosis and increased osteoclast-driven resorption, but not from the suppression of bone formation, are Pyk2 dependent.

Pyk2 KO mice treated with glucocorticoids did not lose bone at any site as detected by DXA or exhibit the hallmark GC-induced thinning of cancellous bone. Pyk2 deficiency also prevented bone fragility induced by glucocorticoids, which was mainly driven by bone loss as indicated by comparing reductions in ultimate force to the lack of reductions in ultimate stress that accounts for the amount of bone (BV/TV) and cross-sectional area (**Figure 4-1**). This glucocorticoid mouse model also consistently (118) demonstrates the bone weakening effects of detrimental microarchitectural trabeculae thinning induced by glucocorticoids as indicated by reductions in both the energy to ultimate load and toughness mechanical properties.

Consistent with previous *in vitro* reports (54), the current study's *in vivo* results indicate that Pyk2 is required for glucocorticoid-induced apoptosis of osteocytes and osteoblasts. Unexpectedly, prevention of glucocorticoid-induced osteoblast apoptosis did not prevent reductions in bone formation as clearly indicated by circulating levels of P1NP and OCN as well as dynamic histomorphometric indexes (**Figure 4-2**). Reductions in P1NP levels were detected between Pyk2$^{-/-}$ and WT placebo treated 4 weeks after pellet implantation; however, the mechanism for this finding remains unknown. Further, no differences in circulating OCN levels were found between the genotypes at either 2 or 4 weeks after pellet implantation. These findings are in contrast to previous reports of

increased BFR/BS, MAR, MS/BS with administration of Pyk2 inhibitor PF-431396 in an OVX rat model (115). However, glucocorticoids have several known mechanisms, such as suppression of OCN (33;34) and Col1A1 (35;36) expression, suppression of canonical WNT signaling via increased WNT antagonist Sost/sclerostin (118) or Dkk1 (119;120) expression, and reductions of β-catenin/TCF/LEF transcription activity (55) to reduce bone formation that Pyk2 deficiency/inhibition would not be anticipated to alter. Consistent with the *in vivo* evidence, the synthetic glucocorticoid dexamethasone reduced mineral deposition of primary osteoblast cultures derived from Pyk2 KO mice or from C57BL/6 mice treated with a Pyk2 inhibitor (**Figure 4-2**). Therefore, the mechanisms of glucocorticoid inhibition of bone formation and mineral matrix production in osteoblasts occur independently of Pyk2 *in vivo* and *in vitro*.

These studies also demonstrate *in vivo* that Pyk2 deficiency prevents glucocorticoid stimulated resorption as Pyk2 is required for normal osteoclast attachment, activity, and anti-apoptotic/survival signaling. Glucocorticoid treated mice exhibited increased resorption due to increased osteoclast numbers as indicated by elevation of circulating CTX and TRAP 5b levels as well as osteoclast number and surface (**Figure 4-3**). However, resorption was not elevated in glucocorticoid treated Pyk2 KO mice as shown by a lack of increased CTX or osteoclast surface. Consistent with previous reports of defective podosome cell attachment and pit resorption of dentin coated slides in Pyk2 deficient osteoclasts *in vitro* (116), Pyk2 KO mice exhibited osteoclasts partially attached to bone surfaces (**Figure 4-3F**) as well as increased number of TRAPase positive multi-nucleated osteoclasts not attached to bone surfaces located in the bone marrow. While the marrow osteoclasts contributed to the elevation of circulating TRAP 5b levels in Pyk2 KO mice, the resorption activity and individual cell activity of these partially attached osteoclasts and marrow osteoclasts was diminished even in the presence of excessive glucocorticoid conditions as indicated by CTX and the

CTX/TRAP 5b ratio. Further, the lack of proper cell attached in Pyk2 KO osteoclasts treated with glucocorticoids led to a mismatch between the number of osteoclasts and osteoclast surface (**Figure 4-3D**).

These findings also suggest a novel role for Pyk2 regarding osteoclast survival/anti-apoptotic signaling *in vivo* and *in vitro*, which also contributed to the inhibition of glucocorticoid stimulated resorption in Pyk2 KO mice. An elevation of apoptotic osteoclasts both on the bone surface and in the marrow was exhibited by Pyk2 deficient mice, and glucocorticoid administration did not reverse this apoptotic accumulation (**Figure 4-4**). Consistent with previous results (24), dexamethasone partially rescued bisphosphonate induced apoptosis of mature, fully differentiated osteoclasts derived from C57BL/6 or WT mice. However, the anti-apoptotic glucocorticoid effects did not occur in either Pyk2$^{-/-}$ derived osteoclasts or Pyk2 inhibitor treated osteoclasts derived from C57BL/6 mice *in vitro.* Taken together, these pieces of evidence indicate that the anti-apoptotic effects of glucocorticoids in osteoclasts are dependent on Pyk2 *in vivo* and *in vitro.* Thus, the impaired attachment, defective activity, and hindered anti-apoptotic signaling conferred by lack of Pyk2 in osteoclasts overrides glucocorticoid stimulated resorption.

We conclude that Pyk2 deficiency protects from GC-induced osteoblast/osteocyte apoptosis and bone resorption to prevent bone loss. These findings provide a basis for therapies to target glucocorticoid-induce resorption.

Acknowledgments

A final BMD

total | spine | femur

placebo | GC1 | GC2

B BV/TV | Tb.Th. | Tb.Sp. | Tb.N.

C structural properties

ultimate force | energy to ultimate load | stiffness

material properties

ultimate stress | toughness | elastic modulus
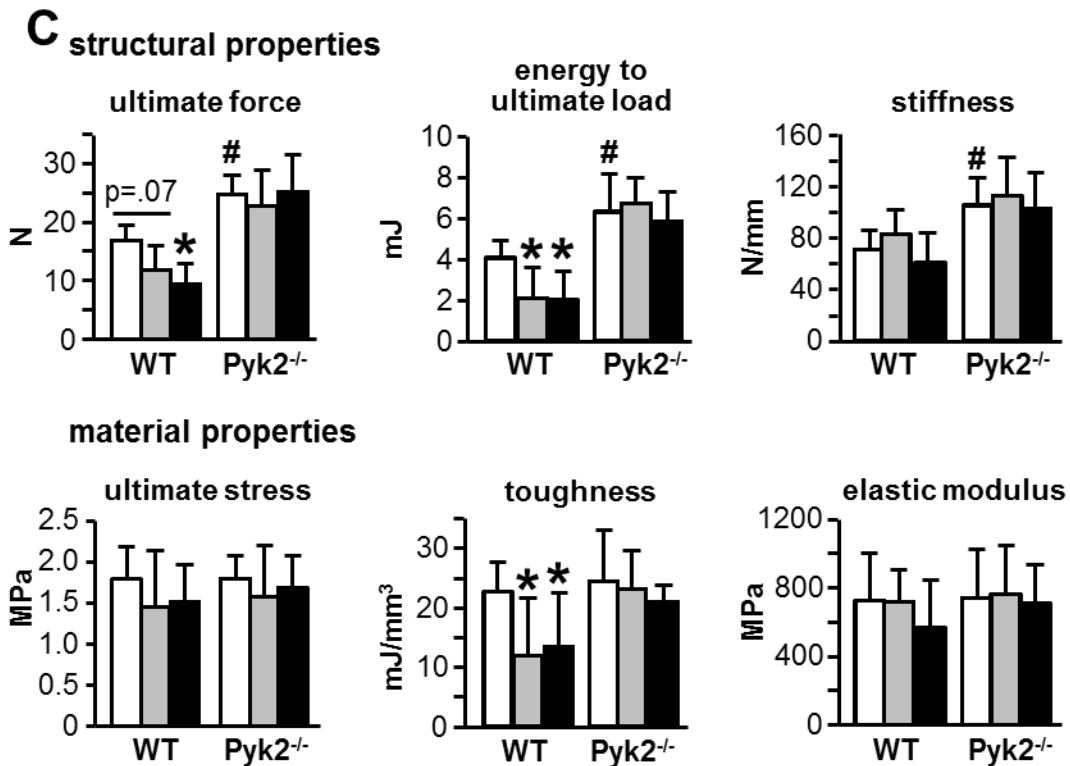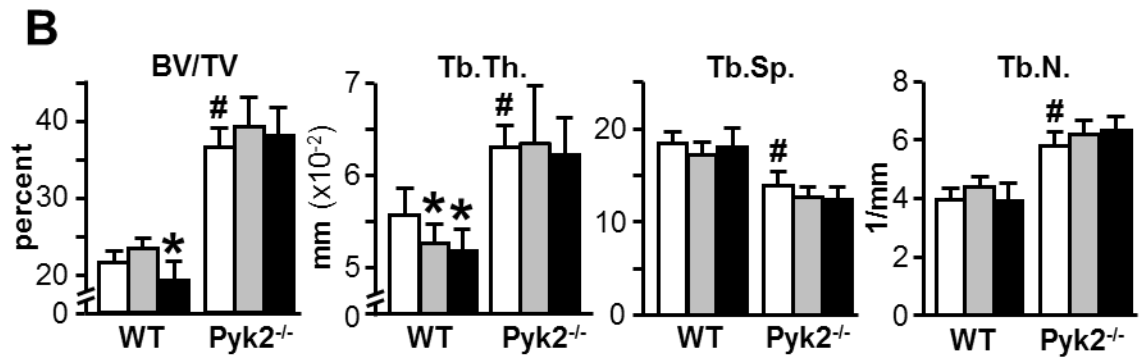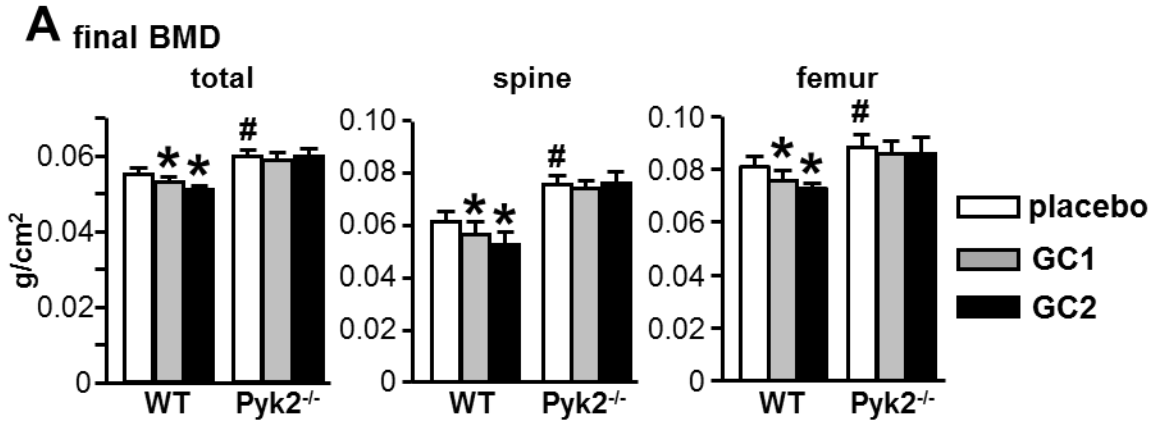
Figure 4-1. Pyk2$^{-/-}$ mice are protected from bone loss and decreased bone strength induced by glucocorticoids. (A) BMD for WT or Pyk2$^{-/-}$ mice treated with placebo, 1.4 mg/kg/day prednisolone (GC1), or 2.1 mg/kg/day prednisolone (GC2) for 28 days, measured by DXA. N=7-10. **(B)** Bone volume/tissue volume (BV/TV), trabecular thickness (Tb.Th.), separation (Tb.Sp.), and number (Tb.N.) of lumbar vertebrae L6 are shown. N=7-10. **(C)** Biomechanical properties were measured in vertebral bone (L6) by axial compression testing; N=7-10. Bars represent means ± SD. *p<0.05 vs. corresponding placebo-treated mice and #p<0.05 vs. placebo-treated WT mice, by two-way ANOVA, Tukey post-hoc test.
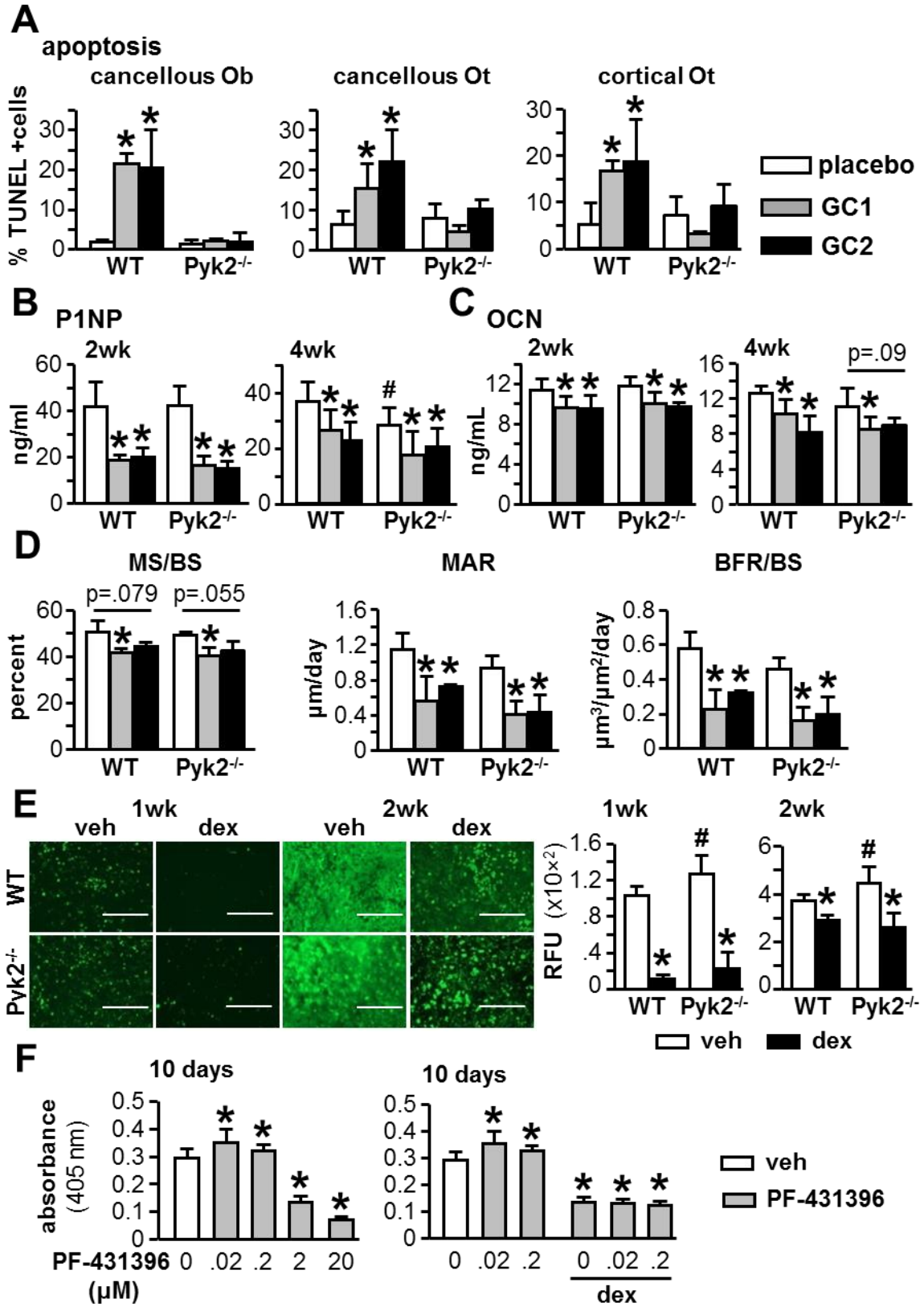
Figure 4-2. Pyk2 deficiency protects from osteoblast and osteocyte apoptosis, but not suppression of bone formation or mineral deposition induced by GC. (A) Apoptosis of osteoblasts (Ob) and osteocytes (Ot) was quantified in cancellous and cortical bone in longitudinal sections of lumbar vertebrae (L1-L3) stained for TUNEL. N=3-4. P1NP, N=8-10 **(B)**, and osteocalcin (OCN), N=6-7 **(C)** were measured in blood collected 2 or 4 weeks after pellet implantation. **(D)** Mineralizing bone surface per bone surface (MS/BS), mineral apposition rate (MAR), and bone formation rate per bone surface (BFR/BS) were quantified in longitudinal sections of lumbar vertebra (L1-L3). N=3-4. **(E)** Quantification of mineralization in cultures of calvaria-derived primary osteoblastic cells from WT or Pyk2$^{-/-}$ mice treated with vehicle (veh) or dexamethasone (dex) for 1 or 2 weeks stained using the OsteoImage Mineralization Assay Kit (RFU 492nm/520nm excitation/emission fluorescence). Scale bars: 400 µm. N=7-8. **(F)** Mineralization quantification of calvaria-derived primary osteoblastic cell cultures from C57BL/6 mice treated with or without Pyk2 inhibitor PF-431396 with veh or dex for 10 days stained using Alizarin Red S (405nm absorbance). N=4, measured in triplicate. Bars represent means ± SD. **(A-D)** *$p<0.05$ vs. corresponding placebo-treated mice and #$p<0.05$ vs. placebo-treated WT mice by two-way ANOVA, Tukey post-hoc test. **(E-F)** *$p<0.05$ vs. corresponding vehicle-treated cells and #$p<0.05$ vs. vehicle-treated cells from WT mice by two-way ANOVA, Tukey post-hoc test.
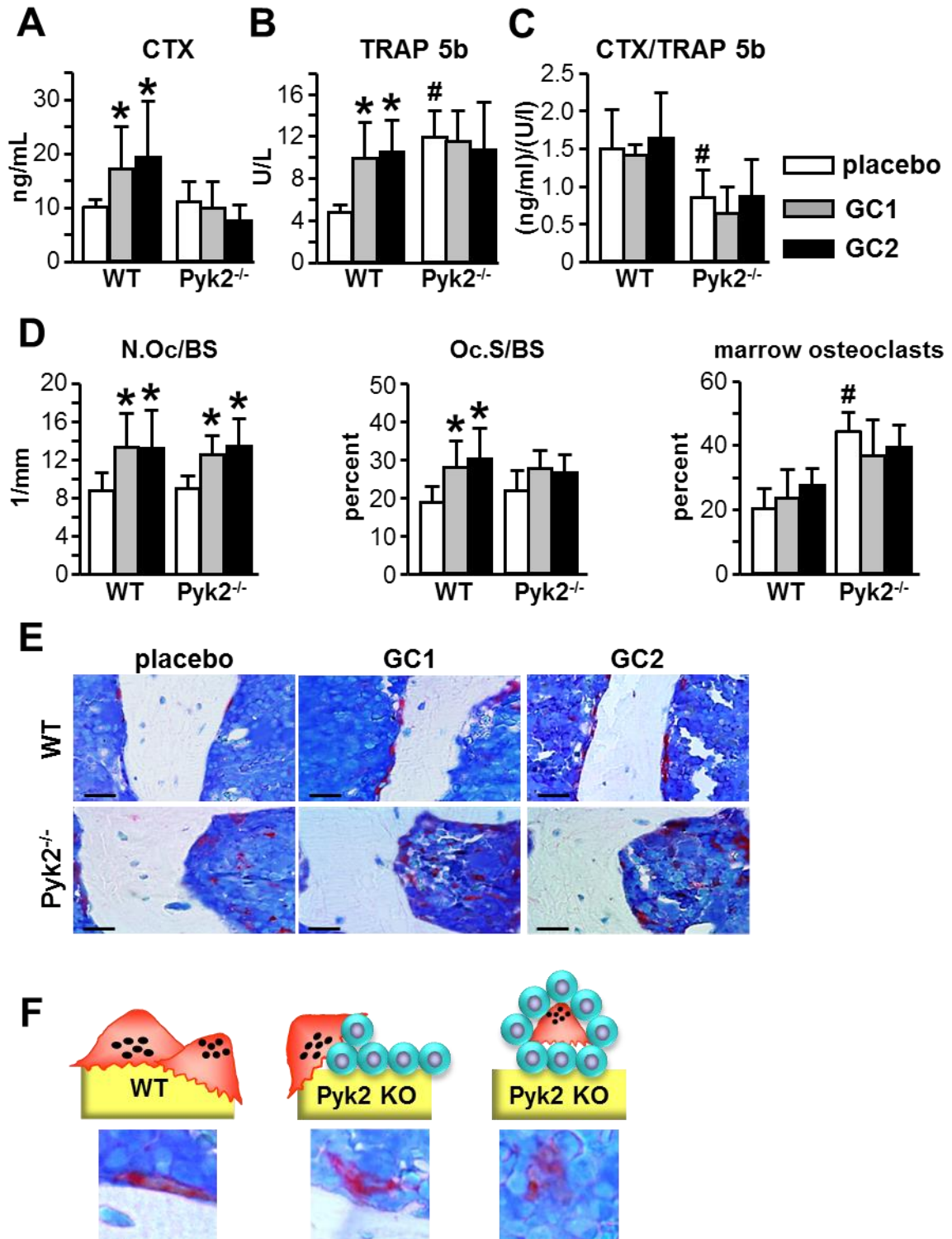
Figure 4-3. Pyk2 deficiency protects from GC-induced bone resorption and increased osteoclast surface. (A) CTX, N=6-7 **(B)** TRAP 5b, N=6-7 **(C)** CTX/TRAP 5b,

N= 5-6. were measured in blood collected 4 weeks after pellet implantation. **(D)** Osteoclast number (N.Oc/BS) and surface (Oc.S/BS) normalized to bone surface were measured and the percentage of marrow osteoclasts were determined in longitudinal sections of lumbar vertebra (L1-L3). N=6. **(E)** Representative microscopy images of osteoclasts on cancellous bone surface in lumbar vertebra (L2) stained for TRAPase. Scale bars: 25 μm. **(F)** Schematic and representative images of WT osteoclast, Pyk2 KO osteoclasts with impaired attachment, and Pyk2 KO marrow osteoclast. Bars represent means ± SD. *p<0.05 vs. corresponding placebo-treated mice and #p<0.05 vs. placebo-treated WT mice by two-way ANOVA, Tukey post-hoc test.
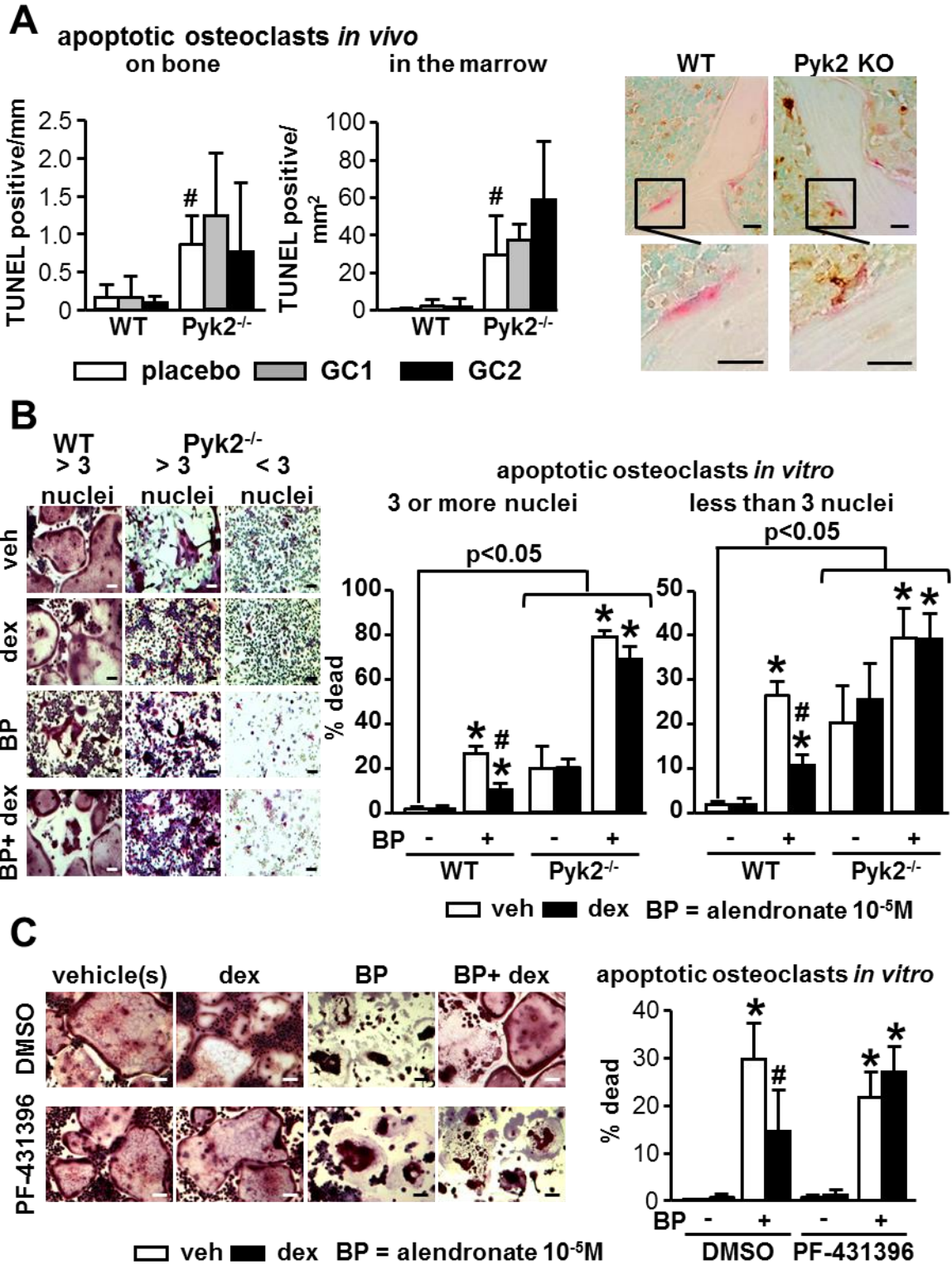
Figure 4-4. Pyk2 deficient mice exhibit increased osteoclast apoptosis, which is not altered by GC, and GC prevention of osteoclast apoptosis requires Pyk2

kinase activity *in vitro*. (A) Apoptotic osteoclasts on bone surfaces and in the marrow were quantified in TRAPase and TUNEL double stained longitudinal sections of the distal femur. N=3. Representative microscopy images of osteoclasts on cancellous bone surface are shown. Scale bars: 20 μm. **(B-C)** Quantification of apoptosis of differentiated primary osteoclasts derived from C57BL/6 mice or Pyk2$^{-/-}$ and WT mice treated with and without alendronate and vehicle (veh) or dexamethasone (dex) for 24 hours using TRAPase and hematoxylin staining. Scale bars: 20 μm. N=6. Bars represent means ± SD. **(A)** *p<0.05 vs. corresponding placebo-treated mice and #p<0.05 vs. placebo-treated WT mice by two-way ANOVA, Tukey post-hoc test. **(B-C)** *p<0.05 vs. corresponding vehicle-treated cells and #p<0.05 vs. corresponding alendronate-treated cells by two-way ANOVA, Tukey post-hoc test.

Chapter 5

Glucocorticoids induce bone and muscle atrophy by tissue-specific mechanisms

upstream of E3 ubiquitin ligases

Introduction

Excess of glucocorticoids is the third most common cause of bone loss, after aging and menopause, and the leading iatrogenic cause of osteoporosis (2). Immunosuppressant therapy with glucocorticoids is highly beneficial for a wide range of inflammatory conditions. However, glucocorticoid treatment has devastating effects on the musculoskeletal system, with bone fractures occurring in approximately 30-50% of long-term glucocorticoid-treated patients (2;10;22;27;114). Glucocorticoids induce bone loss, decrease bone formation, and cause trabecular and cortical bone thinning, leading to increased bone fragility. In addition, glucocorticoids induce loss of skeletal muscle mass and weakness of particularly muscles of the hip and shoulder girdle, which in turn increases the risk for falls. The combined effects on bone and muscle are largely responsible for the increased fracture risk with glucocorticoid excess.

The debilitating effects of glucocorticoids in muscle are of rapid onset, detected as early as 7 days after initiation of their administration in humans (121;122). Glucocorticoids reduce sarcolemmal excitability, decrease serum levels of creatine kinase and myoglobin, decrease cross sectional area of type 1, 2A and 2B myofibers, and reduce the specific force (strength) of muscle fibers. Muscle atrophy induced by glucocorticoids is accompanied by suppression of protein synthesis with simultaneous increase in protein catabolism, leading to reduced myotube diameter (100;123). The formation of new myotubes is also impaired as glucocorticoids inhibit myogenesis by downregulating myogenin gene expression. Glucocorticoid-induced protein catabolism in skeletal muscle is associated with enhanced Forkhead Box O (FoxO)-dependent transcription of members of the protein degradation machinery, including the ubiquitin-proteasome system of E3 ubiquitin ligases, the lysosomal system of cathepsins, and the calcium-dependent system of calpains (123;124). E3 ubiquitin ligases muscle atrophy F-

box (MAFbx, also known as atrogin1) and muscle RING finger 1 (MuRF1, also known as TRIM63) are known regulators of glucocorticoid-induced muscle atrophy both *in vivo* and *in vitro*, as well as a number of other sarcopenia-inducing conditions including denervation, immobilization, disuse, diabetes, and renal failure (125-127). Mice lacking MuRF1 are partially protected from muscle loss induced by glucocorticoids, and muscle-specific deletion of the glucocorticoid receptor prevents the increased atrophy gene expression and muscle loss induced by glucocorticoids (128-130). The ubiquitin ligase MUSA1 (muscle ubiquitin ligase of the SCF complex in atrophy-1, also known as Fbxo30) has also been associated with increased protein catabolism and reductions in total protein content in muscle models of denervation injury/disuse (131). However, the mechanisms by which glucocorticoids upregulate the expression of atrophy-related genes have not been described. In addition, it is not known whether reduction in bone mass induced by glucocorticoids is also accompanied by stimulation of atrophy-related genes.

In this study, we demonstrate that excess of glucocorticoids increase the expression in bone *in vivo* and in osteoblasts and osteocytes *in vitro* of the traditionally considered muscle-specific E3 ligases atrogin1, MuRF1, and MUSA1. In addition, we show that glucocorticoids increase the expression of Notch ligands, receptors, and target genes in muscle, but not in bone. Furthermore, glucocorticoid-induced expression of atrophy-related genes and muscle cell atrophy were prevented by pharmacologic inhibition of the Notch pathway. These findings demonstrate that glucocorticoid-induced loss of bone and muscle mass is accompanied by increased expression of atrophy-related genes, although the upstream mechanisms are tissue-specific. Moreover, our results identify the Notch signaling pathway as a potential therapeutic intervention to prevent skeletal muscle atrophy and weakness induced by glucocorticoids. Our study provides the mechanistic basis for combining therapies that target each tissue to treat

glucocorticoid-induced osteopenia and sarcopenia and offer new molecular approaches

to prevent glucocorticoid-induced atrophy of the musculoskeletal system.

Materials and Methods

Mice. Female 16-week-old C57BL/6 mice (n=10 per group) were randomized based on spinal BMD and allotted into 4 groups, and implanted subcutaneously with pellets containing placebo or prednisolone (2.1 mg/kg/day) (Innovative Research of America, Sarasota, FL, USA), for 14 or 28 days. There were no differences in total body weight between the groups before or at 14 or 28 days after pellet implantation. Bone fluorochrome labeling was performed by intraperitoneal injections of 0.6% calcein and 1.0% alizarin red at 10 and 3 days before the end of the experiment, respectively (94). Analyses were performed in a blind fashion.

Muscle weight and function. Muscles were weighted immediately after dissection. *In vivo* and *ex vivo* muscle function testing was performed in female 20-week-old C57BL/6 mice (n=10 per group) that were randomized based on spinal BMD and lean body mass and allotted into 2 groups: placebo-controls or prednisolone-treated animals for 28 days.

In vivo muscle function was quantified using the 1305A Whole Mouse/Rat Test System, Aurora Scientific Inc., Aurora, ON, Canada (132). Mice were anesthetized with isoflurane, and the right leg was shaved and cleaned with alcohol. Then, mice were placed in supine position with the right ankle at 90 degrees of dorsiflexion and the leg positioned perpendicular to the foot pedal. Two sterile monopolar stimulated electrodes were inserted subcutaneously near the tibial nerve with one electrode medial to the nerve and the other lateral in the posterior hind limb musculature. Electrode placement and stimulation current were adjusted to achieve maximum twitch response and then increased to ~35mA for plantarflexion to ensure supramaximal stimulation of muscle fibers. Maximum isometric torque (N/m) was recorded for stimulation frequencies between 25 and 300Hz, with a pulse width of 0.2ms and train duration of 200ms. Data were recorded by the Dynamic Muscle Control/Data Acquisition (DMC) and Dynamic

Muscle Control Data Analysis (DMA) programs (Aurora Scientific Inc., Aurora, ON, Canada).

Ex vivo muscle contractility of the extensor digitorum longus (EDL) and soleus muscles was performed as previously described (133). Briefly, muscles were dissected from the hind limbs while immersed in Ringer's Solution consisting of 136.9mM NaCl, 2.68mM KCl, 1.84mM $CaCl_2$ dihydrate, 1.03mM $MgCl_2$ hexahydrate, 5.55mM dextrose, 11.91mM $NaHCO_3$, and 0.44mM NaH_2PO_4 anhydrous at pH 7.4. Stainless-steel hooks were fastened to the tendons of the muscles using 4-0 silk sutures, and muscles were placed between a force transducer (Aurora Scientific Inc., Aurora, ON, Canada) and an adjustable hook. Muscles were then submerged in a stimulation chamber containing O_2/CO_2 (95/5%) bubbled in Ringer's solution and placed between two platinum electrodes. Muscles were stimulated to contract by the electrodes, and the contraction data was recorded by the Dynamic Muscle Control/Data Acquisition (DMC) and Dynamic Muscle Control Data Analysis (DMA) programs (Aurora Scientific Inc., Aurora, ON, Canada). The muscle length was then adjusted to yield the maximum force before the initiation of force-frequency or fatigue stimulation regimens. The force-frequency stimulation regimen triggered contraction using incremental stimulation frequencies (0.5ms pulses at 1-150Hz for 350ms at supramaximal voltage of 1A). Between stimulations the muscle was allowed to rest for 1 minute for frequencies ranging between 1 and 70Hz, or for 3 minutes for frequencies ranging between 100 and 150Hz. For the force-frequency analysis, the specific force was calculated by dividing the absolute force by the whole muscle cross sectional area (CSA), which was calculated using the following equation: CSA (mm^2) = mass (mg) / [($L_o$mm) x (L/L_o) x (1.06 mg/mm^3)], where $L_o$mm is the optimal length, L/L_o is the fiber to muscle length ratio, and 1.06 mg/mm^3 is the density of muscle (134). L/L_o of 0.51 and 0.72 were used for the EDL and soleus muscles, respectively, following previous reports (135). The fatigue

stimulation regimen consisted of 50 or 150 repeated stimulation pulses for the EDL or soleus muscles respectively, at 70Hz occurring every 0.7 seconds.

Study approval. All animal protocols were approved by the Institutional Animal Care and Use Committee at Indiana University School of Medicine, and animal care was carried out in accordance with institutional guidelines.

Tissue and BMD measurements and micro-computed tomography (μCT) analysis. Mice anesthetized by inhalation of 1.7% isoflurane (Abbott Laboratories) mixed with O_2 (1.5 liters/minute) were scanned using dual energy x-ray absorptiometry (DXA) with a PIXImus II densitometer (GE Medical Systems, Lunar Division, Madison, WI, USA) (94). BMD of the total body excluding the head and tail, the lumbar spine (L_1-L_6), and the femur, and lean body mass were quantified. Body weight and DXA measurements were performed 2-4 days prior to implantation (initial) and after 14 or 28 days (final). Percent changes in body weight, lean body mass, and BMD were calculated with the following formula: [(final-initial)/initial] x 100.

For μCT analysis, bones were dissected, cleaned of soft tissue, and stored in 70% ethanol until used. The distal femur and proximal tibia metaphysis was scanned at 6μm resolution (Skyscan 1172; SkyScan, Aartselaar, Belgium). Measurements were done 60μm away from the growth plates, as described (93;94).

Bone dynamic histomorphometry. Following μCT analysis, tibiae were then embedded in methyl methacrylate, and thick cross-sections at the mid-diaphysis were prepared using a diamond-embedded wire saw (Histosaw, Delaware Diamond Knives, Wilmington, DE, USA) and ground to a final thickness of 30–35μm for periosteal and endosteal bone formation measurements (136). Four μm-thick longitudinal sections of the proximal half of the tibia were also prepared for cancellous bone measurements. Fluorochrome labels were quantified using OsteoMeasure High Resolution Digital Video System (OsteoMetrics, Decatur, GA, USA) (137). To calculate bone formation rate

91

(BFR/BS) when only single labels were present, a value of 0.1μm/day was used for mineral apposition rate (MAR) (137;138). Terminology and units are those recommended by the Histomorphometry Nomenclature Committee of the ASBMR (139).

Ex vivo bone and muscle organ cultures. Femoral and tibial long bones were harvested from C57BL/6 female and male mice, and marrow was flushed out using a sterile syringe. Bones were then maintained in α-MEM containing 10% FBS and 1% penicillin/streptomycin for 24 hours, followed by addition of 1μM dexamethasone or vehicle (ethanol), in the absence or presence of 5mM GSI XX, and cultured for an additional 6 hours. Tibialis anterior muscles were isolated from 1-month-old C57BL/6 female and male mice and placed in 48-well plates. Muscles were rinsed with PBS and incubated in DMEM containing 10% FBS, 1% penicillin/streptomycin (Life Technologies Carlsbad, CA, USA) overnight. Media was replaced with DMEM + 10% FBS containing DMSO or 0.1μM GSI XX, together with vehicle or 1μM dexamethasone for 12 or 24 hours. mRNA was isolated from bone and muscle samples to examine gene expression.

Cell culture. Murine bone marrow derived OB-6 osteoblastic cells (61) and long bone-derived MLO-Y4 osteocytic cells (28) were cultured as previously published. Murine C2C12 myoblasts were purchased from ATCC and maintained at low confluence in DMEM medium containing high glucose, sodium pyruvate, 1% penicillin/streptomycin (Life Technologies Carlsbad, CA, USA), and 10% fetal bovine serum at 5% CO_2. To induce differentiation, C2C12 cells were grown to confluency and then switched to 10% CO_2 and 2% horse serum DMEM medium (140). After 72 hours, 1μM dexamethasone, 0.03-0.1μM GSI XX, or this combination were added for 24 hours, and RNA was extracted to analyze gene expression, or cells were fixed for myotube diameter measurement.

RNA extraction and qPCR. Total RNA was extracted using Trizol (Invitrogen, Carlsbad, CA, USA), and cDNA was synthesized with a high-capacity cDNA reverse

transcriptase kit (Applied Biosystems, Inc., Foster City, CA, USA). qPCR was performed as previously described (137). Relative mRNA expression levels were normalized to the housekeeping genes mitochondrial ribosomal protein S2 (Rplp2) or glyceraldehyde 3-phosphate dehydrogenase (GAPDH) by using the ΔCt method (93;137). All primers and probes were designed using the Assay Design Center (Roche Applied Science, Indianapolis, IN, USA) or were commercially available (Applied Biosystems, Inc., Foster City, CA, USA).

Myotube diameter measurement. C2C12 myotube diameter was measured as previously published (140). Briefly, cells were fixed and permeabilized in ice cold acetone/methanol (1:1) at -20°C for 20 minutes, rehydrated for 10 minutes in PBS at room temperature. Subsequently, cells were incubated with an antibody against myosin heavy chain (Developmental Studies Hybridoma Bank, Iowa City, IA, USA) overnight at 4°C with gentle agitation, followed by incubation with anti-mouse IgG labeled with green-fluorescent Alexa Fluor 488 dye as secondary antibody (Life Technologies, Carlsbad, CA, USA), for 1 hour at room temperature and protected from light. Nuclei were stained with DAPI and the images captured on an Axio Observer.Z1 (Zeiss) microscope. Myotube diameter was measured using ImageJ analysis software (Wayne Rasband, U.S. National Institutes of Health). All treatment conditions were performed in triplicate.

Statistical analysis. Data are expressed as means ± standard deviations (SD). Sample differences were evaluated using SigmaPlot 12.0 (Systat Software, Inc., San Jose, CA, USA). Differences between groups were detected by Student's *t*-test or two-way ANOVA followed by the Tukey post-hoc method. Force-frequency relationships of muscle contraction, both *ex vivo* absolute and specific force and *in vivo* plantarflexion torque, and fatigue curves were analyzed by mixed-model, two-way repeated-measures ANOVA followed by Tukey post-hoc tests. To determine potential differences in fatigability, *ex vivo* fatigue data were also analyzed with Ordinary Least Squares

regression on group mean data for each stimulation number. For both treatment groups (glucocorticoid and placebo), two regressions were calculated: one fit to the first 10% of the stimulations and one fit to the last 90% of the stimulations. Differences in slope between groups for the 10% data and the 90% data were compared by Student t-test, as previously reported (141-143).

Results

Glucocorticoids induce atrophy in bone and muscle in vivo. Total BMD and total, femoral and spinal BMD were decreased by glucocorticoids after 14 or 28 days, respectively (**Figure 5-1A**). Trabecular thickness of cancellous bone of the distal femur and proximal tibia metaphysis were also reduced after 14 days (**Figure 5-1B** and **C**). Bone formation rate (BFR/BS) was suppressed by 14 days in the cancellous bone of the proximal tibia, as well as in the periosteal and endocortical surfaces of the tibia mid-diaphysis (**Figure 5-1C** and **D**). The decrease in BFR/BS was the result of a decrease in mineral apposition rate (MAR) and of mineralizing surface (MS/BS) in all bone envelopes.

Glucocorticoids also caused muscle atrophy, as measured by reductions in total lean mass, an index of skeletal muscle mass, after 14 or 28 days (**Figure 5-2A**). In addition, glucocorticoids decreased at both time points the mass of the tibialis anterior (**Figure 5-2B** and **C**) and extensor digitorum longus (EDL) muscles (**Figure 5-2B** and **D**), the latter composed mainly of fast-twitch fibers and known to be affected by glucocorticoids (144-146). The weight of the soleus muscle, mainly composed of slow-twitch fibers and known to be more resistant to glucocorticoid-induced atrophy, was not affected after 14 days of glucocorticoid administration (**Figure 5-2C**); and at 28 days, soleus mass was minimally but significantly decreased in one experiment (**Figure 5-2C**), but not affected in another experiment (**Figure 5-2D**). In the experiment in which the soleus mass was not decreased, glucocorticoids still reduced the *ex vivo* contractility force generated by both EDL and soleus muscles in response to force frequency and fatigue electrode stimulation regimens (**Figure 5-2D**). Both EDL and soleus muscles from mice receiving glucocorticoids exhibited a reduction in absolute contraction force compared to muscles from mice receiving placebo, as quantified by the force frequency test (**Figure 5-2D**, middle panels). However, only soleus muscles from glucocorticoid-

95

treated mice exhibited a reduced specific contraction force compared to placebo, whereas specific contraction forces exhibited by EDL muscles were not different between groups, indicating that the decreased absolute force displayed by the EDL muscles is driven by tissue loss. During fatigue testing, the contraction force decreases rapidly for the first 10% of stimulations and more slowly for the last 90% of stimulations, independently of muscle type or treatment. Both EDL and soleus muscles from glucocorticoid-treated mice exhibited lower contraction force compared to muscles from placebo-treated mice (**Figure 5-2D**, right panels). The EDL muscles fatigued at a lower rate in glucocorticoid-treated mice compared to placebo-treated mice in both regions of the curve, as demonstrated by statistically lower slope values of the regression lines compared by *t*-test (legend of **Figure 5-2**). In contrast, soleus muscles from glucocorticoid-treated mice fatigued at the same rates as placebo-treated mice in both the first 10% and last 90% of stimulations, as the slopes of regression lines were not statistically different between groups. The EDL muscles from glucocorticoid-treated mice reached their lowest contraction force sooner than the placebo treated mice (approximately at 40 versus 50 stimulations) (**Figure 5-2D**, right panels). In contrast, the soleus muscles from glucocorticoid-treated and placebo treated mice reached their lowest contraction force at the same stimulation number (approximately 120 simulations). These results suggest that glucocorticoid affects differently the endurance of fast- versus slow-twitch muscles.

In addition, glucocorticoids reduced maximum plantarflexion torque assessed *in vivo* at 14 and 28 days of treatment (**Figure 5-2E**). This test reflects the combined strength of posterior compartment leg muscles (gastrocnemius, soleus, tibialis posterior, fibularis brevis and longus, flexor hallucis longus, flexor digitorum longus and plantaris muscles). Thus, prednisolone administration consistently induces muscle atrophy as well as muscle weakness in our murine model of glucocorticoid excess.

Glucocorticoids increase the expression of atrophy genes in bone and muscle in vivo and in vitro. Earlier evidence showed that muscle atrophy induced by injury or disuse is associated with increased expression of the E3 ubiquitin ligases atrogin1, MuRF1, and MUSA1 with the consequent increase in protein ubiquitination, proteasomal protein catabolism, and reductions in total protein content (125;131;147). Traditionally, atrogin1, MuRF1, and MUSA1 have been considered as selectively expressed in skeletal muscle. However, detectable levels of these transcripts were found also in bone at lower detection levels, with average Ct values of approximately 30 in bone, compared to 20-25 Ct values in tibialis anterior and soleus muscles. Glucocorticoids increased the expression of atrogin1 and MuRF1 after 14 or 28 days in both bone and the tibialis anterior muscle (**Figure 5-3A**). MUSA1 expression was also increased in bone and the tibialis anterior muscle from mice receiving prednisolone for 28 days. Consistent with the previously reported resistance to glucocorticoids of type I slow twitch muscle fibers (144;145), 14 days of glucocorticoid exposure did not increase atrophy gene mRNA expression in the slow-twitch dominated soleus muscle. However, after 28 days of glucocorticoid exposure MuRF1 expression levels were increased in the soleus. Glucocorticoids also increased atrophy gene expression in *ex vivo* bone organ cultures (**Figure 5-3B**), in osteoblastic OB-6 cells (**Figure 5-3C**) and osteocytic MLO-Y4 cells (**Figure 5-3D)** treated with the synthetic glucocorticoid dexamethasone. Furthermore, dexamethasone also increased the expression of atrogin1 and MuRF1 in C2C12 cultured under non-differentiating (myoblasts) and differentiating (myotubes) conditions (**Figure 5-3E**). Overall, these results indicate that atrophy-related gene expression is increased by glucocorticoids in bone and muscle *in vivo* and *in vitro*.

Glucocorticoids increase expression of Notch signaling pathway components in skeletal muscle, but not in bone. In vivo glucocorticoid administration to mice for 14 or 28 days did not alter the levels of the Notch receptors 1-4, the Notch ligands Dll1 and Jag1,

or the Notch target genes Hey1 and Hes1 in bone (**Figure 5-4A**). In addition, dexamethasone decreased the expression of Notch ligand Dll1 and Notch target genes Hey1 and Hes1 without altering the levels of Notch receptors 1-4 in both femoral and tibial *ex vivo* bone organ cultures (**Figure 5-4B**). Notch ligand Jag1 mRNA levels were also decreased by dexamethasone in femoral bone organ cultures; however, Jag1 expression was not affected in tibial organ cultures. Glucocorticoids also decreased the expression of most Notch receptors and ligands, with the exception of Notch 4 expression in OB-6 cells, without altering the levels of the target gene Hey1 in either cell type (**Figure 5-4C** and **D**). The expression of the Notch target gene Hes1 was also lowered by dexamethasone in OB-6 and MLO-Y4 cells. Thus, overall glucocorticoids did not increase, and in some cases decreased, the expression of Notch signaling components in bone *in vivo, ex vivo,* or *in vitro.*

In contrast, *in vivo* glucocorticoids increased the levels of Notch receptors, ligands, and target genes in the tibialis anterior at both 14 and 28 days (**Figure 5-5A**). Further, addition of dexamethasone for 12 or 24 hours increased the expression of multiple Notch target genes in *ex vivo* organ cultures of tibialis anterior (**Figure 5-5B**). Moreover, addition of the Notch signaling pharmacologic inhibitor GSI XX to muscle organ cultures effectively blocked both the increase in Notch target genes (**Figure 5-5B**) and the increase in atrogin1, MuRF1, and MUSA1 gene expression increased by dexamethasone (**Figure 5-5C**). In contrast, GSI XX did not prevent the increase in atrogin1 and MuRF1 in bone organ cultures. In addition, dexamethasone induced a ~20% reduction in myotube diameter of C2C12 cells, which was also prevented by the GSI XX inhibitor (**Figure 5-5D**). These results suggest that upregulation of atrophy-related genes and myotube atrophy induced by glucocorticoids is at least partially mediated by activation of the Notc signaling pathway in muscle, but not in bone.

Discussion

The current study demonstrates that glucocorticoids activate different signaling pathways in bone and muscle that result in upregulation of atrophy-related E3 ubiquitin ligases and identifies the Notch signaling pathway as a potential target to prevent glucocorticoid-induced muscle atrophy (**Figure 5-6**).

Our findings demonstrate that glucocorticoids increased the expression of several E3 ubiquitin ligases in both bone and muscle *in vivo* in the well-established model of glucocorticoid excess, in *ex vivo* bone and muscle organ cultures, and *in vitro* in osteoblastic and osteocytic cell lines, as well as in myoblasts and myotubes. To our knowledge, this is the first report of expression in bone of atrogin1, MuRF1, and MUSA1, heretofore considered muscle-specific atrophy genes, as well as their upregulation by glucocorticoids. The relevance of atrophy gene expression for the action of glucocorticoids in bone is unknown. However, earlier studies showed that genetic global deletion in mice of MuRF1 protects from the loss of bone induced by hind limb unloading (148). MuRF1 KO mice were also protected from the decrease in histomorphometric measures of bone formation and the increase in osteoclasts in this model (148). This evidence, together with our current findings, raises the possibility that upregulation of MuRF1, and potentially other atrophy-related genes, contribute to the reduced bone formation and increased bone resorption induced by glucocorticoids, and suggests that targeting the atrophy pathway could interfere with glucocorticoid action in bone. Future studies will be required to directly examine the role of atrophy-related genes in glucocorticoid-induced bone disease.

Extensive evidence demonstrates that the C57BL/6 mouse model of glucocorticoid excess used in our study reproduces their deleterious effects on bone (26;41;118). In addition, we recently reported that glucocorticoids also decrease muscle mass in this model (118), and we now show that glucocorticoids decreased skeletal

muscle mass as early as after 14 days, quantified by lean body mass, as well as the mass of individual muscles, in particular those rich in fast-twitch fibers like the EDL. Importantly, muscles from glucocorticoid-treated mice exhibited decreased strength (force) quantified *ex vivo* by contractility tests of individual muscles and *in vivo* by measuring isometric plantarflexion torque generated by muscles of the posterior compartment of the leg. Remarkably, we detected decreased strength (specific force) in the slow-twitch soleus muscle in the absence of reduction of soleus mass, suggesting that glucocorticoids might alter muscle function in the absence of detectable tissue loss, at least in muscles traditionally considered resistant to glucocorticoids (144;145). In contrast, the reduction in strength in the EDL muscle can be explained by loss of muscle mass, as it is corrected by normalizing per tissue mass. The lower rate of fatigue detected in the fast-twitch EDL muscles treated with glucocorticoids compared to placebo-treated muscles is potentially explained by the fact that EDL muscles are mainly composed of the highly fatigable myosin-rich type 2 fibers, which are preferential targets of glucocorticoid-induced muscle atrophy (149;150). Therefore, glucocorticoid treatment might induce loss mainly of highly fatigable fibers and thus the remaining fibers fatigue more slowly in EDL muscles from animals treated with prednisolone. In contrast, slow-twitch soleus muscles fatigue at the same rate in glucocorticoid- and placebo-treated mice despite reductions in overall strength induced by glucocorticoids, revealing another distinction between the effects of glucocorticoids depending on the muscle type. This effect may in part explain the proximal myopathy seen in patients with diseases of excess corticosteroid secretion and patients treated with pharmacological doses of corticosteroids. The current findings with the C57BL/6 mouse model of glucocorticoid excess are consistent with the previously reported reduction in muscle fiber specific force in humans treated with glucocorticoids (122). Importantly, the reduction in muscle mass correlated with increased expression of the atrophy genes. Future studies are

warranted to establish the role of E3 ubiquitin ligases in muscle weakness induced by glucocorticoids.

Activation of the Notch signaling pathway has been shown to be required for expansion of the satellite cell population, a known critical event for skeletal muscle repair (151;152). In addition, Notch signaling inhibits myogenic differentiation of progenitor cells by decreasing MyoD and myogenin expression and by reducing MyoD activity (151;153;154). These findings support the notion that Notch signaling is crucial for maintaining the self-renewal capacity of muscle satellite cells. Our current study reveals a novel role of the Notch pathway in the frame of glucocorticoid excess, as it shows that the expression of components of this pathway was strikingly upregulated by glucocorticoids in skeletal muscle. Moreover, inhibition of Notch signaling with the gamma secretase inhibitor GSI XX blocked the upregulation of atrophy-related genes and prevented the reduction in C2C12 myotube diameter induced by glucocorticoids.

In contrast to the effects of glucocorticoids on muscle, glucocorticoids did not increase the expression of components of the Notch pathway in our *in vivo, ex vivo*, or *in vitro* models of bone and osteoblastic/osteocytic cells. Earlier work showed transient increases in Notch1 and Notch2 gene expression in osteoblastic MC3T3 cells treated with cortisol (155). However, similar to our study, the expression Dll1 and Jag1 Notch ligands was not altered by cortisol treatment in this previous study. Therefore, we can conclude that glucocorticoids activates Notch signaling in muscle, but not in bone, to induce atrophy. The mechanism underlying the upregulation of atrophy genes by glucocorticoids in bone remains unknown. However, it is possible that FoxO transcription factors are involved. In muscle, FoxO family members (FoxO1, 3, and 4) regulate the expression of atrogin1, MuRF1, and MUSA1 and are required for the full atrophic response to several inducers of skeletal muscle wasting, including starvation/fasting, denervation, and chronic kidney disease (156-158). In bone, FoxOs are activated by and

are critical for the defense against oxidative stress (ROS) (159). In addition, at least part of the effects of glucocorticoids in bone are due to accumulation of ROS as well as to endoplasmic reticulum (ER) stress, and are abolished by ROS or ER stress inhibitors (41). Furthermore, activation of FoxO in osteoblasts by glucocorticoids is blocked by ROS inhibition (55). Moreover, FoxO-mediated transcription is favored over Wnt/β-catenin transcription (55); and activation of Wnt/β-catenin signaling protects from glucocorticoid-induced osteoporosis (118). Future studies will be required to reveal the role of FoxOs in the upregulation of atrophy-related genes by glucocorticoids in bone.

In conclusion, our study identifies atrophy-related E3 ubiquitin ligases as potential mediators of bone and muscle atrophy induced by excess of glucocorticoids and points towards the Notch signaling pathway as a novel target to prevent glucocorticoid-induced muscle atrophy. These findings provide the basis for combination therapy using inhibitors that target signaling upstream of atrophy-related genes in each tissue to prevent glucocorticoid-induced osteopenia and sarcopenia.

Acknowledgments

Figure 5-1. Glucocorticoids induce atrophy of bone and suppression of bone formation. Female C57BL/6 mice were implanted with pellets releasing 2.1 mg/kg/day of prednisolone or placebo and BMD was assessed 14 or 28 days later. **(A)** Percent change in BMD was measured by DXA and calculated utilizing initial scans performed before pellet implantation and final scans performed at the indicated time points. **(B and C)** Trabecular thickness was measured by µCT analysis at the distal femur **(B)** and

proximal tibia metaphysis **(C)**. **(C** and **D)** Dynamic histomorphometric parameters on the cancellous bone of proximal tibia **(C)** and periosteal and endocortical surfaces of the tibia mid-diaphysis **(D)** were measured in mice treated for 14 days with placebo or prednisolone. Bars represent means ± SD. N=7-10. *p<0.05 vs. placebo-treated mice by Student's *t*-test.

Figure 5-2. Glucocorticoids induce muscle loss and weakness. (A) Percent change whole body lean mass determined by DXA. **(B)** Scheme depicting the position of the muscles tibialis anterior (TA), extensor digitorum longus (EDL), and soleus (SOL)

106

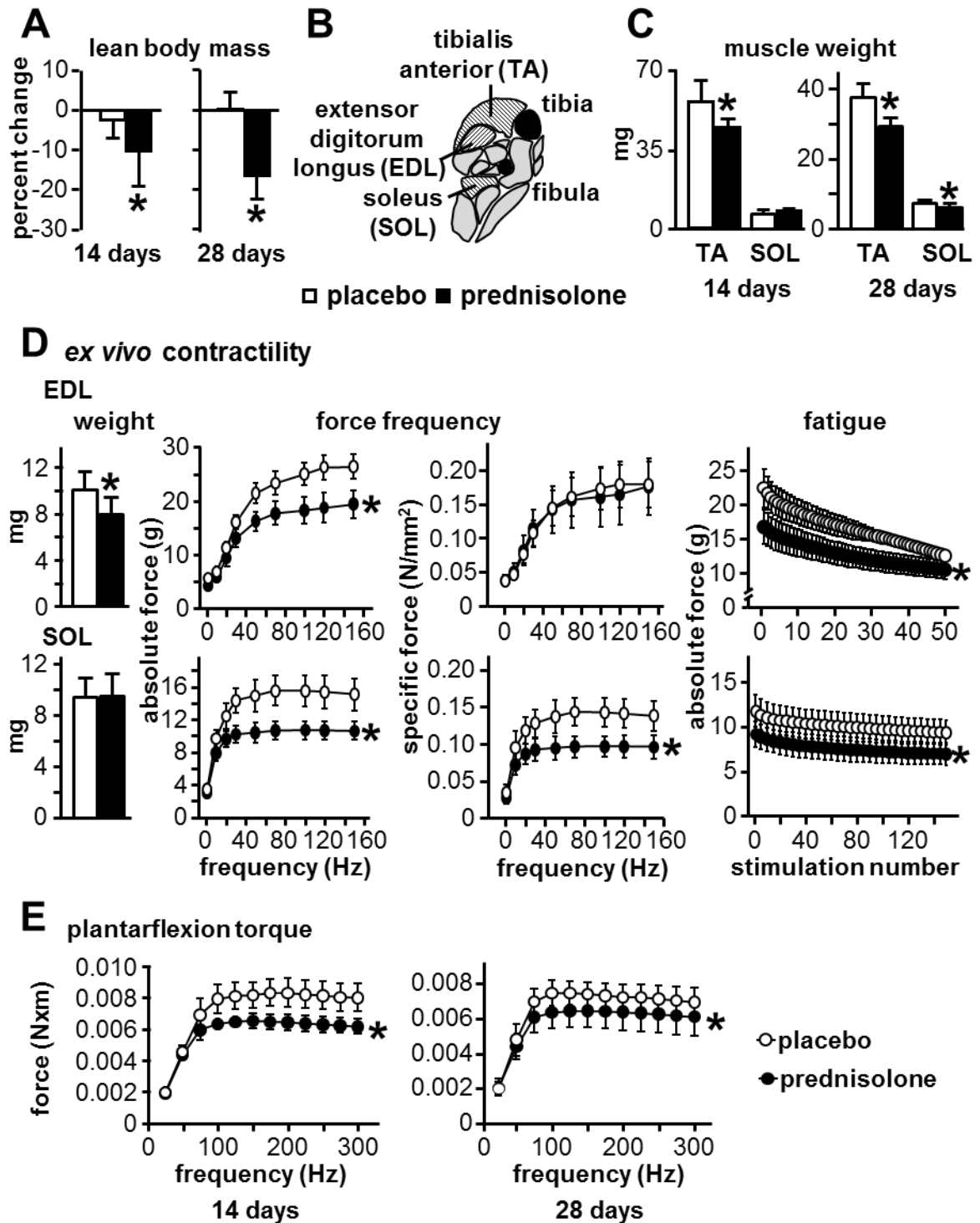relative to the tibia. **(C)** Wet weight of tibialis anterior and soleus muscles recorded 14 or 28 days after pellet implantation. **(D)** Wet weight of EDL and soleus muscles and *ex vivo* contractility muscle function testing recorded 28 days after pellet implantation. **(E)** Muscle function testing performed *in vivo* 14 and 28 days after pellet implantation. Bars represent means ± SD. N=7-10 for **A** and **C** and N=8-10 for **D** and **E**. *p<0.05 vs. placebo by Student's *t*-test for **A-C** and muscle weights in **D**. *p<0.05 vs. placebo by two-factor, mixed-model repeated measures ANOVA followed by Tukey post-hoc method for muscle functionality tests in **D** and **E**. For the fatigue tests in **D**, regression line equations for EDL muscles were the following: for the first 10% of the stimulations, y = -0.5387x + 22.784 (placebo) and y = -0.3549x + 17.033 (glucocorticoids), p<0.05 by *t*-test; and for the last 90% of the stimulations, y = -0.1601x + 20.474 (placebo) and y = -0.102x + 15.181 (glucocorticoids), p<0.05 by *t*-test. Regression line equations for soleus muscles were the following: for the first 10% of the stimulations, y = -0.0658x + 11.72 (placebo) and y = -0.0641x + 9.2375 (glucocorticoids), not significant by *t*-test; and for the last 90% of the stimulations, y = -0.0102x + 10.778 (placebo) and y = -0.0097x + 8.2384 (glucocorticoids), not significant by *t*-test.
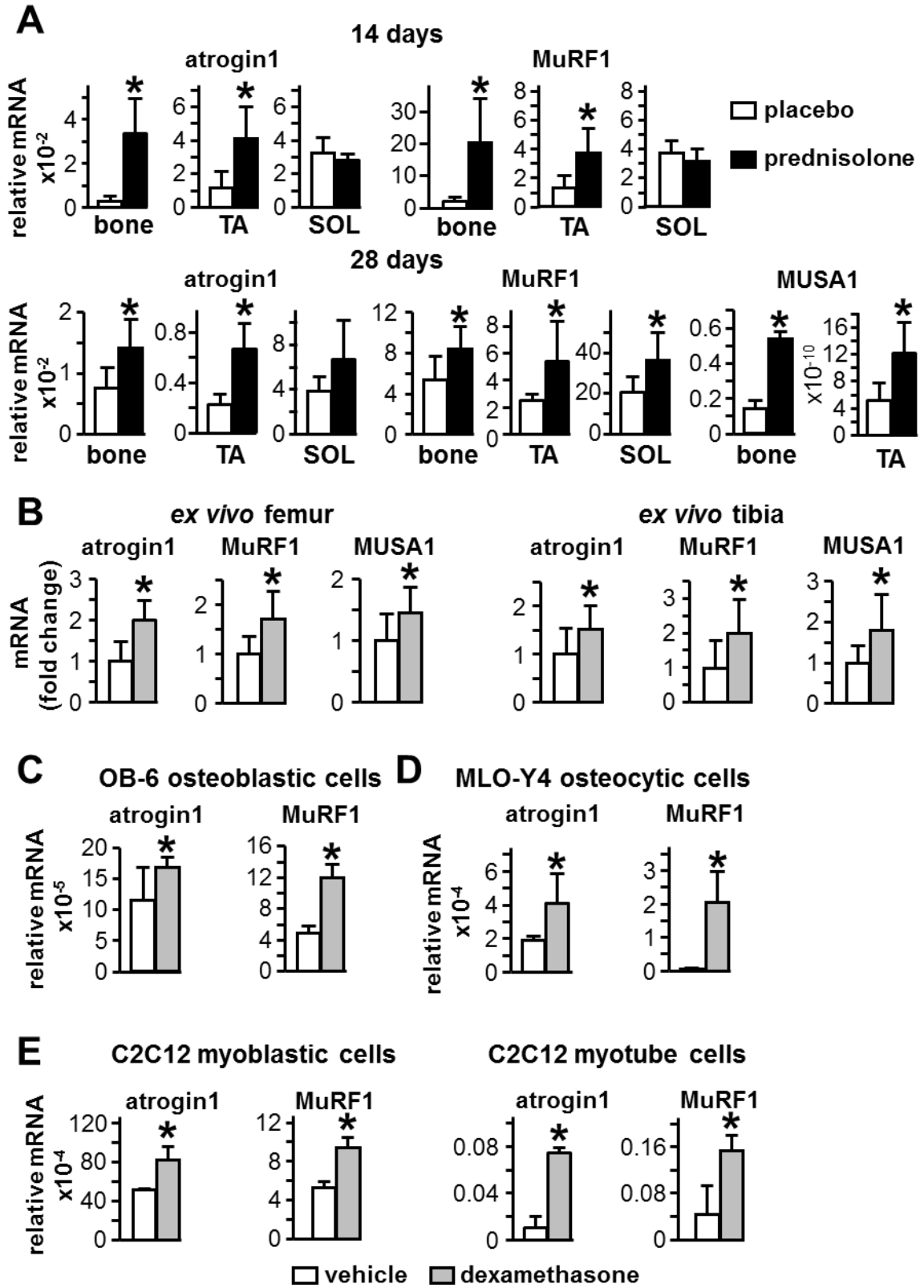
Figure 5-3. Glucocorticoids promote the transcription of atrophy genes *in vivo, ex vivo,* and *in vitro*. (A) mRNA levels were quantified in vertebral bone L4 (bone), and TA and SOL muscle preparations. The transcripts were normalized to the levels of the housekeeping gene glyceraldehyde 3-phosphate dehydrogenase (GAPDH). Bars represent means ± SD. N=5-7 for L4, N=8-10 for TA and SOL. *p<0.05 vs. placebo-treated mice by Student's *t*-test. **(B)** Gene expression in bones from C57BL/6 mice cultured with vehicle or 1μM dexamethasone for 6 hours. Bars represent means ± SD. N=9-12. *p<0.05 vs. vehicle-treated cells by Student's *t*-test. **(C)** OB-6 osteoblastic cells and **(D)** MLO-Y4 osteocytic cells were treated with vehicle or 1μM dexamethasone for 24 hours. RNA was extracted and atrogin1 and MuRF1 levels were quantified by qPCR. Bars represent means ± SD. N=5-6. *p<0.05 vs. vehicle-treated cells by Student's *t*-test. **(E)** C2C12 myoblasts were kept in growing media or induced to differentiate into myotubes for 6 days. Cells were treated with vehicle or 1μM dexamethasone for 24 hours, RNA was extracted and atrogin1 and MuRF1 levels were quantified by qPCR. The transcripts were normalized to the levels of the housekeeping GAPDH. Bars represent means ± SD. N=3 for myoblasts N=6 for myotubes. *p<0.05 vs. vehicle-treated cells by Student's *t*-test.
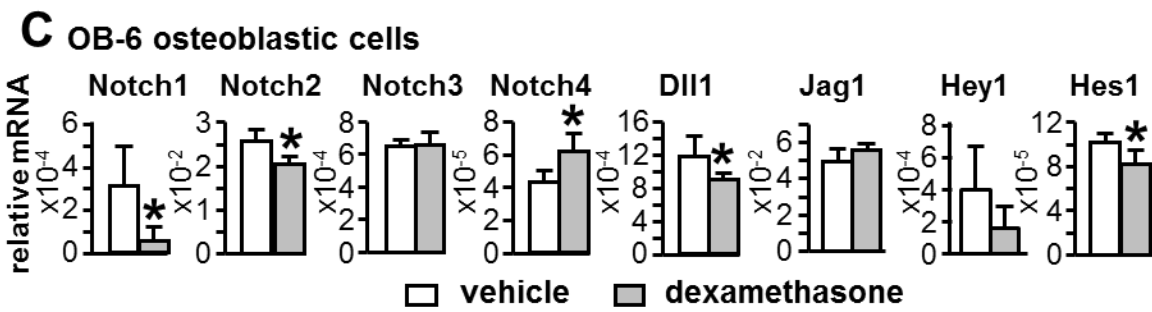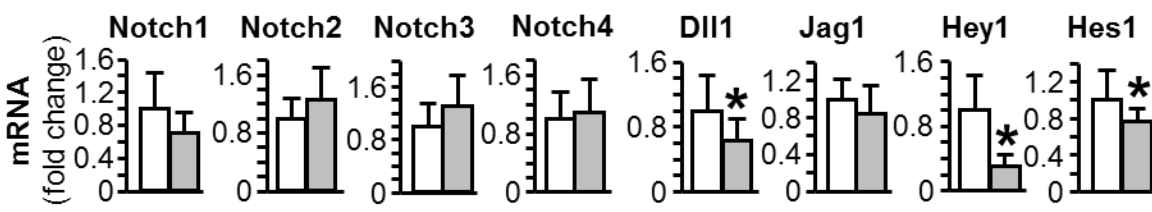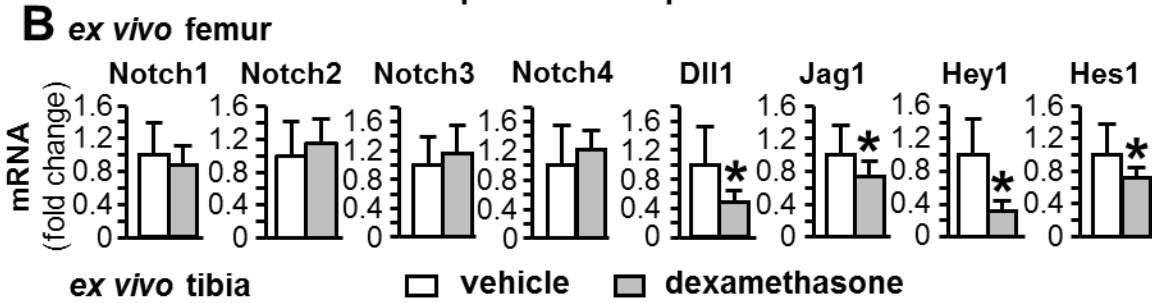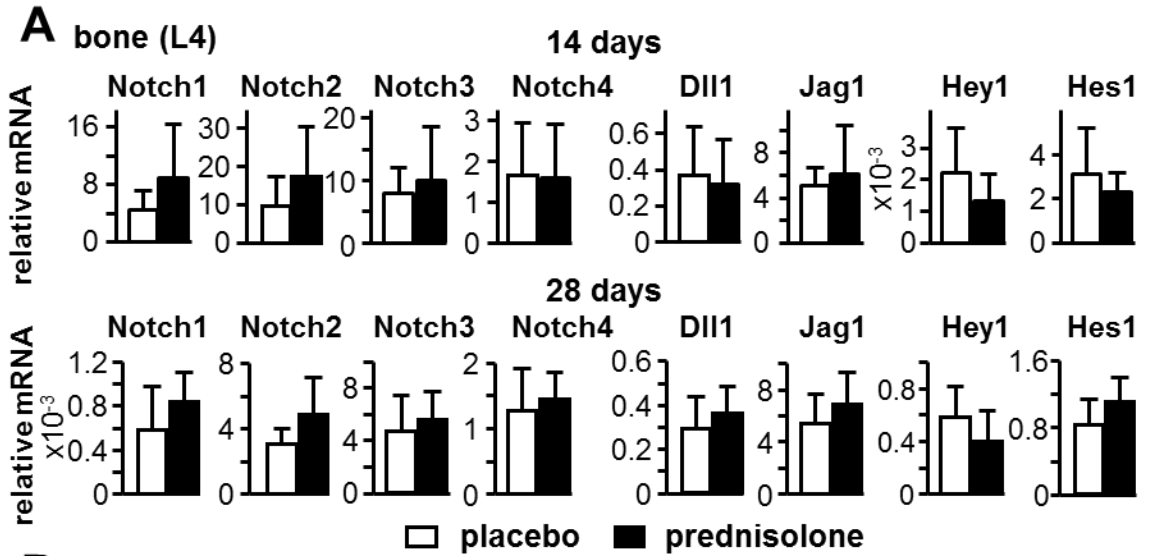
Figure 5-4. Glucocorticoids do not induce Notch activation in bone *in vivo, ex vivo*, or *in vitro*. The expression of the indicated genes normalized to GAPDH was measured by qPCR in **(A)** bone preparations obtained from mice treated with placebo or prednisolone for 14 or 28 days, and **(B)** in bones from C57BL/6 mice cultured with vehicle or 1μM dexamethasone for 6 hours. Bars represent means ± SD. N=9-10 for **(A)** and N=10-12 for **(B)**. *p<0.05 vs. placebo-treated mice or vehicle-treated bones by Student's *t*-test. Gene expression was measured in **(C)** OB-6 osteoblastic or **(D)** MLO-Y4 osteocytic cells treated with vehicle or 1μM dexamethasone for 24 hours. Bars represent means ± SD. N=5-6 for **(C),** and N=6 for **(D)**. *p<0.05 vs. vehicle-treated cells by Student's *t*-test.
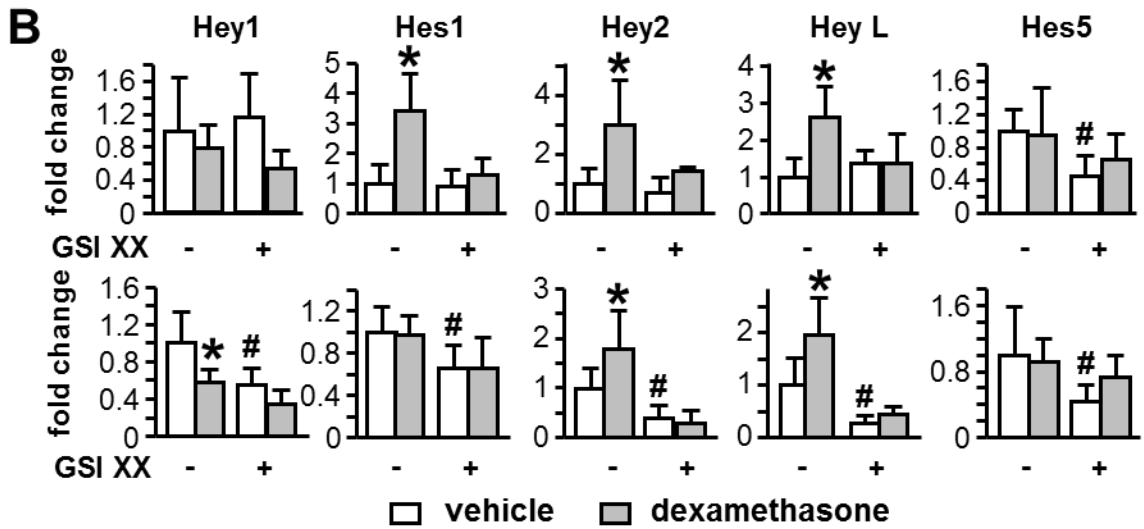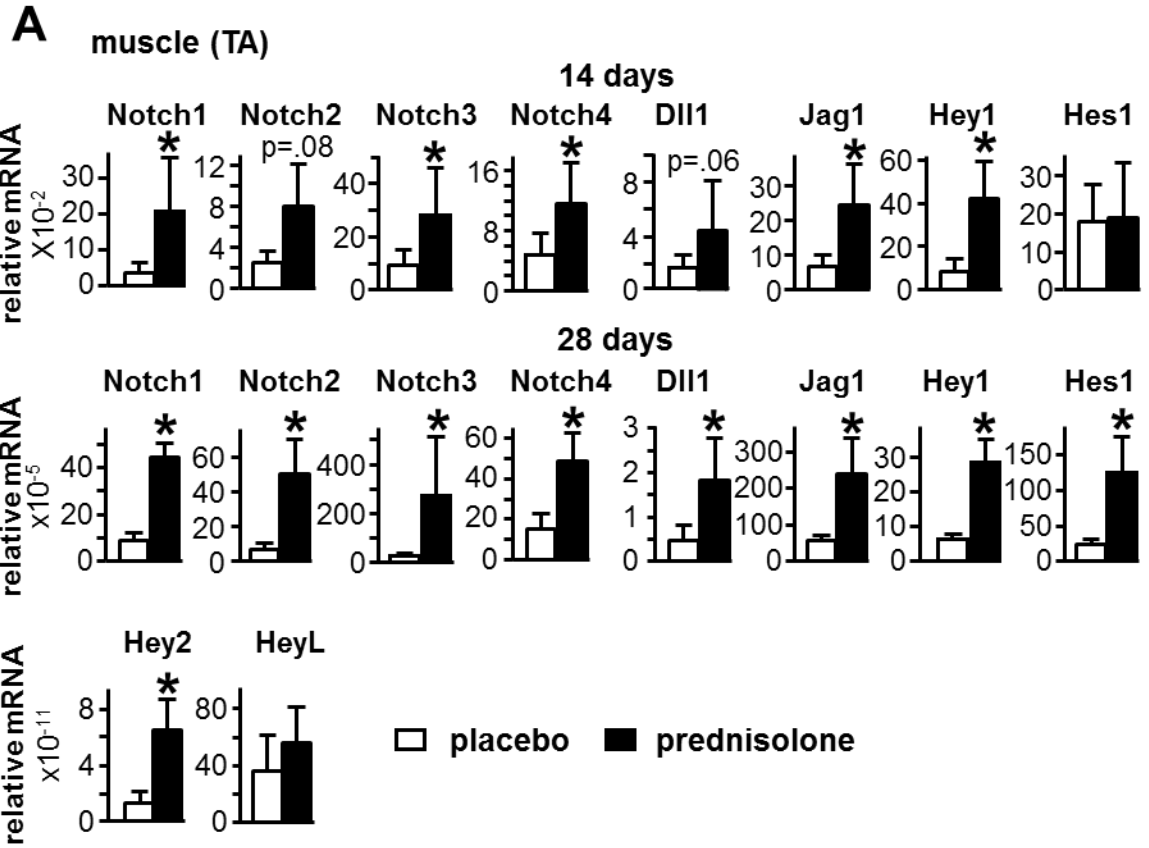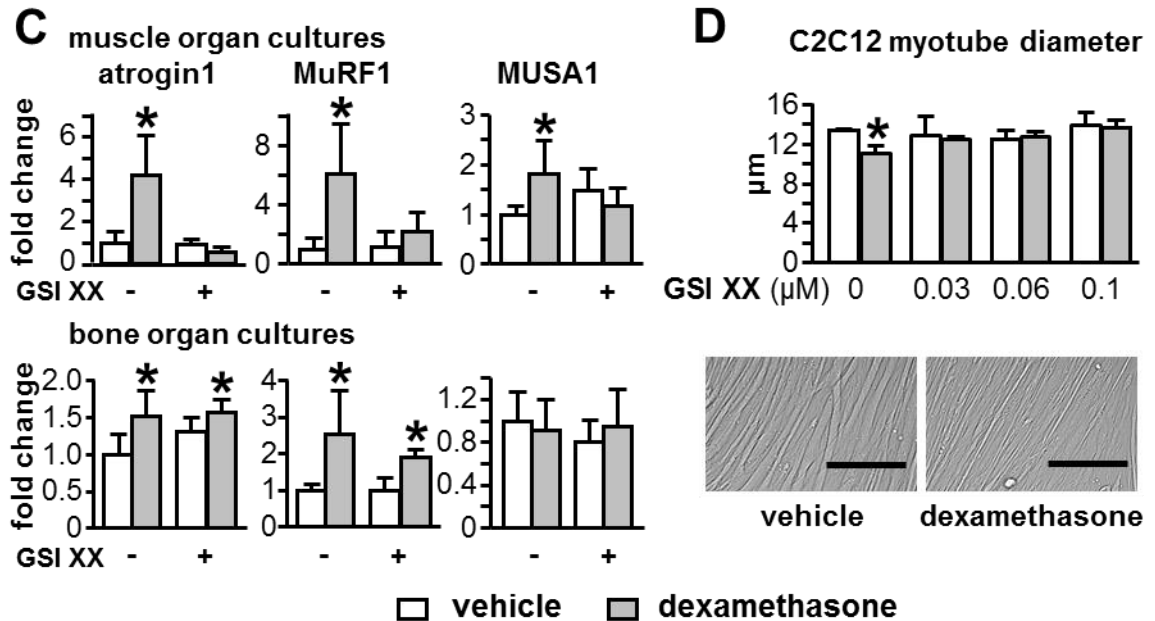
Figure 5-5. Glucocorticoids increase the expression of Notch signaling pathway components in muscle, and Notch inhibitor GSI XX prevents glucocorticoid-induced atrophy-related gene expression and reduction in myotube diameter. (A) The expression of the indicated genes normalized to GAPDH was measured by qPCR in TA muscles from mice treated with placebo or prednisolone for 14 or 28 days. Bars represent means ± SD. N=6. *p<0.05 vs. placebo-treated mice by Student's *t*-test. **(B-C)** TA muscles or tibial bones were isolated from C57BL/6 mice and cultured with vehicle or 1μM dexamethasone in the presence and in the absence of the Notch inhibitor GSI XX for 12 (**B** top row and C top row) or 24 (**B** bottom row) hours for TA and 6 hours for tibia (**C** bottom row). RNA was isolated and the levels of the indicated genes were measured by qPCR and normalized to Rplp2. Bars are mean ± SD. N=5-7. *p<0.05 vs. corresponding vehicle-treated muscles and #p<0.05 vs. vehicle-treated muscles in the absence of GSI XX by two-way ANOVA, Tukey post-hoc test. **(D)** C2C12 cells were differentiated into myotubes and treated with vehicle or 1μM dexamethasone in the absence or in the presence of the indicated concentrations of GSI XX. Myotube diameter was measured as indicated in the Materials and Methods section. Scale bars = 200μm.

Bars represent means ± SD. N=3. *$p<0.05$ vs. vehicle-treated cells by two-way ANOVA,

Tukey post-hoc test.
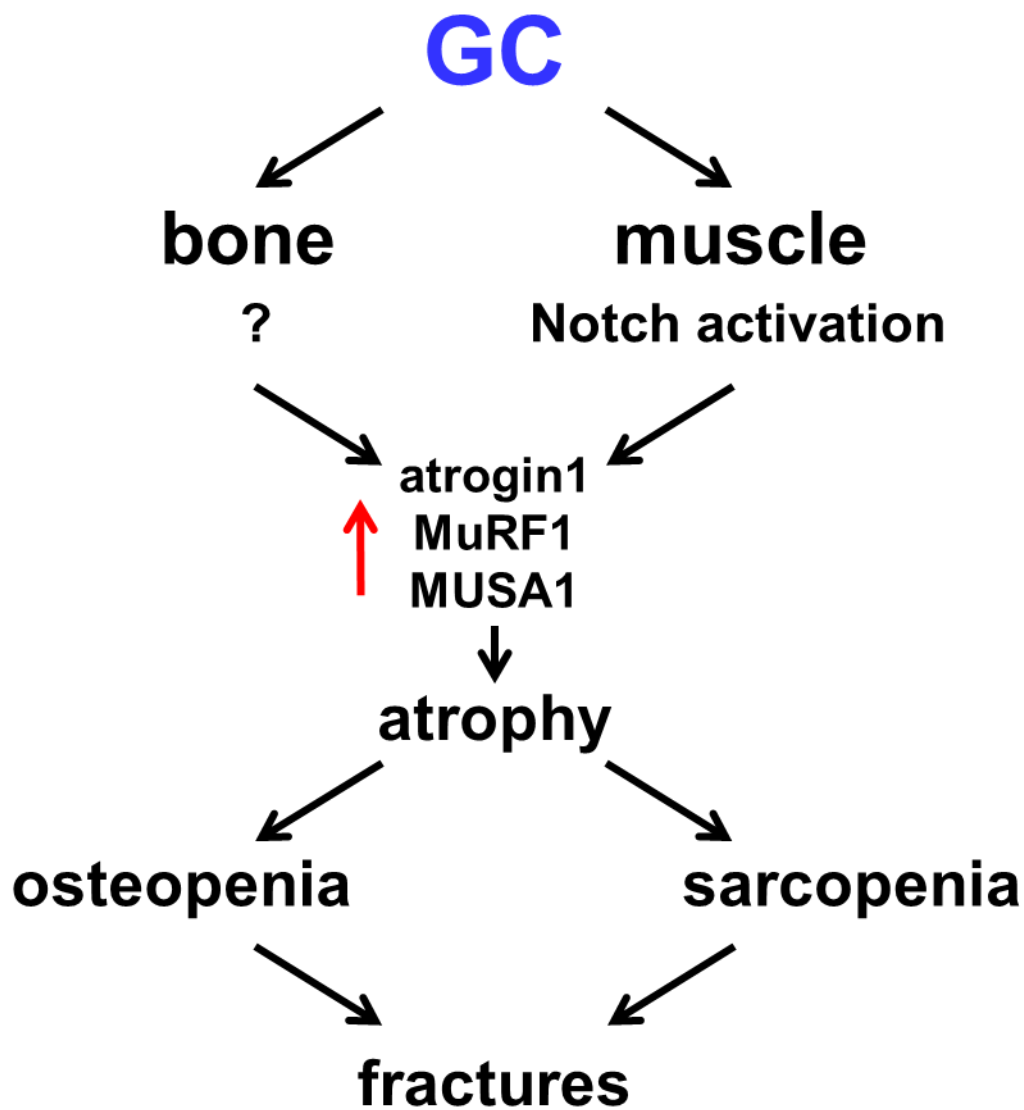
Figure 5-6. Glucocorticoids induce bone and muscle atrophy by distinct tissue-specific mechanisms upstream of atrogin1, MuRF1 and MUSA1. Glucocorticoids induce atrophy of both bone and muscle, although by different upstream mechanisms that converge in upregulation of atrophy-related E3 ubiquitin ligase genes atrogin1, MuRF1, and MUSA1.

Chapter 6

Conclusions and Future Directions

Overall, these studies highlight the contribution of resorption to the early bone loss and fragility induced by GC. Interestingly, both the inhibition of Sost/sclerostin and Pyk2 signaling prevented GC-stimulated resorption and effectively protected bone mass and strength, even without reversal of GC suppressive bone formation effects. However, the contribution of decreased bone formation and osteoblast/osteocyte viability is also significant during the early phase of GC treatment as salubrinal's reversal of these effects also protected against bone loss in the low GC dose treated mice. Taking together, these pieces of evidence indicate that the bone cellular responses of GC stimulated resorption, osteoblast/osteocyte apoptosis, and decreased bone formation all mechanistically contribute to the rapid bone loss of 6-12% exhibited during the first year of GC therapy in patients (29;161).

While current anti-catabolic interventions prevent bone loss during the first year of GC therapy, these therapeutic options do not address the marked decrease in bone formation that characterizes chronic GC excess. After the first treatment year of GC therapy, patients exhibit up to 3-5% reductions in bone per consecutive year of continued treatment; however, currently there is a lack of long-term anabolic interventions (29). Since, the 28 day prednisolone mouse model consistently recapitulates the early GC resorption phase, as indicated by circulating CTX and TRAP 5b levels as well as increases in osteoclast number and surface, prolonging the GC exposure in this model is necessary to access interventions for bone loss associated with long-term GC therapy. Previously, reports utilizing similar mouse models have indicated that the elevations in resorption circulating markers of CTX (162;163) and TRAP 5b (163) after 28 days are no longer elevated after 56 days of GC treatment (162;163). Therefore, future studies extending GC exposure to 56 days will be utilized to

investigate potential anabolic therapeutic agents during the low bone turnover phase of GC-induced bone loss.

Specifically, whether the interventions of ER stress alleviation, increased canonical Wnt signaling, or inhibition of Pyk2 signaling protects the skeleton in the context of long-term GC exposure remains unanswered. In the absence of high GC resorption activity, salubrinal or guanabenz may more effectively protected from bone loss and fragility by promoting osteoblast/osteocyte viability and osteoblast matrix mineral production even in the presence of GC. Further, guanabenz more effectively reversed GC suppression of osteoblast activity *in vitro*; however, whether guanabenz's effects translate to increased bone formation *in vivo* remains unanswered. Also, further investigation is needed to address whether increased canonical Wnt signaling could preserve bone anabolism during the chronic phase of GC-induced bone loss. The absence of Sost/sclerostin did not prevent GC inhibitory effects upon bone formation or the downregulation of anabolic β-catenin targets; however, given the vast number of Wnts and several pathway antagonists (84), it is more than likely that targeting other pathway components could promote bone anabolism even in the context of excessive GC.

The use of a Pyk2 inhibitor could also potentially promote bone formation during the chronic low bone turnover GC phase. While previous reports have shown an age-related loss of both the increased osteoblast surface and increased bone formation in the Pyk2 KO mice after 10 weeks of age (116), *in vivo* use of a Pyk2 inhibitor could exhibit the anabolic benefits of Pyk2 deficiency without the time-related diminished effects depending upon dose and duration. Also, the Pyk2 inhibitor PF-431396 was previously reported to protect against decreased bone formation in an OVX rat model (115), and this inhibitor also increased matrix mineralization production of primary osteoblasts in our studies. Overall, future investigations are warranted to determine whether interventions of ER stress alleviation, increased Wnt/β-catenin signaling, or Pyk2

inhibition will preserve bone formation thus preventing the bone loss induced by chronic GC exposure.

There also is an unmet need for a therapeutic agent that simultaneously addresses the GC-induced loss of tissue mass and strength for both bone and skeletal muscle. Our subcutaneous prednisolone pellet implantation mouse model consistently exhibits glucocorticoid-induced osteopenia and sarcopenia, which provides an opportunity to investigate crosstalk between these tissues as well as potential interventions for the atrophy of both tissues. Interventions using either genetic deletion of atrophy gene(s) or use of proteasomal/Notch signaling inhibitors are warranted to determine the therapeutic potential for targeting E3 ligases involved in musculoskeletal atrophy by GC. Interestingly, the GC induced preferential increase in FoxO transcription over β-catenin/TCF/LEF transcription occurs in cells of the osteoblastic and myogenic linage (55), indicating a potential for increased canonical Wnt signaling to benefit both tissues. Although sost/sclerostin deficiency did not translate into protection from GC-induced skeletal muscle atrophy, suggesting a lack of bone-to-muscle crosstalk, whether muscle-to-bone crosstalk was involved in the low bone formation and increased osteoblast/osteocyte apoptosis exhibited in the GC treated Sost KO mice remains unknown. Another finding that merits further investigation is the discovery of GC atrophy distinctions between fast (EDL) and slow (SOL) twitch dominated muscles, which prompts the question of what mechanistic GC alterations are involved in the loss of strength without affecting muscle mass for the slow twitch dominated muscles. Future experiments are required to identify interventions that simultaneously prevent bone and muscle atrophy as well as the crosstalk nature between these tissues under excessive GC conditions.

In closing, the current studies demonstrate that the deleterious effects of glucocorticoids on the skeleton are initially linked to robust resorption activity and that

inhibition of catabolic processes by Sost/sclerostin or Pyk2 deficiency is sufficient to prevent bone loss and fragility. However, given the long-term usage of GC therapy, future experiments are required for the identification and investigation of potential interventions to stimulate anabolic bone responses as well as prevent muscle atrophy.

References

1. **Fitzpatrick L** 1994 Glucocorticoid-induced osteporosis. In: Marcus R, ed. Osteoporosis. 1st. ed. Boston, MA: Blackwell Scientific Publications; 202-226

2. **Weinstein RS** 2011 Clinical practice. Glucocorticoid-induced bone disease. N Engl J Med 365:62-70

3. **Necela BM, Cidlowski JA** 2004 Mechanisms of glucocorticoid receptor action in noninflammatory and inflammatory cells. Proc Am Thorac Soc 1:239-246

4. **Rhen T, Cidlowski JA** 2005 Antiinflammatory action of glucocorticoids--new mechanisms for old drugs. N Engl J Med 353:1711-1723

5. **Tomlinson JW, Walker EA, Bujalska IJ, Draper N, Lavery GG, Cooper MS, Hewison M, Stewart PM** 2004 11beta-hydroxysteroid dehydrogenase type 1: a tissue-specific regulator of glucocorticoid response. Endocr Rev 25:831-866

6. **Cushing H** 1932 The basophil adenomas of the pituitary body and their clinical manifestations (pituitary basophilism). Bull Johns Hopkins Hosp 50:137-195

7. **Cooper MS, Rabbitt EH, Goddard PE, Bartlett WA, Hewison M, Stewart PM** 2002 Osteoblastic 11beta-hydroxysteroid dehydrogenase type 1 activity increases with age and glucocorticoid exposure. J Bone Miner Res 17:979-986

8. **Cooper MS, Blumsohn A, Goddard PE, Bartlett WA, Shackleton CH, Eastell R, Hewison M, Stewart PM** 2003 11beta-hydroxysteroid dehydrogenase type 1 activity predicts the effects of glucocorticoids on bone. J Clin Endocrinol Metab 88:3874-3877

9. **Weinstein RS** 2001 Glucocorticoid-induced osteoporosis. Rev Endocr Metab Disord 2:65-73

10. **Rizzoli R, Adachi JD, Cooper C, Dere W, Devogelaer JP, Diez-Perez A, Kanis JA, Laslop A, Mitlak B, Papapoulos S, Ralston S, Reiter S, Werhya G, Reginster JY** 2012 Management of glucocorticoid-induced osteoporosis. Calcif Tissue Int 91:225-243

11. **Tauchmanova L, Pivonello R, Di SC, Rossi R, De Martino MC, Camera L, Klain M, Salvatore M, Lombardi G, Colao A** 2006 Bone demineralization and vertebral fractures in endogenous cortisol excess: role of disease etiology and gonadal status. J Clin Endocrinol Metab 91:1779-1784

12. **Vestergaard P, Lindholm J, Jorgensen JO, Hagen C, Hoeck HC, Laurberg P, Rejnmark L, Brixen K, Kristensen LO, Feldt-Rasmussen U, Mosekilde L** 2002 Increased risk of osteoporotic fractures in patients with Cushing's syndrome. Eur J Endocrinol 146:51-56

13. **Manolagas SC** 2010 From Estrogen-Centric to Aging and Oxidative Stress: A Revised Perspective of the Pathogenesis of Osteoporosis. Endocr Rev 31:266-300

14. **Saag KG, Emkey R, Schnitzer TJ, Brown JP, Hawkins F, Goemaere S, Thamsborg G, Liberman UA, Delmas PD, Malice MP, Czachur M, Daifotis AG** 1998 Alendronate for the prevention and treatment of glucocorticoid-induced osteoporosis. Glucocorticoid-Induced Osteoporosis Intervention Study Group. N Engl J Med 339:292-299

15. **Van Staa TP, Leufkens HGM, Abenhaim L, Zhang B, Cooper C** 2000 Use of oral corticoisteroids and risk of fractures. J Bone Min Res 15:993-1000

16. **Lukert B** 1996 Glucocorticoid-induced osteoporosis. In: Marcus R, Felman D, Kelsey J, eds. Osteoporosis. San Diego, CA: Academic Press; 801-820

17. **Newell-Price J, Bertagna X, Grossman AB, Nieman LK** 2006 Cushing's syndrome. Lancet 367:1605-1617

18. **Van Staa TP** 2006 The pathogenesis, epidemiology and management of glucocorticoid-induced osteoporosis. Calcif Tissue Int 79:129-137

19. **Mazziotti G, Angeli A, Bilezikian JP, Canalis E, Giustina A** 2006 Glucocorticoid-induced osteoporosis: an update. Trends Endocrinol Metab 17:144-149

20. **Luengo M, Picado C, Del Rio L, Guanabens N, Montserrat JM, Setoain J** 1991 Vertebral fractures in steroid dependent asthma and involutional osteoporosis: a comparative study. Thorax 46:803-806

21. **Van Staa TP, Laan RF, Barton IP, Cohen S, Reid DM, Cooper C** 2003 Bone density threshold and other predictors of vertebral fracture in patients receiving oral glucocorticoid therapy. Arthritis Rheum 48:3224-3229

22. **Van Staa TP, Leufkens HG, Cooper C** 2002 The epidemiology of corticosteroid-induced osteoporosis: a meta-analysis. Osteoporos Int 13:777-787

23. **Lems WF, Saag K** 2015 Bisphosphonates and glucocorticoid-induced osteoporosis: cons. Endocrine 49:628-634

24. **Weinstein RS, Chen JR, Powers CC, Stewart SA, Landes RD, Bellido T, Jilka RL, Parfitt AM, Manolagas SC** 2002 Promotion of osteoclast survival and antagonism of bisphosphonate-induced osteoclast apoptosis by glucocorticoids. J Clin Invest 109:1041-1048

25. **Weinstein RS, Nicholas RW, Manolagas SC** 2000 Apoptosis of osteocytes in glucocorticoid-induced osteonecrosis of the hip. J Clin Endocrinol Metab 85:2907-2912

26. **O'Brien CA, Jia D, Plotkin LI, Bellido T, Powers CC, Stewart SA, Manolagas SC, Weinstein RS** 2004 Glucocorticoids act directly on osteoblasts and osteocytes to induce their apoptosis and reduce bone formation and strength. Endocrinology 145:1835-1841

27. **Reid IR** 1997 Glucocorticoid osteoporosis--mechanisms and management. Eur J Endocrinol 137:209-217

28. **Plotkin LI, Weinstein RS, Parfitt AM, Roberson PK, Manolagas SC, Bellido T** 1999 Prevention of osteocyte and osteoblast apoptosis by bisphosphonates and calcitonin. J Clin Invest 104:1363-1374

29. **LoCascio V, Bonucci E, Imbimbo B, Ballanti P, Adami S, Milani S, Tartarotti D, DellaRocca C** 1990 Bone loss in response to long-term glucocorticoid therapy. Bone Miner 8:39-51

30. **Jia D, O'Brien CA, Stewart SA, Manolagas SC, Weinstein RS** 2006 Glucocorticoids act directly on osteoclasts to increase their lifespan and reduce bone density. Endocrinology 147:5592-5599

31. **Hofbauer LC, Zeitz U, Schoppet M, Skalicky M, Schuler C, Stolina M, Kostenuik PJ, Erben RG** 2009 Prevention of glucocorticoid-induced bone loss in mice by inhibition of RANKL. Arthritis Rheum 60:1427-1437

32. **Plotkin LI, Bivi N, Bellido T** 2011 A bisphosphonate that does not affect osteoclasts prevents osteoblast and osteocyte apoptosis and the loss of bone strength induced by glucocorticoids in mice. Bone 49:122-127

33. **Leclerc N, Noh T, Cogan J, Samarawickrama DB, Smith E, Frenkel B** 2008 Opposing effects of glucocorticoids and Wnt signaling on Krox20 and mineral deposition in osteoblast cultures. J Cell Biochem 103:1938-1951

34. **Mortensen RF, Shapiro J, Lin BF, Douches S, Neta R** 1988 Interaction of recombinant IL-1 and recombinant tumor necrosis factor in the induction of mouse acute phase proteins. J Immunol 140:2260-2266

35. **Advani S, LaFrancis D, Bogdanovic E, Taxel P, Raisz LG, Kream BE** 1997 Dexamethasone suppresses in vivo levels of bone collagen synthesis in neonatal mice. Bone 20:41-46

36. **Rauch A, Seitz S, Baschant U, Schilling AF, Illing A, Stride B, Kirilov M, Mandic V, Takacz A, Schmidt-Ullrich R, Ostermay S, Schinke T, Spanbroek R, Zaiss MM, Angel PE, Lerner UH, David JP, Reichardt HM, Amling M, Schutz G, Tuckermann JP** 2010 Glucocorticoids Suppress Bone Formation by Attenuating Osteoblast Differentiation via the Monomeric Glucocorticoid Receptor. Cell Metab 11:517-531

37. **Laan RFJM, Van Riel PLCM, Van de Putte LBA, Van Erning LJTO, Van't Hof MA, Lemmens JAM** 1993 Low-dose prednisone induces rapid reversible axial bone loss in patients with rheumatoid arthritis: A randomized, controlled study. Ann Intern Med 119:963-968

38. **Devogelaer JP, Adler RA, Recknor C, See K, Warner MR, Wong M, Krohn K** 2010 Baseline glucocorticoid dose and bone mineral density response with teriparatide or alendronate therapy in patients with glucocorticoid-induced osteoporosis. J Rheumatol 37:141-148

39. **Sambrook PN, Roux C, Devogelaer JP, Saag K, Lau CS, Reginster JY, Bucci-Rechtweg C, Su G, Reid DM** 2012 Bisphosphonates and glucocorticoid

osteoporosis in men: results of a randomized controlled trial comparing zoledronic acid with risedronate. Bone 50:289-295

40. **Saag KG, Shane E, Boonen S, Marin F, Donley DW, Taylor KA, Dalsky GP, Marcus R** 2007 Teriparatide or alendronate in glucocorticoid-induced osteoporosis. N Engl J Med 357:2028-2039

41. **Sato AY, Tu X, McAndrews KA, Plotkin LI, Bellido T** 2015 Prevention of glucocorticoid induced-apoptosis of osteoblasts and osteocytes by protecting against endoplasmic reticulum (ER) stress in vitro and in vivo in female mice. Bone 73:60-68

42. **Allen MR, Burr DB** 2007 Mineralization, Microdamage, and Matrix: How Bisphosphonates Influence Material Properties of Bone. BoneKEy-osteovision 4:49-60

43. **Mashiba T, Turner CH, Hirano T, Forwood MR, Johnston CC, Burr DB** 2001 Effects of suppressed bone turnover by bisphosphonates on microdamage accumulation and biomechanical properties in clinically relevant skeletal sites in beagles. Bone 28:524-531

44. **Allen MR, Burr DB** 2008 Changes in vertebral strength-density and energy absorption-density relationships following bisphosphonate treatment in beagle dogs. Osteoporos Int 19:95-99

45. **Mok CC, Ho LY, Ma KM** 2015 Switching of oral bisphosphonates to denosumab in chronic glucocorticoid users: a 12-month randomized controlled trial. Bone 75:222-228

46. **Allen MR, Iwata K, Phipps R, Burr DB** 2006 Alterations in canine vertebral bone turnover, microdamage accumulation, and biomechanical properties following 1-year treatment with clinical treatment doses of risedronate or alendronate. Bone 39:872-879

47. **O'Ryan FS, Khoury S, Liao W, Han MM, Hui RL, Baer D, Martin D, Liberty D, Lo JC** 2009 Intravenous bisphosphonate-related osteonecrosis of the jaw: bone scintigraphy as an early indicator. J Oral Maxillofac Surg 67:1363-1372

48. **Saag KG, Zanchetta JR, Devogelaer JP, Adler RA, Eastell R, See K, Krege JH, Krohn K, Warner MR** 2009 Effects of teriparatide versus alendronate for treating glucocorticoid-induced osteoporosis: thirty-six-month results of a randomized, double-blind, controlled trial. Arthritis Rheum 60:3346-3355

49. **Dore RK** 2013 Long-term safety, efficacy, and patient acceptability of teriparatide in the management of glucocorticoid-induced osteoporosis. Patient Prefer Adherence 7:435-446

50. **Jin HO, Seo SK, Woo SH, Kim ES, Lee HC, Yoo DH, An S, Choe TB, Lee SJ, Hong SI, Rhee CH, Kim JI, Park IC** 2009 Activating transcription factor 4 and CCAAT/enhancer-binding protein-beta negatively regulate the mammalian target

of rapamycin via Redd1 expression in response to oxidative and endoplasmic reticulum stress. Free Radic Biol Med 46:1158-1167

51. **Dempster DW** 1989 Bone histomorphometry in glucocorticoid-induced osteoporosis. J Bone Miner Res 4:137-141

52. **Weinstein RS, Jilka RL, Parfitt AM, Manolagas SC** 1998 Inhibition of osteoblastogenesis and promotion of apoptosis of osteoblasts and osteocytes by glucocorticoids: potential mechanisms of their deleterious effects on bone. J Clin Invest 102:274-282

53. **Jilka RL, Weinstein RS, Bellido T, Roberson P, Parfitt AM, Manolagas SC** 1999 Increased bone formation by prevention of osteoblast apoptosis with parathyroid hormone. J Clin Invest 104:439-446

54. **Plotkin LI, Manolagas SC, Bellido T** 2007 Glucocorticoids induce osteocyte apoptosis by blocking focal adhesion kinase-mediated survival: evidence for inside-out signaling leading to anoikis. J Biol Chem 282:24120-24130

55. **Almeida M, Han L, Ambrogini E, Weinstein RS, Manolagas SC** 2011 Glucocorticoids and tumor necrosis factor (TNF) alpha increase oxidative stress and suppress WNT signaling in osteoblasts. J Biol Chem 286:44326-44335

56. **Harding HP, Zhang Y, Zeng H, Novoa I, Lu PD, Calfon M, Sadri N, Yun C, Popko B, Paules R, Stojdl DF, Bell JC, Hettmann T, Leiden JM, Ron D** 2003 An integrated stress response regulates amino acid metabolism and resistance to oxidative stress. Mol Cell 11:619-633

57. **Walter P, Ron D** 2011 The unfolded protein response: from stress pathway to homeostatic regulation. Science 334:1081-1086

58. **Boyce M, Bryant KF, Jousse C, Long K, Harding HP, Scheuner D, Kaufman RJ, Ma D, Coen DM, Ron D, Yuan J** 2005 A selective inhibitor of eIF2alpha dephosphorylation protects cells from ER stress. Science 307:935-939

59. **Tsaytler P, Harding HP, Ron D, Bertolotti A** 2011 Selective inhibition of a regulatory subunit of protein phosphatase 1 restores proteostasis. Science 332:91-94

60. **Bellido T, Ali AA, Plotkin LI, Fu Q, Gubrij I, Roberson PK, Weinstein RS, O'Brien CA, Manolagas SC, Jilka RL** 2003 Proteasomal degradation of Runx2 shortens parathyroid hormone-induced anti-apoptotic signaling in osteoblasts. A putative explanation for why intermittent administration is needed for bone anabolism. J Biol Chem 278:50259-50272

61. **Lecka-Czernik B, Gubrij I, Moerman EA, Kajkenova O, Lipschitz DA, Manolagas SC, Jilka RL** 1999 Inhibition of Osf2/Cbfa1 expression and terminal osteoblast differentiation by PPAR-gamma 2. J Cell Biochem 74:357-371

62. **Kato Y, Windle JJ, Koop BA, Mundy GR, Bonewald LF** 1997 Establishment of an osteocyte-like cell line, MLO-Y4. J Bone Miner Res 12:2014-2023

63. **Ogawa R, Mizuno H, Watanabe A, Migita M, Shimada T, Hyakusoku H** 2004 Osteogenic and chondrogenic differentiation by adipose-derived stem cells harvested from GFP transgenic mice. Biochem Biophys Res Commun 313:871-877

64. **Tsai SW, Liou HM, Lin CJ, Kuo KL, Hung YS, Weng RC, Hsu FY** 2012 MG63 osteoblast-like cells exhibit different behavior when grown on electrospun collagen matrix versus electrospun gelatin matrix. PLoS ONE 7:e31200

65. **Plotkin LI, Lezcano V, Thostenson J, Weinstein RS, Manolagas SC, Bellido T** 2008 Connexin 43 is required for the anti-apoptotic effect of bisphosphonates on osteocytes and osteoblasts in vivo. J Bone Miner Res 23:1712-1721

66. **Aguirre JI, Plotkin LI, Stewart SA, Weinstein RS, Parfitt AM, Manolagas SC, Bellido T** 2006 Osteocyte apoptosis is induced by weightlessness in mice and precedes osteoclast recruitment and bone loss. J Bone Min Res 21:605-615

67. **Zhang P, Hamamura K, Jiang C, Zhao L, Yokota H** 2012 Salubrinal promotes healing of surgical wounds in rat femurs. J Bone Miner Metab 30:568-579

68. **Bellido T, Plotkin LI** 2011 Novel actions of bisphosphonates in bone: Preservation of osteoblast and osteocyte viability. Bone 49:50-55

69. **Holmes B, Brogden RN, Heel RC, Speight TM, Avery GS** 1983 Guanabenz. A review of its pharmacodynamic properties and therapeutic efficacy in hypertension. Drugs 26:212-229

70. **Hamamura K, Yokota H** 2007 Stress to endoplasmic reticulum of mouse osteoblasts induces apoptosis and transcriptional activation for bone remodeling. FEBS Lett 581:1769-1774

71. **Saito A, Ochiai K, Kondo S, Tsumagari K, Murakami T, Cavener DR, Imaizumi K** 2011 Endoplasmic reticulum stress response mediated by the PERK-eIF2(alpha)-ATF4 pathway is involved in osteoblast differentiation induced by BMP2. J Biol Chem 286:4809-4818

72. **Lisse TS, Thiele F, Fuchs H, Hans W, Przemeck GKH, Abe K, Rathkolb B, Quintanilla-Martinez L, Hoelzwimmer G, Helfrich M, Wolf E, Ralston SH, Habré de Angelis M** 2008 ER stress-mediated apoptosis in a new mouse model of osteogenesis imperfecta. PLoS Genet 4(2): e7 4:1-11

73. **Wu Y, Yang M, Fan J, Peng Y, Deng L, Ding Y, Yang R, Zhou J, Miao D, Fu Q** 2014 Deficiency of osteoblastic Arl6ip5 impaired osteoblast differentiation and enhanced osteoclastogenesis via disturbance of ER calcium homeostasis and induction of ER stress-mediated apoptosis. Cell Death Dis 5:e1464

74. **Yokota H, Hamamura K, Chen A, Dodge TR, Tanjung N, Abedinpoor A, Zhang P** 2013 Effects of salubrinal on development of osteoclasts and osteoblasts from bone marrow-derived cells. BMC Musculoskelet Disord 14:197

75. **Hamamura K, Tanjung N, Yokota H** 2013 Suppression of osteoclastogenesis through phosphorylation of eukaryotic translation initiation factor 2 alpha. J Bone Miner Metab 31:618-628

76. **Zhang P, Chen A, Dodge TTN, Zheng Y, Fuqua C, Yokota H** 2013 Salubrinal Regulates Bone Remodeling and Fat Metabolism in Ovariectomized Mice. Proceedings of the Orthopedic Research Society Annual Meeting

77. **Fullwood MJ, Zhou W, Shenolikar S** 2012 Targeting phosphorylation of eukaryotic initiation factor-2alpha to treat human disease. Prog Mol Biol Transl Sci 106:75-106

78. **Delepine M, Nicolino M, Barrett T, Golamaully M, Lathrop GM, Julier C** 2000 EIF2AK3, encoding translation initiation factor 2-alpha kinase 3, is mutated in patients with Wolcott-Rallison syndrome. Nat Genet 25:406-409

79. **Harding HP, Zhang Y, Bertolotti A, Zeng H, Ron D** 2000 Perk is essential for translational regulation and cell survival during the unfolded protein response. Mol Cell 5:897-904

80. **Harding HP, Zeng H, Zhang Y, Jungries R, Chung P, Plesken H, Sabatini DD, Ron D** 2001 Diabetes mellitus and exocrine pancreatic dysfunction in perk-/- mice reveals a role for translational control in secretory cell survival. Mol Cell 7:1153-1163

81. **Wei J, Sheng X, Feng D, McGrath B, Cavener DR** 2008 PERK is essential for neonatal skeletal development to regulate osteoblast proliferation and differentiation. J Cell Physiol 217:693-707

82. **Warriner AH, Saag KG** 2013 Glucocorticoid-related bone changes from endogenous or exogenous glucocorticoids. Curr Opin Endocrinol Diabetes Obes 20:510-516

83. **Overman RA, Yeh JY, Deal CL** 2013 Prevalence of oral glucocorticoid usage in the United States: a general population perspective. Arthritis Care Res (Hoboken) 65:294-298

84. **Baron R, Kneissel M** 2013 WNT signaling in bone homeostasis and disease: from human mutations to treatments. Nat Med 19:179-192

85. **Balemans W, Ebeling M, Patel N, Van Hul E, Olson P, Dioszegi M, Lacza C, Wuyts W, Van Den Ende J, Willems P, Paes-Alves AF, Hill S, Bueno M, Ramos FJ, Tacconi P, Dikkers FG, Stratakis C, Lindpaintner K, Vickery B, Foernzler D, Van Hul W** 2001 Increased bone density in sclerosteosis is due to the deficiency of a novel secreted protein (SOST). Hum Mol Genet 10:537-543

86. **Dixon JM, Cull RE, Gamble P** 1982 Two cases of Van Buchem's disease. J Neurol Neurosurg Psychiatry 45:913-918

87. **Leupin O, Piters E, Halleux C, Hu S, Kramer I, Morvan F, Bouwmeester T, Schirle M, Bueno-Lozano M, Fuentes FJ, Itin PH, Boudin E, de FF, Jennes**

K, Brannetti B, Charara N, Ebersbach H, Geisse S, Lu CX, Bauer A, Van HW, **Kneissel M** 2011 Bone overgrowth-associated mutations in the LRP4 gene impair sclerostin facilitator function. J Biol Chem 286:19489-19500

88. **Glass DA, Bialek P, Ahn JD, Starbuck M, Patel MS, Clevers H, Taketo MM, Long F, McMahon AP, Lang RA, Karsenty G** 2005 Canonical Wnt signaling in differentiated osteoblasts controls osteoclast differentiation. Dev Cell 8:751-764

89. **Holmen SL, Zylstra CR, Mukherjee A, Sigler RE, Faugere MC, Bouxsein ML, Deng L, Clemens TL, Williams BO** 2005 Essential role of beta-catenin in postnatal bone acquisition. J Biol Chem 280:21162-21168

90. **Jilka RL, Bellido T, Almeida M, Plotkin LI, O'Brien CA, Weinstein RS, Manolagas SC** 2008 Apoptosis in bone cells. In: Bilezikian JP, Raisz LG, Martin TJ, eds. Principles of Bone Biology. 3er ed. San Diego, San Francisco, New York, London, Sydney, Tokyo: Academic Press; 237-261

91. **Li X, Ominsky MS, Niu QT, Sun N, Daugherty B, D'Agostin D, Kurahara C, Gao Y, Cao J, Gong J, Asuncion F, Barrero M, Warmington K, Dwyer D, Stolina M, Morony S, Sarosi I, Kostenuik PJ, Lacey DL, Simonet WS, Ke HZ, Paszty C** 2008 Targeted deletion of the sclerostin gene in mice results in increased bone formation and bone strength. J Bone Miner Res 23:860-869

92. **Tu X, Delgado-Calle J, Condon KW, Maycas M, Zhang H, Carlesso N, Taketo MM, Burr DB, Plotkin LI, Bellido T** 2015 Osteocytes mediate the anabolic actions of canonica Wnt/β-catenin signaling in bone. Proc Natl Acad Sci U S A 112:E478-E486

93. **O'Brien CA, Plotkin LI, Galli C, Goellner J, Gortazar AR, Allen MR, Robling AG, Bouxsein M, Schipani E, Turner CH, Jilka RL, Weinstein RS, Manolagas SC, Bellido T** 2008 Control of bone mass and remodeling by PTH receptor signaling in osteocytes. PLoS ONE 3:e2942

94. **Rhee Y, Allen MR, Condon K, Lezcano V, Ronda AC, Galli C, Olivos N, Passeri G, O'Brien CA, Bivi N, Plotkin LI, Bellido T** 2011 PTH receptor signaling in osteocytes governs periosteal bone formation and intra-cortical remodeling. J Bone Miner Res 26:1035-1046

95. **Tu X, Rhee Y, Condon KW, Bivi N, Allen MR, Dwyer D, Stolina M, Turner CH, Robling AG, Plotkin LI, Bellido T** 2012 Sost downregulation and local Wnt signaling are required for the osteogenic response to mechanical loading. Bone 50:209-217

96. **Bellido T, Ali AA, Gubrij I, Plotkin LI, Fu Q, O'Brien CA, Manolagas SC, Jilka RL** 2005 Chronic elevation of PTH in mice reduces expression of sclerostin by osteocytes: a novel mechanism for hormonal control of osteoblastogenesis. Endocrinology 146:4577-4583

97. **Pacheco-Costa R, Hassan I, Reginato RD, Davis HM, Bruzzaniti A, Allen MR, Plotkin LI** 2014 High Bone Mass in Mice Lacking Cx37 Due to Defective Osteoclast Differentiation. J Biol Chem 289:8508-8520

98. **Hill Gallant KM, Gallant MA, Brown DM, Sato AY, Williams JN, Burr DB** 2014 Raloxifene prevents skeletal fragility in adult female Zucker Diabetic Sprague-Dawley rats. PLoS ONE 9:e108262

99. **Ota K, Quint P, Ruan M, Pederson L, Westendorf JJ, Khosla S, Oursler MJ** 2013 Sclerostin is expressed in osteoclasts from aged mice and reduces osteoclast-mediated stimulation of mineralization. J Cell Biochem 114:1901-1907

100. **Schakman O, Kalista S, Barbe C, Loumaye A, Thissen JP** 2013 Glucocorticoid-induced skeletal muscle atrophy. Int J Biochem Cell Biol 45:2163-2172

101. **Iyer S, Ambrogini E, Bartell SM, Han L, Roberson PK, de CR, Jilka RL, Weinstein RS, O'Brien CA, Manolagas SC, Almeida M** 2013 FOXOs attenuate bone formation by suppressing Wnt signaling. J Clin Invest 123:3409-3419

102. **Iyer S, Han L, Bartell SM, Kim HN, Gubrij I, de CR, O'Brien CA, Manolagas SC, Almeida M** 2014 Sirtuin1 (Sirt1) promotes cortical bone formation by preventing beta-catenin sequestration by FoxO transcription factors in osteoblast progenitors. J Biol Chem 289:24069-24078

103. **Zou W, Yang S, Zhang T, Sun H, Wang Y, Xue H, Zhou D** 2015 Hypoxia enhances glucocorticoid-induced apoptosis and cell cycle arrest via the PI3K/Akt signaling pathway in osteoblastic cells. J Bone Miner Metab 33:615-624

104. **Kramer I, Halleux C, Keller H, Pegurri M, Gooi JH, Weber PB, Feng JQ, Bonewald LF, Kneissel M** 2010 Osteocyte Wnt/beta-catenin signaling is required for normal bone homeostasis. Mol Cell Biol 30:3071-3085

105. **Marenzana M, Greenslade K, Eddleston A, Okoye R, Marshall D, Moore A, Robinson MK** 2011 Sclerostin antibody treatment enhances bone strength but does not prevent growth retardation in young mice treated with dexamethasone. Arthritis Rheum 63:2385-2395

106. **Yao W, Dai W, Jiang L, Lay EY, Zhong Z, Ritchie RO, Li X, Ke H, Lane NE** 2016 Sclerostin-antibody treatment of glucocorticoid-induced osteoporosis maintained bone mass and strength. Osteoporos Int 27:283-294

107. **Marcus R, Bouxsein ML** 2008 The nature of osteoporosis. In: Marcus R, Feldman D, Nelson DA, Rosen CJ, eds. Osteoporosis. 3rd edition ed. Burlington, MA: Elsevier Academic Press; 27-36

108. **van Lierop AH, Hamdy NA, Papapoulos SE** 2010 Glucocorticoids are not always deleterious for bone. J Bone Miner Res 25:2796-2800

109. **Aspenberg P, Schilcher J** 2014 Atypical femoral fractures, bisphosphonates, and mechanical stress. Curr Osteoporos Rep 12:189-193

110. **Shane E, Burr D, Abrahamsen B, Adler RA, Brown TD, Cheung AM, Cosman F, Curtis JR, Dell R, Dempster DW, Ebeling PR, Einhorn TA, Genant HK, Geusens P, Klaushofer K, Lane JM, McKiernan F, McKinney R, Ng A, Nieves J, O'Keefe R, Papapoulos S, Howe TS, van der Meulen MC,**

Weinstein RS, Whyte MP 2014 Atypical subtrochanteric and diaphyseal femoral fractures: second report of a task force of the American Society for Bone and Mineral Research. J Bone Miner Res 29:1-23

111. **Sato AY, Au E, Richardson D, Bivi N, Cregor M, McAndrews K, Davis HM, Zimmers TA, Plotkin LI, Bellido T** 2015 Glucocorticoids induce bone and muscle atrophy by distinct mechanisms upstream of atrogin1 and MuRF1. J Bone Miner Res 30:-S1

112. **Bellido T** 2010 Antagonistic interplay between mechanical forces and glucocorticoids in bone: a tale of kinases. J Cell Biochem 111:1-6

113. **Frenkel B, White W, Tuckermann J** 2015 Glucocorticoid-Induced Osteoporosis. Adv Exp Med Biol 872:179-215

114. **Suzuki Y, Nawata H, Soen S, Fujiwara S, Nakayama H, Tanaka I, Ozono K, Sagawa A, Takayanagi R, Tanaka H, Miki T, Masunari N, Tanaka Y** 2014 Guidelines on the management and treatment of glucocorticoid-induced osteoporosis of the Japanese Society for Bone and Mineral Research: 2014 update. J Bone Miner Metab 32:337-350

115. **Buckbinder L, Crawford DT, Qi H, Ke HZ, Olson LM, Long KR, Bonnette PC, Baumann AP, Hambor JE, Grasser WA, Pan LC, Owen TA, Luzzio MJ, Hulford CA, Gebhard DF, Paralkar VM, Simmons HA, Kath JC, Roberts WG, Smock SL, Guzman-Perez A, Brown TA, Li M** 2007 Proline-rich tyrosine kinase 2 regulates osteoprogenitor cells and bone formation, and offers an anabolic treatment approach for osteoporosis. Proc Natl Acad Sci U S A 104:10619-10624

116. **Gil-Henn H, Destaing O, Sims NA, Aoki K, Alles N, Neff L, Sanjay A, Bruzzaniti A, De Camilli P, Baron R, Schlessinger J** 2007 Defective microtubule-dependent podosome organization in osteoclasts leads to increased bone density in Pyk2(-/-) mice. J Cell Biol 178:1053-1064

117. **Okigaki M, Davis C, Falasca M, Harroch S, Felsenfeld DP, Sheetz MP, Schlessinger J** 2003 Pyk2 regulates multiple signaling events crucial for macrophage morphology and migration. Proc Natl Acad Sci U S A 100:10740-10745

118. **Sato AY, Cregor M, Delgado-Calle J, Condon KW, Allen MR, Peacock M, Plotkin LI, Bellido T** 2016 Protection from Glucocorticoid-Induced Osteoporosis by Anti-Catabolic Signaling in the Absence of Sost/Sclerostin. J Bone Miner Res doi: 10.1002/jbmr.2869.:

119. **Ohnaka K, Taniguchi H, Kawate H, Nawata H, Takayanagi R** 2004 Glucocorticoid enhances the expression of dickkopf-1 in human osteoblasts: novel mechanism of glucocorticoid-induced osteoporosis. Biochem Biophys Res Commun 318:259-264

120. **Ohnaka K, Tanabe M, Kawate H, Nawata H, Takayanagi R** 2005 Glucocorticoid suppresses the canonical Wnt signal in cultured human osteoblasts. Biochem Biophys Res Commun 329:177-181

121. **Minetto MA, Botter A, Lanfranco F, Baldi M, Ghigo E, Arvat E** 2010 Muscle fiber conduction slowing and decreased levels of circulating muscle proteins after short-term dexamethasone administration in healthy subjects. J Clin Endocrinol Metab 95:1663-1671

122. **Minetto MA, Qaisar R, Agoni V, Motta G, Longa E, Miotti D, Pellegrino MA, Bottinelli R** 2015 Quantitative and qualitative adaptations of muscle fibers to glucocorticoids. Muscle Nerve 52:631-639

123. **Schakman O, Gilson H, Thissen JP** 2008 Mechanisms of glucocorticoid-induced myopathy. J Endocrinol 197:1-10

124. **Sandri M, Lin J, Handschin C, Yang W, Arany ZP, Lecker SH, Goldberg AL, Spiegelman BM** 2006 PGC-1alpha protects skeletal muscle from atrophy by suppressing FoxO3 action and atrophy-specific gene transcription. Proc Natl Acad Sci U S A 103:16260-16265

125. **Bodine SC, Latres E, Baumhueter S, Lai VK, Nunez L, Clarke BA, Poueymirou WT, Panaro FJ, Na E, Dharmarajan K, Pan ZQ, Valenzuela DM, DeChiara TM, Stitt TN, Yancopoulos GD, Glass DJ** 2001 Identification of ubiquitin ligases required for skeletal muscle atrophy. Science 294:1704-1708

126. **Gomes MD, Lecker SH, Jagoe RT, Navon A, Goldberg AL** 2001 Atrogin-1, a muscle-specific F-box protein highly expressed during muscle atrophy. Proc Natl Acad Sci U S A 98:14440-14445

127. **Menconi M, Gonnella P, Petkova V, Lecker S, Hasselgren PO** 2008 Dexamethasone and corticosterone induce similar, but not identical, muscle wasting responses in cultured L6 and C2C12 myotubes. J Cell Biochem 105:353-364

128. **Furlow JD, Watson ML, Waddell DS, Neff ES, Baehr LM, Ross AP, Bodine SC** 2013 Altered gene expression patterns in muscle ring finger 1 null mice during denervation- and dexamethasone-induced muscle atrophy. Physiol Genomics 45:1168-1185

129. **Baehr LM, Furlow JD, Bodine SC** 2011 Muscle sparing in muscle RING finger 1 null mice: response to synthetic glucocorticoids. J Physiol 589:4759-4776

130. **Watson ML, Baehr LM, Reichardt HM, Tuckermann JP, Bodine SC, Furlow JD** 2012 A cell-autonomous role for the glucocorticoid receptor in skeletal muscle atrophy induced by systemic glucocorticoid exposure. Am J Physiol Endocrinol Metab 302:E1210-E1220

131. **Sartori R, Schirwis E, Blaauw B, Bortolanza S, Zhao J, Enzo E, Stantzou A, Mouisel E, Toniolo L, Ferry A, Stricker S, Goldberg AL, Dupont S, Piccolo S, Amthor H, Sandri M** 2013 BMP signaling controls muscle mass. Nat Genet 45:1309-1318

132. **Organ JM, Srisuwananukorn A, Price P, Joll JE, Biro KC, Rupert JE, Chen NX, Avin KG, Moe SM, Allen MR** 2016 Reduced skeletal muscle function is

associated with decreased fiber cross-sectional area in the Cy/+ rat model of progressive kidney disease. Nephrol Dial Transplant 31:223-230

133. **Waning DL, Mohammad KS, Reiken S, Xie W, Andersson DC, John S, Chiechi A, Wright LE, Umanskaya A, Niewolna M, Trivedi T, Charkhzarrin S, Khatiwada P, Wronska A, Haynes A, Benassi MS, Witzmann FA, Zhen G, Wang X, Cao X, Roodman GD, Marks AR, Guise TA** 2015 Excess TGF-beta mediates muscle weakness associated with bone metastases in mice. Nat Med 21:1262-1271

134. **Moorwood C, Liu M, Tian Z, Barton ER** 2013 Isometric and eccentric force generation assessment of skeletal muscles isolated from murine models of muscular dystrophies. J Vis Expe50036

135. **Burkholder TJ, Fingado B, Baron S, Lieber RL** 1994 Relationship between muscle fiber types and sizes and muscle architectural properties in the mouse hindlimb. J Morphol 221:177-190

136. **Tu X, Delgado-Calle J, Condon KW, Maycas M, Zhang H, Carlesso N, Taketo MM, Burr DB, Plotkin LI, Bellido T** 2015 Osteocytes mediate the anabolic actions of canonical Wnt/β-catenin signaling in bone. Proc Natl Acad Sci U S A 112:E478-E486

137. **Bivi N, Condon KW, Allen MR, Farlow N, Passeri G, Brun L, Rhee Y, Bellido T, Plotkin LI** 2012 Cell autonomous requirement of connexin 43 for osteocyte survival: consequences for endocortical resorption and periosteal bone formation. J Bone Min Res 27:374-389

138. **Hauge E, Mosekilde L, Melsen F** 1999 Missing observations in bone histomorphometry on osteoporosis: implications and suggestions for an approach. Bone 25:389-395

139. **Parfitt AM, Drezner MK, Glorieux FH, Kanis JA, Malluche H, Meunier PJ, Ott SM, Recker RR** 1987 Bone histomorphometry: standardization of nomenclature, symbols, and units. J Bone Min Res 2:595-610

140. **Bonetto A, Aydogdu T, Jin X, Zhang Z, Zhan R, Puzis L, Koniaris LG, Zimmers TA** 2012 JAK/STAT3 pathway inhibition blocks skeletal muscle wasting downstream of IL-6 and in experimental cancer cachexia. Am J Physiol Endocrinol Metab 303:E410-E421

141. **Roy E.Plotnick** 1989 Application of Bootstrap Methods to Reduced Major Axis Line Fitting. Systematic Zoology . Abingdon: Taylor & Francis, Ltd. for the Society of Systematic Biologists; 144-153

142. **Organ JM, Ward CV** 2006 Contours of the hominoid lateral tibial condyle with implications for Australopithecus. J Hum Evol 51:113-127

143. **Organ JM** 2007 The functional anatomy of prehensile and nonprehensile tails of the platyrrhini (primates) and procyonidae (carnivora). Ph.D. dissertation, Johns Hopkins University

144. **Fournier M, Huang ZS, Li H, Da X, Cercek B, Lewis MI** 2003 Insulin-like growth factor I prevents corticosteroid-induced diaphragm muscle atrophy in emphysematous hamsters. Am J Physiol Regul Integr Comp Physiol 285:R34-R43

145. **Dekhuijzen PN, Gayan-Ramirez G, Bisschop A, de B, V, Dom R, Decramer M** 1995 Corticosteroid treatment and nutritional deprivation cause a different pattern of atrophy in rat diaphragm. J Appl Physiol 78:629-637

146. **Shimizu N, Yoshikawa N, Ito N, Maruyama T, Suzuki Y, Takeda S, Nakae J, Tagata Y, Nishitani S, Takehana K, Sano M, Fukuda K, Suematsu M, Morimoto C, Tanaka H** 2011 Crosstalk between glucocorticoid receptor and nutritional sensor mTOR in skeletal muscle. Cell Metab 13:170-182

147. **Bonaldo P, Sandri M** 2013 Cellular and molecular mechanisms of muscle atrophy. Dis Model Mech 6:25-39

148. **Kondo H, Ezura Y, Nakamoto T, Hayata T, Notomi T, Sorimachi H, Takeda S, Noda M** 2011 MURF1 deficiency suppresses unloading-induced effects on osteoblasts and osteoclasts to lead to bone loss. J Cell Biochem 112:3525-3530

149. **Rosenblatt JD, Parry DJ** 1992 Gamma irradiation prevents compensatory hypertrophy of overloaded mouse extensor digitorum longus muscle. J Appl Physiol (1985) 73:2538-2543

150. **Falduto MT, Czerwinski SM, Hickson RC** 1990 Glucocorticoid-induced muscle atrophy prevention by exercise in fast-twitch fibers. J Appl Physiol 69:1058-1062

151. **Mourikis P, Sambasivan R, Castel D, Rocheteau P, Bizzarro V, Tajbakhsh S** 2012 A critical requirement for notch signaling in maintenance of the quiescent skeletal muscle stem cell state. Stem Cells 30:243-252

152. **Wen Y, Bi P, Liu W, Asakura A, Keller C, Kuang S** 2012 Constitutive Notch activation upregulates Pax7 and promotes the self-renewal of skeletal muscle satellite cells. Mol Cell Biol 32:2300-2311

153. **Buas MF, Kabak S, Kadesch T** 2010 The Notch effector Hey1 associates with myogenic target genes to repress myogenesis. J Biol Chem 285:1249-1258

154. **Kopan R, Nye JS, Weintraub H** 1994 The intracellular domain of mouse Notch: a constitutively activated repressor of myogenesis directed at the basic helix-loop-helix region of MyoD. Development 120:2385-2396

155. **Pereira RM, Delany AM, Durant D, Canalis E** 2002 Cortisol regulates the expression of Notch in osteoblasts. J Cell Biochem 85:252-258

156. **Sandri M, Sandri C, Gilbert A, Skurk C, Calabria E, Picard A, Walsh K, Schiaffino S, Lecker SH, Goldberg AL** 2004 Foxo transcription factors induce the atrophy-related ubiquitin ligase atrogin-1 and cause skeletal muscle atrophy. Cell 117:399-412

157. **Milan G, Romanello V, Pescatore F, Armani A, Paik JH, Frasson L, Seydel A, Zhao J, Abraham R, Goldberg AL, Blaauw B, DePinho RA, Sandri M** 2015 Regulation of autophagy and the ubiquitin-proteasome system by the FoxO transcriptional network during muscle atrophy. Nat Commun 6:6670

158. **Xu J, Li R, Workeneh B, Dong Y, Wang X, Hu Z** 2012 Transcription factor FoxO1, the dominant mediator of muscle wasting in chronic kidney disease, is inhibited by microRNA-486. Kidney Int 82:401-411

159. **Ambrogini E, Almeida M, Martin-Millan M, Paik JH, DePinho RA, Han L, Goellner J, Weinstein RS, Jilka RL, O'Brien CA, Manolagas SC** 2010 FoxO-Mediated Defense against Oxidative Stress in Osteoblasts Is Indispensable for Skeletal Homeostasis in Mice. Cell Metab 11:136-146

160. **Sato AY, Richardson D, Cregor M, Davis HM, Au ED, McAndrews K, Zimmers TA, Organ JM, Peacock M, Plotkin LI, Bellido T** 2017 Glucocorticoids induce bone and muscle atrophy by tissue-specific mechanisms upstream of E3 ubiquitin ligases. Endocrinology doi.org/10.1210/en.2016-1779:

161. **Reid IR** 1989 Pathogenesis and treatment of steroid osteoporosis. Clin Endocrinol (Oxf) 30:83-103

162. **Yao W, Cheng Z, Busse C, Pham A, Nakamura MC, Lane NE** 2008 Glucocorticoid excess in mice results in early activation of osteoclastogenesis and adipogenesis and prolonged suppression of osteogenesis: A longitudinal study of gene expression in bone tissue from glucocorticoid-treated mice. Arthritis Rheum 58:1674-1686

163. **Yao W, Cheng Z, Pham A, Busse C, Zimmermann EA, Ritchie RO, Lane NE** 2008 Glucocorticoid-induced bone loss in mice can be reversed by the actions of parathyroid hormone and risedronate on different pathways for bone formation and mineralization. Arthritis Rheum 58:3485-3497

CURRICULUM VITAE

Amy Yoshiko Sato

Education

Indiana University, Ph.D.,	**2011-2017**

Major: Anatomy & Cell Biology, Minor: Life Sciences

Cumulative GPA: 3.838

DePauw University Class of 2011, B.A.,	**2006-2011**

Majors: Biology & Psychology, Minor: Japanese

Cumulative GPA: 3.78

Graduate Awards

American Society for Bone and Mineral Research (ASBMR) Young Investigator Travel Grant Award	2016
Erica M. Daniel Kepner Award for Scientific Achievement Honorable Mention Award	2016
Golden Key International Honour Society	2016
American Society for Bone and Mineral Research (ASBMR) Young Investigator Award	2015
Orthopaedic Research Society (ORS) 45th Sun Valley Workshop Alice L. Jee Award	2015
Endocrine Fellows Foundation (EFF)/ASBMR Seventh Fellows Forum on Osteoporosis and Metabolic Bone Diseases Travel Award	2013
Graduate Student Representative for Anatomy & Cell Biology Department	2013-2014
Indiana University School of Medicine (IUSM) Graduate Student Travel Grant Award	2012

Undergraduate Awards

Honor: *Magna Cum Laude*	2011
Dean's List: 10 semesters	2006-2011
Marcella Fletcher Memorial Award, Department of Biology	2011
Biology 335 Animal Physiology, Teaching Assistant	2010-2011
Honors Thesis: *The Effects of Gdf8 and Activin A on Muscle Atrophy*	2010
Dr. Irving Serlin Distinguished Honor Scholar Award	2010
Honors Scholar: Academic Program of Distinction	2006-2010
Psychology Thesis: *The Effects of Prior Knowledge on the Perception of Attractiveness for Faces and Voice,* Senior Thesis Seminar Award, Psychology Department	2010
Theodore Englehart Scholarship, Awarded to the Outstanding Senior Psychology Major	2010
Experimental Research in Cognitive Psychology, Research Assistant	2008
DePauw Faculty Distinguished Scholar Award	2006

Publications

Sato AY, Richardson D, Cregor M, Davis HM, Au ED, McAndrews K, Zimmers TA, Organ JM, Peacock M, Plotkin LI, Bellido T. 2017. Glucocorticoids induce bone and muscle atrophy by tissue-specific mechanisms upstream of E3 ubiquitin ligases. *Endocrinology: in press.*   2017

Delgado-Calle J, **Sato AY**, Bellido T. 2016. Role and mechanism of action of sclerostin in bone. *Bone.* 2016 doi: 10.1016/j.bone.2016.10.007. Epub 2016 Oct 12.   2016

Maycas M, McAndrews K, **Sato AY**, Pellegrini GG, Brown DM, Allen MR,   2016
Plotkin LI, Gortazar AR, Esbit P, Bellido T. 2016. PTHrP-derived peptides
restore bone mass and strength in diabetic mice: additive effect of mechanical
loading. *J Bone Miner Res:* doi: 10.1002/jbmr.3007. Epub 2016 Sep 28.

Sato AY, Cregor M, Delgado-Calle J, Condon KW, Allen MR, Peacock M,   2016
Plotkin LI, Bellido T. 2016.Protection from glucocorticoid-induced osteoporosis
by anti-catabolic signaling in the absence of Sost/sclerostin.
J Bone Miner Res 31(1791-1802): doi: 10.1002/jbmr.2869. Epub 2016 Jun 5.

Sato AY, Tu X, McAndrews KA, Plotkin LI, Bellido T. 2015. prevention of   2015
 glucocorticoid induced-apoptosis of osteoblasts and osteocytes by protecting
against endoplasmic reticulum (ER) stress in vitro and in vivo in female mice.
Bone 73(60-68): doi: 10.1016/j.bone.2014.12.012. Epub 2014 Dec 19.

Hill Gallant KM, Gallant MA, Brown DM, **Sato AY**, Williams JN, Burr DB. 2014.   2014
Raloxifene prevents skeletal fragility in adult female zucker diabetic
sprague-dawley rats. *PLoS ONE* 9(9): e108262. doi: 10.1371/journal.pone.0108262.
eCollection 2014.

Abstracts

Sato AY, Cregor M, Condon KW, Plotkin LI, Bellido T. 2016. Pyk2 deficiency   2016
 protects from glucocorticoid-induced bone resorption and osteoblast and osteocyte
apoptosis, but not from the decrease in bone formation. *J Bone Miner Res. 31*
(Suppl. 1). **Oral Presentation and ASBMR Young Investigator Travel Grant Award.**

Sato AY, Cregor M, Tzeggai J, McAndrews K, Delgado-Calle J, Robling AG, Plotkin LI, Bellido T. 2015. Sost/sclerostin deficiency protects the murine skeleton from glucocorticoid-induced bone loss by inhibiting bone resorption. *Orthopaedic Research Society (ORS) 45th Sun Valley Workshop.* **Alice L. Jee Award.**

2015

Sato AY, Au E, Richardson D, Bivi N, Cregor M, McAndrews K, Davis HM, Zimmers T, Plotkin LI, Bellido T. 2015. Glucocorticoids induce bone and muscle atrophy by distinct mechanisms upstream of atrogin1 and MuRF1. *J Bone Miner Res. 30* (Suppl. 1). **Oral Presentation and ASBMR Young Investigator Award.**

2015

Sato AY, Cregor M, Tzeggai J, McAndrews K, Delgado-Calle J, Robling AG, Plotkin LI, Bellido T. 2015. Sost/sclerostin deficiency protects the murine skeleton from glucocorticoid-induced bone loss by inhibiting bone resorption. *J Bone Miner Res. 30* (Suppl. 1). **Plenary Poster**.

2015

Maycas M, McAndrews KA, **Sato AY**, Pellegrini GG, Brown DM, Allen MR, Plotkin LI, Esbrit P, Gortzar AR, Bellido T. 2015. PTHrP-derived peptides restore bone mass and strength in diabetic mice: additive effect of mechanical loading. *J Bone Miner Res. 30* (Suppl. 1).

2015

Pellegrini GG, Cregor M, McAndrews K, Delgado-Calle J, **Sato AY**, Davis HM, Plotkin LI, Burr D, Weaver C, Bellido T. 2015. N Nrf2 mediates gender specific mechanisms on bone accrual and maintenance. *J Bone Miner Res. 30* (Suppl. 1).

2015

Sato A, Plotkin LI, Bellido T. 2013. Prevention of glucocorticoid
induced-apoptosis of osteoblasts and osteocytes by protecting against
endoplasmic reticulum (ER) stress. *J Bone Miner Res.* 28 (Suppl. 1).

2013

Delgado-Calle J, Tu X, **Sato A**, Cregor M, McAndrews K, Plotkin LI, Bellido T.
2013. PTH upregulates RANKL and MMP13 expression through direct actions on
osteocytes, but MMP13 is derived from non-osteocytic cells. *J Bone Miner Res.* 28
(Suppl. 1). **Plenary Poster**.

2013

Bivi N, Olivos N, **Sato A**, Southern D, Bellido T. 2012. Glucocorticoids induce
atrophy of bone andmuscle by FoxO- and ATF4-dependent mechanisms.
J Bone Miner Res. 27 (Suppl. 1).

2012

Hill K, Gallant M, Brown D, **Sato A**, Burr D. 2012. Raloxifene prevents skeletal
fragility in adult female zucker diabetic sprague-dawley (ZDSD) rats.
J Bone Miner Res. 27 (Suppl. 1).

2012

Bivi N, Olivos N, **Sato A**, Southern D, Bellido T. 2012 Atrophy is a common
pathway activated by glucocorticoids in bone and muscle. *IBMS Sun Valley
Workshop: Musculoskeletal Biology. 42*. **Oral presentation**.

2012

Sato A, Yaden B, Kline A, Krishnan V. 2010. Use of non-invasive MRI/MRS
techniques to assess recovery in muscle tissue. *Endocrine Reviews.* 31 (Suppl. 1).

2010

Halladay D, **Sato A**, Ma Y, Shetler P, Bullock H, Krishnan V. 2010. Exploring   2010

the LRP5 SOST interacting surface to identify small molecule inhibitor of SOST

Action. *J Bone Miner Res.* 25 (Suppl. 1).

Professional Associations

ASBMR, American Society for Bone and Mineral Research   2012-2017

Orthopaedic Research Society (ORS)   2015-2017

Golden Key International Honour Society   2016

Endocrine Society   2010-2011

Phi Beta Kappa   2010-2011

Psi Chi, International Honor Society in Psychology   2009-2011

Order of Omega, Leadership Honor Society   2008-2010

Employment & Positions

DePauw University– Greencastle, IN   2010-2011

Undergraduate Teaching Assistant with Dr. K. S. Kinney, Professor of Biology

Spent two semesters serving as the teaching assistant (T.A.) for Dr. K. S. Kinney's

Animal Physiology course involving instruction for course materials in T.A. led review

sessions, basic laboratory techniques, and standard animal husbandry and handling

skills. These efforts led to an unprecedented awarding of course credit.

Eli Lilly and Company– Indianapolis, IN   2009-2010

Summer Replacement Student with Dr. G. Krishnan, Musculoskeletal DHT

Spent two summers and a winter term with Dr. G. Krishnan researching muscle atrophy

using MRS analyses of the gastrocnemius muscle and the canonical Wnt pathway using

molecular and cell biology techniques. These efforts led to poster presentations at the

annual conferences for the Endocrine Society 2010 and American Society for Bone and Mineral Research 2010 meetings.

InfoSpherix Incorporated– Carmel, IN   2007-2008

Reservation Specialist

Advised clients of risk management policies. Supervised part-time employees. Solved quality assurance concerns. Administered tech support for online division. Executed client billing and notification.

Personal Interests

Conversational Japanese, Classically Trained Pianist, International Travel